

LA-4073-MS

C. 3

CIC-14 REPORT COLLECTION  
REPRODUCTION  
COPY

# LOS ALAMOS SCIENTIFIC LABORATORY

of the

## University of California

LOS ALAMOS • NEW MEXICO

Quarterly Status Report on the

### Advanced Plutonium Fuels Program

July 1 to September 30, 1968

JUN 26 1968

SCANNED

LOS ALAMOS NATIONAL LABORATORY



3 9338 00378 1332

UNITED STATES  
ATOMIC ENERGY COMMISSION  
CONTRACT W-7405-ENG-36

## LEGAL NOTICE

This report was prepared as an account of Government sponsored work. Neither the United States, nor the Commission, nor any person acting on behalf of the Commission:

A. Makes any warranty or representation, expressed or implied, with respect to the accuracy, completeness, or usefulness of the information contained in this report, or that the use of any information, apparatus, method, or process disclosed in this report may not infringe privately owned rights; or

B. Assumes any liabilities with respect to the use of, or for damages resulting from the use of any information, apparatus, method, or process disclosed in this report.

As used in the above, "person acting on behalf of the Commission" includes any employee or contractor of the Commission, or employee of such contractor, to the extent that such employee or contractor of the Commission, or employee of such contractor prepares, disseminates, or provides access to, any information pursuant to his employment or contract with the Commission, or his employment with such contractor.

This LA...MS report presents the status of the LASL Advanced Plutonium Fuels Program. Previous Quarterly Status Reports in this series, all unclassified, are:

LA-3607-MS

LA-3760-MS\*

LA-3650-MS

LA-3820-MS

LA-3686-MS

LA-3880-MS

LA-3708-MS\*

LA-3933-MS

LA-3745-MS

LA-3993-MS

This report, like other special-purpose documents in the LA...MS series, has not been reviewed or verified for accuracy in the interest of prompt distribution.

\*Advanced Reactor Technology (ART) Series

Printed in the United States of America. Available from  
Clearinghouse for Federal Scientific and Technical Information  
National Bureau of Standards, U. S. Department of Commerce  
Springfield, Virginia 22151

Price: Printed Copy \$3.00; Microfiche \$0.65

Distributed January 9, 1969

LA-4073-MS  
SPECIAL DISTRIBUTION

**LOS ALAMOS SCIENTIFIC LABORATORY**  
**of the**  
**University of California**  
LOS ALAMOS • NEW MEXICO

Quarterly Status Report on the  
**Advanced Plutonium Fuels Program**

July 1 to September 30, 1968



## FOREWORD

This is the ninth quarterly report on the Advanced Plutonium Fuels Program conducted at the Los Alamos Scientific Laboratory. The work is centered around problem areas associated with LMFBR development, though some of it has a broader applicability to general reactor technology.

In this report, areas of investigation have been identified by new indices in accordance with AEC-RDT directives that each Schedule 189a prepared in support of specific tasks be assigned a permanent identifying number. These permanent numbers, together with the descriptive title of the corresponding Schedule 189a and the identification number used prior to FY 1969, are listed below for reference:

<u>189a Title, or Program</u>	<u>Former 189a Number</u>	<u>New 189a Number</u>
Examination of Fast Reactor Fuels	822	07401
LASL Sodium Technology Program	801	07462
Ceramic Plutonium Fuel Materials	807	07463
Studies of Na Bonded (U,Pu)C and (U,Pu)N LMFBR Fuels	808	07464
Reactor Physics	811	07465
Fast Reactor Metallic Fuel Studies	824	07466
Other Advanced Systems	901	07471

Only the last three digits of the permanent identifying numbers are used in designating work areas (projects) in this report. Material in the report has been arranged in the sequence of the new identifying numbers.

Most of the investigations discussed here are of the continuing type. Results and conclusions described may therefore be changed or augmented as the work continues. Published reference to results cited in this report should not be made without obtaining explicit permission to do so from the person in charge of the work.

TABLE OF CONTENTS

<u>PROJECT</u>		<u>PAGE</u>
401	EXAMINATION OF FAST REACTOR FUELS	
	I. Introduction	5
	II. Hot Cell Equipment Development	5
	III. Hot Cell Applications of Analytical Methods	8
	IV. Examination of Unirradiated Fuels	9
	V. Requests from DRDT	10
	VI. LMFBR/FFTF Analytical Chemistry Quality Control Program	12
	VII. References	13
462	SODIUM TECHNOLOGY	
	I. Introduction	14
	II. Materials Compatibility	14
	III. Study of Purification Methods for Nonradioactive Impurities	16
	IV. Fission Products in Sodium Systems	20
	V. On-Line Monitoring Methods	22
	VI. Sampling and Analysis	26
	VII. Cover Gas and Maintenance Atmospheres	29
463	CERAMIC PLUTONIUM FUEL MATERIALS	
	I. Introduction	31
	II. Synthesis and Fabrication	31
	III. Properties	32
	IV. Analytical Chemistry	37
	V. Publications	38
464	STUDIES OF SODIUM-BONDED (U,Pu)C and (U,Pu)N LMFBR FUELS	
	I. Introduction	40
	II. Synthesis and Fabrication of (U,Pu)C Pellets	40
	III. Loading Facility for Test Capsules	42
	IV. Carbide Fuel Compatibility Studies	43
	V. EBR-II Irradiation Testing	52
	VI. Gamma Scanning and Related Studies	52
	VII. Sodium-Bond Heat Transfer Studies	55
	VIII. Analytical Chemistry	55
	IX. References	56
465	REACTOR PHYSICS	
	I. Introduction	58
	II. Cross-Section Procurement, Evaluation, and Testing	58
	III. Reactor Analysis Methods and Concept Evaluations	60
	IV. Cooperative Arrangements	65
	V. References	65

TABLE OF CONTENTS  
(continued)

<u>PROJECT</u>		<u>PAGE</u>
466	FAST REACTOR METALLIC FUEL STUDIES	
	I. Introduction	66
	II. Fuel Preparation and Fabrication	66
	III. Irradiation Effects Studies	69
	IV. Metal Fuel Compatibility Testing	70
	V. Analytical Chemistry	70
	VI. References	71
471	OTHER ADVANCED SYSTEMS - RESEARCH AND DEVELOPMENT	
	I. High Temperature Neutron Detector Test	72
	II. Equation of State of Reactor Fuels	74
	III. References	74
	SPECIAL DISTRIBUTION	75

PROJECT 401

EXAMINATION OF FAST REACTOR FUELS

Person in Charge: R. D. Baker  
Principal Investigators: J. W. Schulte  
J. A. Leary  
C. F. Metz

I. INTRODUCTION

This project is directed toward the examination and comparison of the effects of neutron irradiation on LMFBR Program fuel materials. Irradiated materials are examined as requested by the Fuels and Materials Branch of DRD & T.

Another phase of this project is the development of an analytical chemistry program designed to assure the high-quality well-characterized fuel required by the LMFBR/FFTF Program. In close cooperation with PNL, an analytical program has been developed which has the following objectives:

1. To evaluate the present capabilities of potential fuel producers for making the analytical measurements on FFTF fuel that are necessary to assure the uniformly high quality fuel required by the LMFBR/FFTF Program.
2. To provide technical guidance to fuel producers, as may be required, to assure these capabilities are established at the level required by FFTF reactor fuel specifications.
3. To establish and conduct a monitoring program that will assure continuing technical competence of fuel producers for the analysis of FFTF fuel at the level required by fuel specifications.

II. HOT CELL EQUIPMENT DEVELOPMENT

Fuel Capsule Handling  
(D. B. Court)

Design of the shielded cask for shipping irradiated capsules from EBR-II to LASL has been modified to include suggestions from reviewers. The design is currently being re-evaluated for heat dissipation characteristics.

One major change made during this period has been to provide for handling fuel elements up to 50 inches long inside the alpha containment box. This increased length capability also applies to gamma scanning and x-ray operations, both of which were previously limited to 40 inches.

Inert Atmosphere Boxes

(G. R. Brewer, C. E. Frantz, M. D. Keehn,  
R. F. Velkinburg)

Additional tests have been made with the disassembly box located in Cell 14 indicating again that under ideal conditions it is possible to attain atmosphere purities of 4 ppm O<sub>2</sub> and 0.5 ppm H<sub>2</sub>O.

An inspection of the new Ar purification unit at the vendor's plant will be made in early October. It is planned to use this system for providing an inert atmosphere to the 2 metallography cells and the "blister" which houses the remote metallograph.

The alpha-box for Cell 11, where the DTA equipment is installed, has been He leak-checked and found to be satisfactory. Even though there are no immediate plans to provide inert atmosphere to this cell, it was shown to be suitable should the requirement be needed.

#### In-Cell Equipment

(G. R. Brewer, D. B. Court, E. L. Ekberg, F. J. Fitzgibbon, C. E. Frantz, M. E. Lazarus, M. W. McCloskey, F. H. Newbury, D. S. Shaffer, A. E. Tafoya, T. Romanik, J. R. Trujillo)

Considerable time was spent during this period with checking out and making last minute changes to the equipment to accommodate the PNL and BNW capsules and pins. Major modifications or additions to those previously listed are given below.

#### 1. Dimensioning Equipment

Equipment for taking dimensions of pins in the disassembly box has been altered to accept pins up to 50 inches long.

At the request of DRDT the new profilometer (for use in a beta-gamma cell) is being designed to measure capsules (and pins) up to 61 inches long, the length of the unencapsulated pins proposed for the EBR-II.

The apparatus designed and constructed for obtaining dimensions of 1/4 in. x 1/4 in. pellets was used extensively for measuring several hundred unirradiated mixed carbide pellets. According to the users, the machine gave good diametral traces. However, the length, perpendicularity, concave and convex measurements were not easily obtained. Therefore, an improved model is being designed for glovebox use. Those improvements which are adaptable to hot cell application will be incorporated into the remotized unit.

#### 2. Fission Gas Sampling and Void-Volume Determination

Cell 14 is now completely equipped to puncture pins which have an o.d. of 0.235-0.256, 0.294-0.315 and 0.356-0.380 in. This covers all pins that are presently expected. Void volume and quantitative fission gas measurements can be made on any of these pins. A written procedure for use of the equipment is available and two successful dry runs have been completed.

Cell 4 is being equipped to drill capsules for void volume and fission gas measurements and installation is expected to be complete before the end of October. Drilling is necessary of most of the capsules since the puncturing device will not penetrate a wall which is much greater than 0.020 in. The drill will now accommodate capsules which have an o.d. of 1-1/8 in. and 0.568 in. but can be made to accommodate any capsule that is less

than 1-1/8 in. o.d.

#### 3. Gamma Scanning at the DP West Hot Cells

Layouts for the in-cell equipment and collimators have been completed. Revisions to the hoists and corridor equipment for unloading shielded casks are under consideration.

The mechanical portion of the scanning unit, revised to handle 50 in. long capsules (pins), is in fabrication.

#### 4. Support Equipment for the Shielded Microprobe

In order to obtain a surface on oxide samples with sufficient conductivity to be suitable for the microprobe, a carbon evaporator will be installed in Cell 11. It is planned to decontaminate the sample prior to deposition of carbon.

Transfer of the coated specimen to the transfer plug will be handled in the corridor if the alpha activity level is reduced sufficiently by the carbon deposition. Drawings of the transfer plug and mating surfaces between the cask and instrument had not been received by October 1.

#### Differential Thermal Analysis (D. B. Court)

Testing of the entire system was started. It appears that the oscillator, control unit, vacuum system and valve controller perform satisfactorily. There is, however, a leak in the vacuum piping, and active testing has been curtailed until the system can be made leak-free.

Since it was decided to locate the carbon evaporator (for the microprobe samples) in Cell 11, the vacuum piping of the DTA system was modified to incorporate the requirements for the evaporator.

#### Heat Content Measurement (C. E. Frantz)

Essentially the entire calorimeter is fabricated, installed in an alpha-box, and helium leak-checked. Instrumentation for both the calorimeter and welder is complete. Services up to the cell face are nearly finished. The alpha-box must be completely equipped, leak-checked, and installed before the significant tests can be run on the calorimeter.

#### Cathodic Etcher (K. A. Johnson)

Preliminary check-out of optimum operating conditions is being done.

General Metallography

(K. A. Johnson, W. McCloskey, D. Jeffries)

A new premount of polycarbonate plastic has been developed for use in hot cell metallography, as shown in

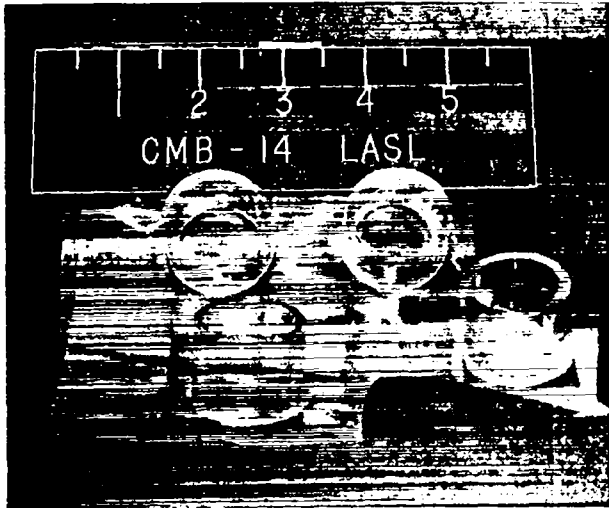


Fig. 1. Polycarbonate premounts.

The polycarbonate plastic is transparent and bonds completely with the epoxy casting resin, as shown in Fig. 2. The former premounts of brass did not fully

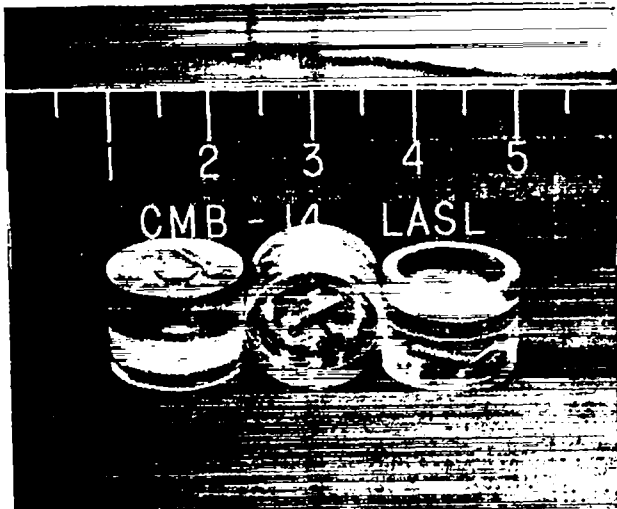


Fig. 2. Polycarbonate premounts with specimens cast in place with epoxy resin. Note the transparency and bonding of epoxy with the polycarbonate premold.

bond, sometimes resulting in cracks which would retain etchants, lubricants, or rinses. The polycarbonate plastic is relatively radiation resistant and is more resistant than the epoxy casting resin.

The outer ring in the premount fits into the ball detents in the multiple specimen holder (Fig. 3). The seven pound pressure detents prevent the mounts from turning. The ring in the premount locates the surface of all six mounts to be ground and polished at the same level (Fig. 4).

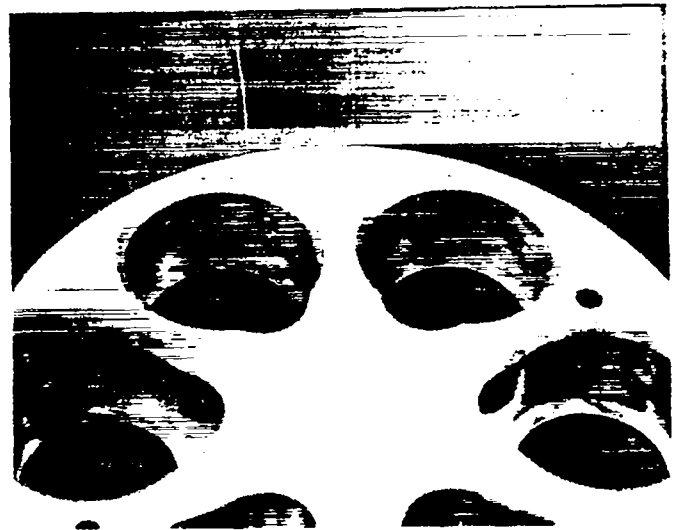


Fig. 3. Ball detents in the multiple specimen holder.

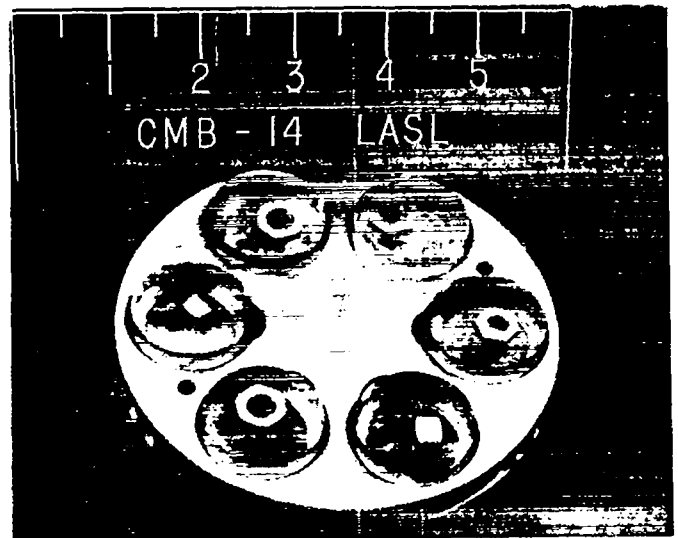


Fig. 4. Polycarbonate premounts with specimens as polished in the multiple specimen holder.

### III. HOT CELL APPLICATIONS OF ANALYTICAL METHODS

#### Microsampling of Irradiated Fuel (G. C. Swanson, J. W. Dahlby)

In preparation for application of a Raytheon Model 2-334 ultrasonic impact grinder to microsampling of irradiated reactor fuels, modifications were made that permitted taking microcores in an inert atmosphere. Modifications included changing the shape of the tip of the tool cone, threading the tip for attachment of threaded hypodermic needles, and replacing the flowing aqueous slurry system for the grinding compound with a small reservoir of slurry containing 800 grit BC in Dow Corning 200 Fluid. Following these modifications, the hypodermic needle vibrated with the tool cone at 25,000 cycles/sec through an amplitude of 0.0004 in. The sample was held in the slurry reservoir beneath the needle tip which drove the abrasive into the sample, thereby producing its counterpart in the sample. The microcore produced had a diameter slightly less than the bore of the needle, and generally remained in the needle. The needle also was abraded; needle to sample wear ratios were 1:1 for stainless steel samples, 1:5 for UC, and 1:10 for  $UO_2$ .

Microcores were taken by full penetration of sintered UC pellets 0.06-in. thick and  $UO_2$  pellets 0.25-in. thick using needles having bores with the following diameters: 0.047-in. (16 gauge), 0.033-in. (18 gauge), 0.027-in. (19 gauge), and 0.020-in. (21 gauge). Samples taken with a 23 gauge (0.013-in. bore) needle were too small to locate in the slurry. The sampling operation was generally satisfactory.

Work to be done in adapting the microsampler to remote operation includes developing an appropriate indexing system to place the needle tip within 0.003 to 0.004 in. of the desired spot on the sample, devising a method for retrieving the microcores, and minor modifications of the instrument controls for manipulator operation.

#### Determination of C in (U,Pu)O<sub>2</sub> Fuel Material (M. E. Smith, C. S. MacDougall, W. B. Hutchinson, G. R. Waterbury)

In preparation for determining C in irradiated mixed oxide fuel a combustion-capillary trap method was

applied to measurement of C in the ppm range in unirradiated sintered pellets of (U,Pu)O<sub>2</sub>. It was found that this material must be ground in order to expose the C to the oxidizing action of O<sub>2</sub>. Limited data indicated that the particular material analyzed contained between 50 and 60 ppm of C. Grinding conditions will be investigated further and necessary modifications to both grinder and combustion furnace will be made for hot cell operation. The method appeared entirely adaptable to hot cell use.

#### Analysis of Irradiated (Th,U)C-Graphite Fuel Compacts

(J. W. Dahlby, W. J. Baughman, T. K. Marshall,  
G. R. Waterbury)

Samples from eight irradiated fuel compacts, containing (Th,U)C particles coated with pyrolytic C in a graphite matrix, were analyzed spectrophotometrically for U and Th. Hot cell operations included grinding the samples in a mixer-mill, and dissolving by refluxing with  $HNO_3-HClO_4$  and finally with  $HClO_4-K_2Cr_2O_7$ . Small aliquots of the solutions were then removed from the hot cell for the spectrophotometric measurements. In addition, the Th and U were determined in  $HNO_3-HClO_4$  leach solutions of fractured particles in two underground samples, and in the  $HClO_4-K_2Cr_2O_7$  solutions of the residues left from leaching. No difficulties were experienced in these operations. The relative standard deviations of the measurements were about 4%.

#### Determination of Burnup

(E. A. Hakila, R. G. Hurley, G. R. Waterbury)

In recent months the idea of determining burnup by measuring the concentration of a non-radioactive fission product isotope has been proposed. Considerations have indicated that an x-ray fluorescence technique might have possibilities for this measurement, especially if a high yield fission element were selected. To test this possibility, neodymium was selected as the fission product element for trial. A solution containing U and fission product elements was used as a stand-in for dissolver solution of an irradiated fuel. Tb was added as an internal standard. The Nd and Tb were separated from the remainder of the elements present by being adsorbed onto an inorganic paper disc impregnated with a strong cation

exchange resin.

Measurement of the intensities of the  $L\beta_1$  x-ray for Nd and  $L\alpha_1$  x-ray for the Tb permitted calculation of intensity ratios which were compared to ratios measured from prepared solutions to obtain the Nd concentration. Under optimum conditions, the precision ( $1\sigma$ ) was 0.7 relative percent in measuring 20 to 5  $\mu\text{g}$  and increased to 8% for  $\mu\text{g}$  of Nd. The effects of various impurity elements are now being studied. It is anticipated the method will apply to irradiated fuel such as a mixed oxide, and further, that it will be amenable to hot cell operation. The size of the sample required for this technique may be too large for some applications.

#### IV. EXAMINATION OF UNIRRADIATED FUELS

##### Examination of Westinghouse Atomic Power Department Carbides

(J. A. Leary, E. A. Hakila, K. A. Johnson, C. Baker, R. T. Phelps, G. R. Waterbury)

Eight pellets of carbides produced by WARD were examined by metallography, electron microprobe examination, x-ray diffractometry, and emission spectroscopy. Four of the samples were  $\text{Cr}_{23}\text{C}_6$  stabilized (U,Pu)C, three were Fe stabilized (U,Pu)C, and one was Fe stabilized with UC. All results have been reported to RDT/AEC and to WARD.

##### Thermal Conductivity (K. W. R. Johnson)

Installation of the comparative thermal conductivity apparatus in an inert glovebox was completed. Associated instrumentation and services were tested and the system was made ready for use with radioactive materials.

Stand-in measurements were made with a 1/2 in. diam alloy A-286 specimen and Inconel 702 meter bars. The thermal conductivity of alloy A-286 varied linearly with temperature and was of the same order of magnitude as the (U,Pu)C of interest. A set of meter bars were fabricated from the same stock as the specimen. Data for alloy A-286 are listed below and are comparable to the data of Moeller and Wilson. <sup>(1)</sup>

#### The Thermal Conductivity of Alloy A-286

Temperature (°C)	Thermal Conductivity (cal./sec. cm. °C)
122	0.0318 ± 0.0009
452	0.0429 ± 0.0005
986	0.0575 ± 0.0027

Measurement of the thermal conductivity of a specimen of  $\text{U}_{0.8}\text{Pu}_{0.2}\text{C}$  is now in progress.

##### Plastic Deformation (M. Tokar)

Measurements of the compressive creep of uranium-plutonium ceramic fuels have been undertaken using equipment adapted from a design now in use on UC-graphite composites (Fig. 5). The specimens are cylindrical pellets, about 1/2 in. diam x 1/2 in. long. As shown, the specimen is held in a graphite die, which is heated by induction. The compressive load is applied by a hydraulic ram, which passes through an O-ring in the bottom of the water-cooled vacuum chamber in which the graphite susceptor, induction coil, etc. are enclosed. The entire assembly has been installed in an inert-atmosphere glovebox.

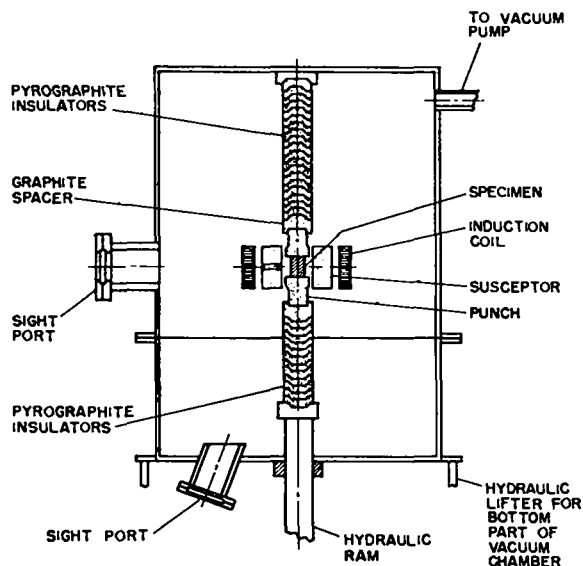


Fig. 5. Deformation testing equipment.

The specimens may be subjected to compressive loads up to 8000 psi at temperatures up to 1800°C. Temperature readings are taken by an optical pyrometer sighted through an opening in the susceptor onto the specimen. The specimen deformation is at present determined from measurements of the specimen dimensions before and after creep tests. These measurements are made with a micrometer calibrated to 0.0001 inch. Changes in the equipment design are being planned to enable continuous creep measurements to be made by optical extensometers.

Compressive creep tests have been started on (U<sub>0.8</sub>Pu<sub>0.2</sub>)C solid solution samples, but most of the preliminary testing program has been undertaken on UC and UC<sub>2</sub>.

#### Hot Hardness

(A. Gonzales, K. A. Johnson)

A new Mo element heating coil is being constructed for the apparatus.

#### V. REQUESTS FROM DRDT

##### Examination of EBR-II Driver Fuels

(K. A. Johnson, J. W. Schulte, G. R. Waterbury)

Six irradiated EBR-II Driver Fuel Rods were investigated extensively. Five unirradiated rods were received for check-out of equipment and methods. The examinations were mostly completed and reported previously.<sup>2</sup> The results of subsequent work are given below.

##### Fuel Pins

Isotopic Analyses: The isotopic compositions of the uranium in sections taken from two unirradiated and three irradiated fuel pins were measured mass spectrometrically. These determinations were made on aliquots of solutions prepared by dissolving 1-gram samples taken from the top, middle, and bottom of the fuel pins. The isotopic compositions of the unirradiated pins (Table I) were within the concentration ranges listed in Product Specifications for the EBR-II Driver Fuel Elements, FCF-1. As expected, burnup of the <sup>235</sup>U in the irradiated fuel pins reduced the concentration of this isotope which resulted in a corresponding increase in the relative concentrations of the other isotopes. Analyses of the two

remaining samples are in progress.

Table I

Sample	Uranium Isotope Concentration, %		
	235	234 + 236 + 238	234 + 236
0121H-05 (Unirrad.)			
Middle	52.20	47.80	< 1.0
Bottom	52.15	47.85	< 1.0
0121H-27 (Unirrad.)			
Middle	62.28	47.71	< 1.0
Bottom	52.14	47.85	< 1.0
4087-53 (Irrad.)			
Top	51.26	48.43	< 1.0
Middle	51.02	48.66	< 1.0
Bottom	51.15	48.43	< 1.0
4088-100 (Irrad.)			
Top	51.37	48.08	1.0
Middle	51.18	48.41	1.0
Bottom	51.25	48.44	1.0
SL42-17 (Irrad.)			
Middle	51.26	48.62	< 1.0
Bottom	51.43	48.30	< 1.0
Specified Concentrations <sup>a</sup>	52.18 ± 0.050	47.82 ± 0.050	< 1.0

<sup>a</sup>Product specifications for unirradiated EBR-II Driver Fuel Elements, FCF-1

#### Electron Microprobe Examinations

A top and a bottom section of fuel pin 0121-H-05 were examined to identify inclusions and to determine distributions of the fission elements. Niobium was not detected in either sample showing that Nb was not segregated to the extent that concentrations higher than the 0.05% detection limit existed in isolated areas. The other fission elements (Mo, Ru, Rh, Pd, and Zr) were found throughout the U matrix of each sample. The fission elements also were found in the two types of inclusions. The more common type contained only Zr and U. The interiors of these inclusions contained more Zr and less U than the surfaces. The less common type of inclusion generally occurred in grain boundaries and contained Ru, Pd, Rh, Mo, Si, and U.

#### Examination of Peach Bottom Fuel Element C-05-05 and Sleeve

Chemical Analysis of Irradiated Fuel Compacts and Other Components of the Peach Bottom Reactor  
(J. W. Dahlby, W. J. Baughman, T. K. Marshall, G. R. Waterbury, O. R. Simi, and R. T. Phelps)

Duplicate samples from eight irradiated fuel compacts, containing (Th, U) C particles coated with pyrolytic C in a graphite matrix, were analyzed spectrophotometrically for U and Th and gravimetrically for weight loss

upon drying at 120°C. The samples were ground in a mixer-mill, and then dissolved by refluxing with HNO<sub>3</sub>-HClO<sub>4</sub> and finally with HClO<sub>4</sub>-K<sub>2</sub>Cr<sub>2</sub>O<sub>7</sub>. Small aliquots of the solutions were removed from the hot cell for the spectrophotometric measurements. In addition, the Th and U were determined in HNO<sub>3</sub>-HClO<sub>4</sub> leach solutions of fractured particles in two unground samples, and in the HClO<sub>4</sub>-K<sub>2</sub>Cr<sub>2</sub>O<sub>7</sub> solutions of the residues left from leaching. The spectrophotometric methods also were applied to measurement of Th and U in two samples of unirradiated pyrolytic carbon coated (Th,U)C particles. No difficulties were experienced in these operations. The relative standard deviation of a single measurement of either metal was about 5%.

Six samples of components were analyzed spectro-chemically for impurities. These samples consisted of an irradiated fuel compact and a "shadow" from an irradiated graphite sleeve which were analyzed qualitatively, and samples taken from the surface and interior of unirradiated and irradiated graphite sleeve which were analyzed semi-quantitatively. The methods performed satisfactorily

Metallographic Examination  
(K. A. Johnson, D. S. Shaffer)

The eight irradiated compacts (or portions thereof) were macrophotographed to record their condition upon arrival at LASL. Random samples from the irradiated compacts were taken and polished; etched cross-sections were examined for bead density and the proportions of undamaged, damaged, and broken beads. Irradiated and unirradiated samples of sleeve graphite were examined metallographically. Metallographic examination was also made on unbroken beads leached from several compacts.

Miscellaneous Tests  
(G. H. Mottaz, F. H. Newbury, A. E. Tafuya,  
R. F. Velkinburg)

Porosity, density and dimensional measurements were made on unirradiated sleeve material and compared to those values obtained on the sleeve from C-05-05.

Measurements were made of the force required to fracture ring sections from unirradiated and irradiated sleeve material subjected to tension and compression.

A pneumatic rupture test was conducted on an unirradiated section of sleeve material in an attempt to demonstrate whether vertical and circumferential cracks could be produced by internal expansion.

Shielding Integrity Test of the Paducah Cask  
(F. Fitzgibbon, J. R. Trujillo)

The hot cell facility was used for testing the attenuation of the radiation from 90,000 Ci of <sup>60</sup>Co which was placed in the cavity of the Demonstration Cask from Paducah. The cask had been previously subjected to the hypothetical accident conditions listed in Chapter 0529 of the AEC manual. The results, on the basis of radiation measurements, indicated the cask had no appreciable voids.

The attenuation provided by the walls of the hot cell facility were adequate for handling the 90,000 Ci of <sup>60</sup>Co. A previous integrity test of the walls indicated that ~ 50,000 Ci of fission products could be safely handled.

Examination of Irradiated Pins and Capsules from Battelle Northwest Laboratory  
(K. A. Johnson, J. W. Schulte, G. R. Waterbury,  
J. F. Torbert (GMX-1), D. Holm (K-1))

Three pins and two capsules of the PNL-1 series as well as two capsules of the BNW-1 type were received on September 16.

To date the following work was completed on the PNL-1 units: radiation and temperature measurements; external viewing and photography; gamma scanning and x-ray radiography on three pins. Attempts at profilometry showed up minor deficiencies in the diametral measurements and major problems with the bow measurements. Action was started immediately to correct the difficulties.

Examination of Irradiated Capsules from United Nuclear  
(K. A. Johnson, J. W. Schulte, G. R. Waterbury,  
J. F. Torbert (GMX-1), D. Holm (K-1))

Three capsules containing mixed carbide fuel irradiated to 50,000 MWD/T were received on September 16. Examination of these capsules will be started at the completion of certain phases of work on the material from BNWL.

VI. LMFBR/FFTF ANALYTICAL CHEMISTRY  
QUALITY CONTROL PROGRAM

The laboratory work required in Phase I of this program as described in instructions to participating laboratories dated May 9, 1968 has been completed. The results are being evaluated and will appear as a special report about November 1, 1968. It was intended that this report would be available by October 1, but discussions with PNL have resulted in re-organization of certain material in order to make the report more compatible with their scheduled pre-qualification plans.

In order to further this program LASL has continued to develop methods to be applied to certain measurements indicated in the PNL specifications for FFTF fuel. In addition, certain problem areas have been encountered in applying existing methods to sintered (U,Pu)O<sub>2</sub> pellets. These are described below.

Determination of C on (U,Pu)O<sub>2</sub> Fuel Material  
(M. E. Smith, C. S. MacDougall,  
W. B. Hutchinson, G. R. Waterbury)

Preliminary work indicated that sintered solid solution (U,Pu)O<sub>2</sub> pellets must be ground before the carbon present will be oxidized by a stream of oxygen. Under these conditions, a combustion-capillary trap separation technique can be applied to the analysis of this material for carbon content. The sintered pellets analyzed, (PNL Lot ME-21) seemed to have a carbon content between 50 and 60 ppm. Optimum conditions of grinding remain to be established.

Gas Evolution from (U,Pu)O<sub>2</sub> Fuel  
(G. C. Swanson, D. E. Vance, M. E. Smith,  
G. R. Waterbury)

One of the specifications of FFTF Fuel presently under consideration is the total gas evolution from (U,Pu)O<sub>2</sub> fuel. This includes water vapor.

An apparatus was constructed for measuring separately the quantities of H<sub>2</sub>O evolved at 200°C and of other gases evolved as the sample was heated inductively to 2000°C in a W crucible. The H<sub>2</sub>O evolved at 200°C was swept by He carrier gas through a heated stainless steel conduit to a CEC moisture monitor, and the total quantity of H<sub>2</sub>O was obtained by digital integration of the monitor signal. The gases evolved above 200°C were

collected with a Toeppler pump, and the volume and pressure measured. Evolution of gases was monitored by a thermocouple vacuum gauge. The equipment was designed so that samples of the collected gas could be taken for mass spectrometric analysis.

Initial calibration of the apparatus was completed by measuring known quantities of H<sub>2</sub>O injected into the He stream. A statistical analysis of forty-four measurements showed that the precision (1 σ) was 6 relative percent in determining 4 μg of H<sub>2</sub>O and increased to 18% for 1 μg of H<sub>2</sub>O. Prior to the analysis of (U,Pu)O<sub>2</sub> fuels, further testing of the equipment and measurement of blanks at selected temperatures will be done.

Matrix Effects in Determining Spectrographic Impurities

(O. R. Simi, R. G. Phelps, W. M. Myers,  
C. J. Martell)

It has been known for years that the composition of the matrix of a sample affects the sensitivities of elements as determined by emission spectroscopy. The underlying reasons for this are not well understood. Neither can it be predicted what the change will be if the matrix composition is changed. In addition, it is true that the density of the matrix likewise causes changes in these sensitivities.

Studies have continued on this problem and it was observed that a U<sub>3</sub>O<sub>8</sub>-PuO<sub>2</sub> matrix decreased the sensitivities for Al, Si, and Fe by as much as a factor of 3 (for Si). Other elements also may be involved. This is important because it establishes the fact that standards must be prepared that have a matrix similar to that of the sample. Work is continuing including preparation of standards with different matrices.

Determination of O/M Ratio in (U,Pu)O<sub>2</sub>  
(C. S. MacDougall)

The method reported last month was applied to additional samples of sintered (U,Pu)O<sub>2</sub> pellets. Additional data indicates that the standard deviation of a single measurement is ± 0.005 out of a ratio of approximately 2.000, or a relative standard deviation of 0.25%.

Analytical Standards  
(R. L. Nance, D. Kelley)

High purity UO<sub>2</sub> and PuO<sub>2</sub> powders have been

synthesized in preparation for producing pure

$U_{0.75}Pu_{0.25}O_2$  pellets for analytical chemistry standards.

VII. REFERENCES

1. Calvin E. Moeller and Donnell R. Wilson, "Thermal Conductivities of Several Metals and Non-Metals from 200° to 1300° C by the Radial Heat-Flow Technique," The Third Thermal Conductivity Conference, Vol. I, p. 224, Gatlinburg, Tennessee, Oct. 16-18, 1963.
2. LA-3993-MS, Quarterly Status Report on the Advanced Plutonium Fuels Program, April to June 30, 1968, and Second Annual Report, FY 1968.

PROJECT 462

SODIUM TECHNOLOGY

Person in Charge: D. B. Hall  
Principal Investigators: G. H. Best  
R. H. Perkins  
E. O. Swickard

---

I. INTRODUCTION

For the successful operation of high temperature sodium systems contemplated for use in fast, central station reactor concepts, impurities in the sodium must be monitored and controlled. Nonradioactive impurities such as oxygen must be maintained at low concentration levels to limit corrosion processes. Radioactive impurities introduced into sodium from failed fuel elements should be removed to facilitate "contact maintenance" and to minimize safety and detection problems. To control the levels of these impurities, a knowledge of their behavior and interactions in sodium must be developed. Acquisition of this information has been subdivided in the LMFBR Program Plan into a number of task areas. The sodium technology program at LASL has projects which contributed to six of these areas. The broad tasks and current LASL projects within those areas are summarized below:

Task Area 1: Materials Compatibility

- A. Correlation of sodium and helium leaks.
- B. Study of carbon transport in thermal convection loops.

Task Area 2: Sodium Purification

- A. Study of sodium oxide kinetics in cold traps.
- B. Study of soluble getters for removal of impurities from sodium.
- C. Study of gas diffusion through metals into sodium.

Task Area 3: Fission Products in Sodium Systems

- A. Study of fission product distribution in loop experiments.
- B. Study of fission product gettering in capsule experiments.
- C. Study of fission product introduction into sodium systems.

Task Area 4: On-Line Monitoring Methods

- A. Plugging meter studies.

- B. D. C. resistivity meter studies.

- C. Evaluation of UNC EMF cells.

Task Area 5: Sampling and Analysis

- A. Vacuum distillation studies.
- B. Study of gamma ray activation analysis for C and O.
- C. Absorption spectrometry development for metal impurity analysis.
- D. Total carbon analysis development.
- E. Development of remotely operated distillation samplers for EBR-II.

Task Area 7: Cover Gas and Maintenance Atmospheres

- A. Development of a high temperature quadrupole mass spectrometer for cover gas analysis.

Details of the work in these programs are presented below.

II. MATERIALS COMPATIBILITY

- A. Correlation of Sodium and Helium Leaks  
(D. C. Kirkpatrick, J. P. Brainard)

I. General

The correlation of sodium leak development with measured helium leak rates observed during acceptance testing provides information on the degree of component integrity which must be attained for safe, long-term sodium plant operation. No firm criteria now exist that establish acceptable levels of leak-tightness for various situations.

This study uses fabricated stainless steel leaks and leaks that occur naturally in stainless steel bar stock. Selected samples having a range of helium leak rates are incorporated into small sodium systems (cells) which are held at a predetermined temperature until sodium leakage occurs. From these observations it may be possible to establish, for mass spectrometer acceptance tests on sodium system components, the maximum tolerable helium rate which

is consistent with adequate long-term containment of sodium by that component.

An interesting side effect from this work has been observation of the elusiveness of what are considered to be large leaks ( $10^{-5}$  to  $10^{-6}$  atm-cc/sec). Normal contaminants such as grease, water and some solvents can completely mask leaks of this size and invalidate a leak test, unless proper pre-treatment of the component is performed; and in some cases this can involve firing of the component in a hydrogen atmosphere. If meaningful helium leak tests are to be performed on LMFBR components, procedures must be developed for treating and handling of the part prior to leak test.

## 2. Current Results

Four sodium cells containing known helium leaks have been operating at 400°C for 3500 h without sodium leakage into air. Pretest data on the test specimens are given in Table 462-I.

Table 462-I

Pretest Characteristics of Na Leaks		
Cell No.	Type of Leak	Initial He Leak Rate (room temp.)
1	Fabricated (compressed tube)	$1.1 \times 10^{-4}$ atm-cm <sup>3</sup> /sec
2	Fabricated (compressed tube)	none (control specimen)
3	Porosity (in bar stock)	$1.7 \times 10^{-4}$ atm-cm <sup>3</sup> /sec
4	Porosity (in bar stock)	none (control specimen)

The absence of leakage at 400°C indicates that the test program must go to higher temperatures and larger leaks to generate time-to-failure data in a reasonable test period. In a given leak, metallic oxides are probably creating a plug and stopping sodium flow, and the time to sodium leakage then depends on the chemical reaction rates at the plug. By going to higher temperature, the reaction rates should greatly increase and the time to sodium leakage by correspondingly reduced.

Four more cells are nearly ready to begin operation at 650°C. Data on the test specimens are given in Table 462-II.

Table 462-II

Pretest Characteristics of Na Leaks		
Cell No.	Type of Leak	Initial He Leak Rate (room temp.)
5	Porosity (in bar stock)	About $1 \times 10^{-5}$ atm cc/sec
6	Solid Bar Stock sample	none (control specimen)
7	Porosity (in bar stock)	About $1 \times 10^{-1}$ atm cc/sec
8	Porosity (in bar stock)	none (steel oxide plugged)

From these studies at 650°C, perhaps very small leaks can be shown not to be a problem. To obtain information about small leaks, large leaks will be tested at high temperatures to obtain failure data in reasonable lengths of time. Then estimates of failure times for the small leaks may possibly be obtained by extrapolation.

The zirconium getters (in the 650°C sodium cells) have been carefully weighed in order to measure the possible oxygen influx from the leaks. The oxygen influx may be correlated to the initial helium leak.

## B. Study of Carbon Transport in Thermal Convection Loops (J. C. Biery, C. R. Cushing)

### 1. General

Studies have indicated that the use of carbon beds may be useful in the gettering of <sup>137</sup>Cs in sodium systems. Carbon, however, is slightly soluble in sodium and can carburize austenitic stainless steels and refractory metals. Therefore, the purpose of this study is to determine the conditions under which carbon mass transfer rates are sufficiently low to allow the use of carbon beds in a sodium system.

The carbon transfer rates from carbon rods will be studied in thermal convection loops. The Type 304 or 316 stainless steel loop itself will serve as the carbon sink when these alloys are studied and vanadium alloy sleeves will serve as getters when vanadium is studied.

### 2. Current Results

The thermal convection loop is ready for preliminary testing and loading with sodium. Sodium will be

circulated through the loop for a period up to a week at the desired operating temperature to allow the stainless steel surface reaction with the oxygen in the sodium to approach an equilibrium.

At present, the evacuated thermal convection loop is being held at 300°C before being filled with sodium. The first filling must await a modification of the sodium supply loop.

### III. STUDY OF PURIFICATION METHODS FOR NONRADIOACTIVE IMPURITIES

#### A. Study of Na<sub>2</sub>O Kinetics in Cold Traps

(C. C. McPheeters, J. C. Biery)

##### 1. General

Nuclear reactors which will incorporate liquid sodium as the heat transfer fluid will require efficiently-designed cold traps because of the large sodium volumes involved. Minimum cold trap sizes adequate to achieve the required cleanup rates and impurity holding capacities are of interest because of the cost of large component construction. In order to design minimum-size cold traps, the mechanisms of impurity precipitation in cold traps and to measure the mass transfer coefficients involved. With adequate knowledge of these rates and mechanisms, cold traps can be designed to accommodate the required amount of impurity deposits and to meet the required system cleanup rates.

Mass transfer coefficients are being determined by observing cleanup rates in a sodium system with cold traps of simple geometries. These cold traps are operated at various temperatures and flow rates to determine the effect of these variables on the mass transfer coefficients. The test system is an isothermal, forced-convection loop containing vacuum-distillation apparatus, an oscillating plugging indicator, and two United Nuclear Corporation oxygen meters for determination of oxygen concentration in the sodium.

The first cold trap design being tested consists of three concentric tubes.<sup>1</sup> The annulus between the outer two carries NaK which removes heat from the cold trap. Sodium flows down the inner annulus where it is cooled and then up the central tube where it is reheated. A notable feature of this design is the absence of any form of extended surface or "packing." The packing was omitted in order to provide a simple surface area on which the

oxide could precipitate. Packed cold traps will also be tested during this study.

Cold trap test runs consist of an equilibration period at an initial temperature followed by a rapid change to a new temperature and flow rate. Oxygen concentration data are taken at small time intervals with all the available analytical techniques until the system concentration reaches the new equilibrium level. The resulting oxygen concentration data as a function of time are then used to determine the mass transfer coefficients.

#### 2. Current Results

##### a. Tests on Packless Cold Trap Number 1

##### (1) Velocity Effect

Experiments with the first packless cold trap design have been completed. Two series of eight cold trapping runs were conducted during this reporting period. The first series consisted of four precipitation runs at a cold trap temperature of 170°C and four dissolution runs at 210°C. Flow rates tested were 0.25, 0.50, 1.0, and 1.5 gpm for both precipitation and dissolution. The effect of sodium velocity (or Reynold's number) on the overall mass transfer coefficient is shown in Figure 462-I and Table 462-III. The relationship is approximately linear on a log-log scale between Reynold's numbers of 200 and 1200, and the mass transfer coefficient increases proportional to the first power of the Reynold's number. A greater increase occurs between Reynold's numbers of 1200 to 1700. A first power relationship between Reynold's number and the mass transfer coefficient would not be expected in the laminar flow region. The first power relationship observed here is thought to be due to cross-flow in the cold trap caused by poor entrance conditions. Sodium enters the cold trap on one side of a 3.75 in. o.d. x 2 in. i.d. annulus through a one-inch pipe. The resultant flow pattern is probably somewhat mixed, and it allows the impurities in solution to have better access to the cool cold trap walls. At the onset of true turbulent flow, the mass transfer coefficient would be expected to increase proportionally to approximately the 0.8 power of the Reynold's Number.

The dissolution mass transfer coefficients were in all cases essentially equal to those for

precipitation, and the same velocity effect was seen in both cases. This indicates that both processes are diffusion rate limited, and that greatly increased Reynold's numbers can lead to greater mass transfer rates.

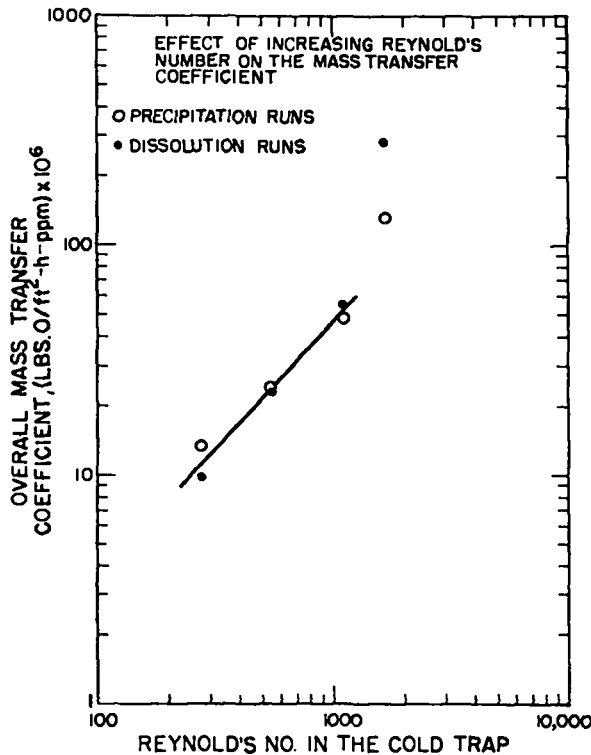


Fig. 462-1. The effect of Reynold's number on the overall mass transfer coefficient.

Table 462-III  
Summary of Cold Trap Runs

Run No.	Minimum Cold Trap Temp. (°C)	Type of Run	Sodium Flow Rate (gpm)	Calculated Mass Transfer Coefficient (lb oxygen/ft <sup>2</sup> -h-ppm) x 10 <sup>6</sup>
1-18	182	Precipitation	1.5	131.0
1-19	208	Dissolution	1.5	281.0
1-20	168	Precipitation	1.0	48.0
1-21	212	Dissolution	1.0	55.0
1-22	168	Precipitation	0.5	24.0
1-23	210	Dissolution	0.5	23.0
1-24	170	Precipitation	0.25	13.5
1-25	211	Dissolution	0.25	9.9
1-26	149	Precipitation	0.5	13.5
1-27	203	Dissolution	0.5	22.5
1-28	130	Precipitation	0.5	23.8
1-29	180	Dissolution	0.5	27.7
1-30	122	Precipitation	0.5	44.6
1-31	122	Precipitation	0.5	39.6
1-34	121	Precipitation	0.5	47.4
1-35	160	Dissolution	0.5	35.0

A typical precipitation run is shown in Figure 462-2. The initial oxygen concentration was 0.1 ppm and the final concentration was 3.6 ppm. The

sodium flow rate was 1.0 gpm. Dimensionless or fractional concentration,  $(C-C_e)/(C_0-C_e)$ , is plotted on a log scale vs time in hours. C is the bulk system oxygen concentration,  $C_0$  is the initial oxygen concentration, and  $C_e$  is the equilibrium or final oxygen concentration. After approximately

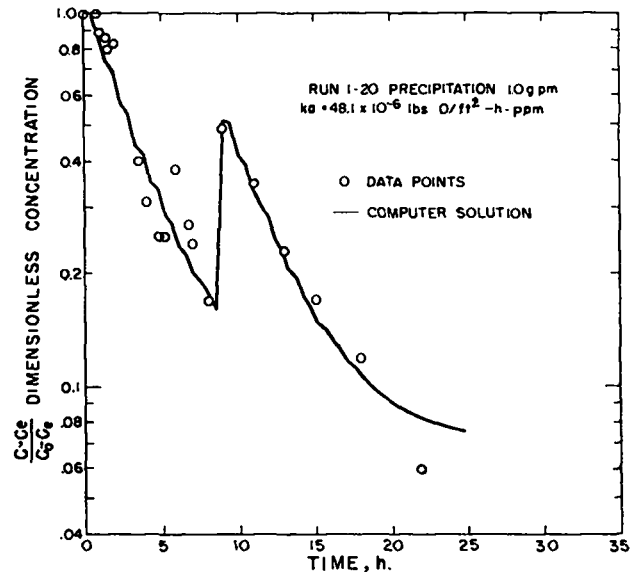


Fig. 462-2. Precipitation run number 1-20 showing an oxygen concentration spike.

eight hours of the run, an oxygen concentration increase occurred. It is thought that the concentration spikes which occurred during approximately half of the cold trapping runs were caused by oxide break-away in the cold trap. All of the spikes were of about the same magnitude. Since the cold trap under test was a packless design, oxide break-away would be expected in some cases. The function of packing in this case would be to support the oxide and to provide a larger surface area for deposition and greater access of the solution to nucleation and growth sites.

The second series of eight runs consisted of four dissolution runs conducted at a common flow rate of 0.5 gpm, and the results are shown in Table 462-III.

Minimum cold trap temperatures tested for the precipitation runs were 170, 150, 130, and 120°C, and the minimum cold trap temperatures for the dissolution runs were 210, 200, 180, and 160°C. Mass transfer coefficients in the range of  $23 \times 10^{-6}$  to  $47 \times 10^{-6}$  lb O/ft<sup>2</sup>-h-ppm were obtained. (To convert to units of gO/cm<sup>2</sup>-h-ppm, multiply by 0.486.)

### (2) Dissolution vs Precipitation Rate Constants

Each precipitation run was followed by a dissolution run. Since the crystallographic nature of the precipitate and the corresponding mass transfer area for the two coupled runs are similar and since both processes are diffusion rate limited, the mass transfer coefficients should be equal. The data support this hypothesis as evidenced in Table 462-III and Figure 462-1. In all cases, the constants from coupled runs were nearly equal or highly correlated. No trend was established as to which constant was bigger if a difference occurred. This dissolution constant was larger in four cases and smaller in four other runs. This result also implies that there is little if any temperature or absolute concentration effect since the cold trap temperatures and equilibrium concentrations for the coupled runs were significantly different. Good agreement between mass transfer coefficients calculated from precipitation and dissolution runs also supports the initial assumption of nucleation and growth of crystals only on solid surfaces. This agreement implies that the same mechanism is operative for both processes. It is highly probable that the mechanism in effect during the dissolution process is the dissolving of solid crystals and the diffusion of the material into the moving fluid stream. Therefore, with the agreement of mass transfer coefficients the reverse process would be expected during precipitation runs, i.e., diffusion through a stagnant film and deposition of the material on crystals growing on the solid surface. If homogeneous nucleation occurred significantly, a higher precipitation mass transfer coefficient would be found in the event that the particles settled to the bottom of the trap and a lower mass transfer coefficient if the particles were carried back into the system. It is therefore concluded that for the conditions studied, homogeneous nucleation is insignificant in comparison to heterogeneous nucleation on solid surfaces.

### (3) Initial Concentration Difference Effect

In Figure 462-3 are plotted the mass transfer coefficients,  $k_a$ , from the 0.5 gpm runs vs the concentration driving force at the beginning of the precipitation run. The plot clearly shows an effect of increasing rate constant with decreasing initial

$\Delta C$ . The reason for the effect is not clear. However, the influence of the initial driving force may be its effect on the number of crystals initially nucleated on the cold trap surface. The larger the  $\Delta C$ , the larger is the number of crystals nucleated.

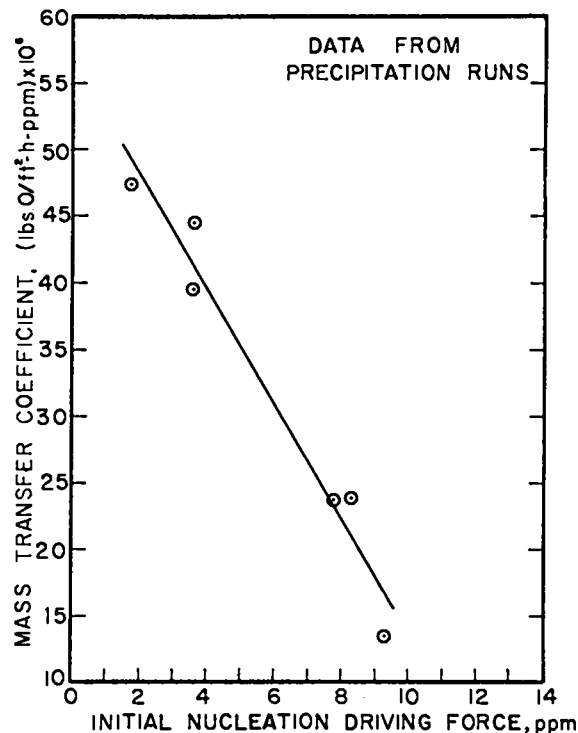


Fig. 462-3. The effect of the initial concentration driving force on the mass transfer coefficient.

However, since the area for lateral growth of crystals is limited, a large number of nuclei may grow together to form a smooth bed with a small available surface area. This condition would result in a lower apparent mass transfer coefficient.

Another reason for the trend shown in Figure 462-3 may be the influence of other impurities in the system. The large  $\Delta C$  runs were also higher cold trap temperature runs and involved a larger quantity of hydrogen in the sodium which was detected by increased hydrogen concentration in the cover gas. Hydrogen may have affected both the character of the precipitate in the cold trap and the saturation temperature indicated by the plugging indicator. However, the agreement between precipitation and dissolution runs and the comparison of the behavior of the plugging indicator between the coupled runs indicate that this effect may be secondary in nature.

b. Cover Gas Analysis

Routine cover gas analyses were performed on the cold trap test loop with a gas chromatograph. The gas was sampled by flowing a continuous stream through the gas chromatograph sampling valve. Impurity gasses in most abundance were hydrogen and nitrogen. Nitrogen remained constant at approximately 200 ppm, and hydrogen concentrations varied with the cold trap temperature. At 170°C, the hydrogen concentration was near the detection limit at 10 to 20 ppm, and 210°C, the hydrogen concentration was 190 ppm. This concentration was equivalent to a hydrogen partial pressure of 0.14 mm Hg which agreed well with the expected hydrogen pressure over sodium saturated at 210°C according to the data of Addison, et al.<sup>2</sup>

The vacuum distillation technique and the oscillating plugging indicator have both indicated the presence of an impurity other than oxygen. When the sodium was sampled for vacuum distillation during operation at high (>200°C) cold trap temperatures, abnormally high results were obtained: however, when the sample cup was heated to 500°C for 30 minutes after the normal distillation was complete, the analytical results were 8 to 10 ppm lower and in good agreement with the oxygen concentrations expected assuming saturation at the cold trap temperature. This result indicates that some compound which did not decompose during normal distillation (at 400°C) decomposed on heating to 500°C. The oscillating plugging indicator results indicated the presence of a second impurity by undergoing a significant shift in the indicated saturation temperature. The shift was consistent during a series of runs where a new plug was formed, and the instrument was allowed to oscillate normally. The indicated saturation temperature shifted from 220°C to 240°C repeatedly. In each case about one hour of normal oscillation preceded the temperature shift. Based on the cover gas analyses, it is thought that the second impurity was some form of hydrogen in solution.

c. Removable-Core Cold Trap Number 2

The present packless cold trap is being used to remove most of the impurities from the test loop in preparation for shutdown. During the down period, a second type of cold trap will be installed. The

second design will include a NaK cooled insert which can be removed for examination and species identification. Cold trapping runs will be made while the system oxygen concentration is measured. Subsequent analysis of the deposit on the cold finger will allow a check on the calculated mass transfer coefficients, a check on the calculated mass distribution and identification of the species precipitated.

This cold trap design also includes an inert gas chamber which will be used to transfer the cold inert to a drybox where sampling and examination of the residue will be done. The second cold trap is currently in the assembly stage.

d. 2D Computer Simulation of Annular Packless Cold Trap No. 1

A series of computer runs are being made to determine the functional relationship between the mass transfer coefficient and velocity in the trap for the pure laminar flow case. The grid size for the numerical calculation must be refined considerably to give meaningful data for the high velocity runs (1 gpm and above). Division of the one such radial annulus into 20 units is sufficient for flow rates below 0.5 gpm.

B. Study of Soluble Getters for Removal of Impurities from Sodium  
(G. E. Meadows, L. A. Waldschmidt)

1. General

For large sodium-cooled reactor systems, it may be desirable to use soluble getters for control of oxygen and other dissolved impurities in lieu of the more conventional hot and cold trapping techniques. The soluble getters of interest occur in the sodium coolant either naturally, as an impurity (calcium), or are produced during reactor operation (as with magnesium). The techniques for the controlled additions of these getters, maintenance of fixed getter levels, and the selective removal of depleted getter metals and other impurities from dynamic sodium systems must be developed if their usefulness is to be evaluated; and the significant chemical reactions occurring in a sodium system containing these soluble getters must be understood and controlled. This mode of purity control has the potential for effectively controlling not only oxygen, but also carbon, hydrogen, nitrogen, and possibly metallic impurities.

## 2. Current Results

### a. Analytical Loop No. 1

Analytical Loop No. 1 is being readied for the first Ca soluble getter run. A leak in the loop was repaired and additional sodium was charged to the system. The Ca level has been determined in preparation for Ca additions. The first run will give some indication of Ca dissolution rates, changes in oxygen levels with Ca addition, and deposition characteristics of CaO.

### b. Analytical Loop No. 2

Assembly of the mechanical portion of Analytical Loop No. 2 which will be used for soluble gettering studies and for development and evaluation of prototype analytical instrumentation is approximately 85% complete. The facility will contain about 40 gal of sodium. A main driver loop will pump through a central well mixed core of the bulk sodium tank. There are three parasitic loops; the EMF cell loop, the dc resistivity meter loop, EMF cell loop and the main driver loop are complete.

### c. Study of Gas Diffusion Through Metals into Sodium (J. P. Brainard, D. C. Kirkpatrick)

#### 1. General

Very little quantitative information is available on the diffusion of gases in reactor system containment materials, although the phenomenon has been observed in several high-temperature, liquid-metal-cooled systems. Diffusion of nitrogen through stainless steel in such systems may be misinterpreted as evidence of an air leak in the plumbing. If quantitative information on diffusion were available, the expected rate of nitrogen influx could be estimated, and the existence of small hard-to-find leaks might be substantiated or dismissed by comparing the expected and observed rates of nitrogen accumulation in the system.

A program for determining the diffusion rate of nitrogen in stainless steels has therefore been undertaken. In later phases of the program the diffusion of O and H in stainless steels will be studied.

#### 2. Current Results

A system has been designed and is being fabricated to measure a wide range of gas permeation rates at temperatures ranging from room temperature

to 1000°C. The measurements will be accomplished by observing the flow of gas through a metal membrane (the diffusion cell) into a mass spectrometer. The initial system will be nitrogen and Type 304 stainless steel. The following equipment components have been completed: The oven with an inert gas buffer region to prevent atmospheric gases from diffusing into the mass spectrometer envelope; the calibration apparatus for the mass spectrometer; and the inlet manifold for introducing nitrogen to the diffusion cell. Remaining to be completed are the following items: The table top and supports for the above assemblies and the diffusion cell.

Since inert gases do not diffuse through metal, at significant rates, a small addition of helium to the nitrogen will allow continuous monitoring of any leakage through the diffusion cell. A leak will be indicated when helium is found with the mass spectrometer on the low pressure side of the membrane.

## IV. FISSION PRODUCTS IN SODIUM SYSTEMS

### A. Study of Fission Product Distribution in Loop Experiments (J. C. Clifford, J. Fellers)

#### 1. General

The behavior of radioactivity released to sodium from failed or vented fuel elements may limit access to portions of the primary coolant system and may effect the consequences of a loss-of-coolant incident. Depending on the fission-product release fraction anticipated in either circumstance, it may be desirable to scavenge these species (as well as uranium and plutonium) from the coolant.

The immediate goals of this investigation are: (1) to identify sodium-soluble fission-product species and (2) to examine the effects of primary-coolant-system construction materials, design features, and operating conditions on these species.

#### 2. Current Results

Studies of the distribution of long-lived fission products have been continued with major emphasis on  $^{137}\text{Cs}$ .

#### a. $^{137}\text{Cs}$ Adsorption Loop

Two experiments have been run in the  $^{137}\text{Cs}$  adsorption loop in which the adsorption characteristics of C-1010 steel, Type 316 stainless steel, zirconium, and nickel were tested. External gamma scans were

made, and samples of the foils have been submitted for chemical analysis. The tests were run at 197 to 205°C in flowing sodium containing less than 1 ppm oxygen at a Reynold's number of 2600.

b. Trace Irradiated Fuel Loop

The trace irradiated fuel loop has been temporarily used for a study of (U,Pu)<sub>2</sub>O<sub>3</sub> powder distribution in flowing sodium. The results of the study will be reported in a later quarterly under the fuels section. The study of multi-component fission product distribution from trace irradiated fuel will be continued in the near future.

B. Study of Fission Product Gettering in Capsule Experiments  
(H. A. O'Brien, C. R. Cushing)

1. General

Capsule experiments have been designed to determine the distribution of gamma-active isotopes in the sodium/stainless steel/helium/adsorber system as a function of time and temperature. Gamma-ray scanning permits a study of transport rates, adsorption and desorption phenomena, and the equilibrium distribution between phases to be made. The isotope <sup>137</sup>Cs is the first radioisotope to be studied in these experiments because it is a major fission product released from irradiated nuclear fuels, and its long (27.7-yr.) half-life simplifies measurements. Other candidates for study, using these experimental techniques, are <sup>131</sup>I and <sup>140</sup>Ba-<sup>140</sup>La.

In the present series of experiments, the <sup>137</sup>Cs getting capacities of carbon and various oxides are to be determined. In each capsule tested a basket containing one of the materials to be tested, will be introduced into the sodium after the cesium and sodium have come into equilibrium. The capsule will be scanned with a collimated NaI(Tl) crystal in order to determine the amount and rate of cesium pickup by the getter.

2. Current Results

a. Run 1 - Activated Charcoal

The first capsule, loaded with about 3 mCi of <sup>137</sup>CsCl in a nickel cup, was equilibrated with sodium for 1 week at 500°C. The basket, containing 2.16 g of Columbia activated carbon, was lowered into the sodium and remained until equilibrium had been attained, i.e., about 46 days.

Scanning of the capsule showed an appreciable pickup of the cesium by the carbon, but erratic behavior of the counting equipment prevented as estimation of the amount or rate. The capsule was subsequently removed and sectioned. Radiation measurements of the various capsule components indicated that 95% of the <sup>137</sup>Cs activity left the nickel cup and went into the sodium. Of the 95% of the cesium in solution, about 99% was located in the carbon basket region.

Analytical analyses indicate that the <sup>137</sup>Cs concentration in the sodium was 0.33 μCi/g Na. Also, it appears that <sup>137</sup>Cs was adsorbed on the wall of the nickel capsule to the extent of 0.30 μCi/in.<sup>2</sup> at 500°C. These results are in apparent agreement with the radiation readings made at the time of sectioning. A chemical error in the analysis of the cesium content in the carbon prohibited the attainment of quantitative results.

b. Run 2 - Activated Carbon

Due to the erratic behavior of the counting equipment in Run 1, it was impossible to estimate the accuracy with which the scanning technique can measure the amount and rate of cesium pickup by the getting material. The counting difficulties were corrected, and it was decided to repeat the experiment with activated carbon. This time the experiment was initiated at 200°C, with the intent of a stepwise increment of the temperature up to 500°C.

The cesium and sodium in the capsule were equilibrated for 1 week at 200°C. Horizontal scanning of the nickel cup indicated that equilibrium had been attained, and the carbon basket was lowered into the sodium. Vertical scanning of the capsule for an additional week failed to detect any appreciable change in <sup>137</sup>Cs activity distribution, nor could the location of the carbon basket in the sodium be found. At that time the basket was removed from the sodium.

Horizontal scans of the nickel cup at the beginning and end of the 200°C experiment indicated that only 14.6% of the cesium activity left the cup and went into solution. Of this amount in solution, only 12.4% was adsorbed by the carbon, as indicated by a horizontal scan of the basket after removal from the sodium. From these results, it appears that cesium is relatively immobile at 200°C, and

the amount of cesium adsorption by activated carbon is small.

With the carbon basket removed from the sodium, the temperature was raised to 300°C and the cesium and sodium were equilibrated for 1 week. The carbon basket was then lowered into the sodium, and vertical scans were made until equilibrium had been obtained. At the end of 1 week, it was apparent that the cesium activity on the nickel cup was essentially constant. Horizontal scans of the cup indicated that an additional 15% of the cesium activity went into solution in comparison with the results at 200°C. The carbon appeared to pick up an additional 5% of the activity in solution.

The temperature was increased to 500°C and the cesium and sodium were equilibrated at this temperature for 5 days while the basket was removed from the sodium. At that time the cesium activity level on the nickel cup appeared to be constant, and the carbon basket was lowered into the sodium. The basket has now been immersed in the sodium for 11 days. During this period, the activity level on the nickel cup has been continually diminishing with a corresponding increase of activity in the carbon region.

In comparison with the results observed at 200 and 300°C, the rate of cesium adsorption by carbon at 500°C appears to be considerably accelerated, but is probably modified by the rate of cesium desorption from the nickel cup. At the present time, 11% of the initial cesium activity remains on the nickel cup, and this is decreasing at the rate of about 2% per day. The major portion of the cesium activity that has left the cup appears to be located in the carbon basket. This is in agreement with the results from Run 1.

The major objective of this study is the measurement of the rate and amount of cesium adsorption by various gettering materials. However, the present experiment suggests that the rate of cesium desorption from the nickel cup is the rate-controlling factor. The elimination of this factor will be attempted in future experiments by evaporating the <sup>137</sup>CsCl solution on an aluminum foil instead of the nickel cup. There is evidence to believe that sodium will attack aluminum thereby releasing the cesium rapidly to the sodium.

## V. ON-LINE MONITORING METHODS

### A. Plugging Meter Studies (C. C. McPheeters, J. C. Biery)

#### 1. General

Plugging meters have been used on sodium systems for many years. They are relatively simple to design, install, and operate; however, the meaning of the data obtained from these instruments has not always been clear, and as a result, the value of the instrument has sometimes been questioned. Work previously reported<sup>3</sup> indicates that the plugging meter is a valuable instrument and that it can be used with confidence. The three areas of investigation indicated below are continuing to better understand the meter.

- a. Studies of the bare orifice meter.
- b. Observations of the operating characteristics of the oscillating plugging meter.
- c. Determination of mass transfer coefficients from plugging meter data.

#### 2. Current Results

##### a. Oscillating Plugging Indicator Development

An MSA-type plugging indicator which is installed on a 500 gallon sodium system was successfully operated in the partially plugged, oscillating mode. This plugging indicator consists of a regenerative heat exchanger, an air cooler, and a slotted stem valve. Approximately four feet of 1-in.-pipe separates the heat exchanger and the air cooler as well as the air cooler and the plugging valve. Consequently, the plugging valve is not necessarily at the coolest point in the system. Impurities may precipitate in the air cooler rather than in the valve. In spite of these difficulties, the plugging indicator system was operated successfully in a manually controlled oscillating mode. The plugging indicator circuit was cooled in the normal manner until a plugging temperature of 160°C was determined. The valve was allowed to further plug until a pre-determined set-point flow rate was reached. The blower was then turned off, and the temperature increased until the flow rate came up to the set-point. At this time, the blower was turned on, and in this manner the temperature and flow rate were made to oscillate. Saturation temperature readings were taken at the maximum and minimum flow rate points.

The saturation temperature as determined by this methods was  $178^{\circ}\text{C} \pm 2^{\circ}\text{C}$ .

Successful operation of this large, inefficient system is encouraging in that other plugging indicator systems can probably be operated similarly. The advantages of this mode of operation include the following:

- (1) A saturation temperature is determined which is independent of cooling rate, geometry of the system or other operational parameters.
- (2) A rapid succession of readings is obtained.
- (3) It is easy and simple to establish operation if sufficient cooling and heating are available and if the concentration is high enough to nucleate a plug.
- (4) No sophisticated electronic controls are necessary. Either manual operation or a simple on-off control can be used.

Some difficulties can be encountered with the oscillating mode of operation. The cooling and heating rates must be sufficient to cause the temperature to change more rapidly than the flow rate. Otherwise, an unstable oscillation may develop which will cause either complete plugging of the valve or a loss of the partial plug.

#### b. Multiple Species in System

Along with the operation of the cold trap loop, a number of runs on the plugging indicator were made in the last two months. The cold trap loop and its cold trap were run at higher than normal temperatures during this period, and some interesting phenomena were recorded with the use of the plugging indicator. Previously, operation of the meter in the oscillating mode indicated that two impurity species were in the system. This condition was shown when the meter indicated equilibrium temperatures near  $220^{\circ}\text{C}$  initially but after an hour of operation slowly shifted to equilibrium temperatures of  $240^{\circ}\text{C}$  which was very close to cold trap temperature. The frequency of oscillation and the rates of mass transfer for the upper temperature impurity were much slower than for the lower temperature impurity. The lower temperature curve could be repeated by dissolving off the plug and then reprecipitating the lowered temperature precipitate. This precipitate formed preferentially because the concentration of the higher temperature specie was not large enough to produce

nucleation of crystals in the period allowed. Thus, the more soluble specie precipitated first when the temperature was sufficiently reduced.

This same type of phenomenon was not observed as the cold trap temperature was increased. With the cold trap at  $280^{\circ}\text{C}$ , the double saturation temperature was not observed. The nucleation of the upper temperature specie occurred before the temperature could be lowered to the level where the low temperature specie could nucleate and precipitate. In this case the saturation temperature of the upper temperature specie was  $278^{\circ}\text{C}$ . At this cold trap temperature there was a sufficient quantity of the specie to saturate the sodium. However, there was an insufficient supply of the lower temperature specie to saturate at the high cold trap temperature, and its saturation temperature remained at  $220^{\circ}\text{C}$ .

A further increase of cold trap temperature was made to  $350^{\circ}\text{C}$  and the plugging indicator indicated that a third specie may be present. In this case a lower temperature specie precipitated first and the meter oscillated about a temperature in the  $290\text{-}300^{\circ}\text{C}$  range. After about 30 minutes, the temperature slowly changed and sought out a saturation temperature in the  $320\text{-}330^{\circ}\text{C}$  range. After a day this temperature increased to  $350^{\circ}\text{C}$ . The lower temperature specie had a kinetic behavior similar to that of the high temperature specie of the previous lower temperature pair. The kinetics of precipitation of the high temperature specie of the high temperature pair were very slow and very little oscillation of the flow curve resulted.

An explanation of the above phenomena might be obtained from Figure 462-4. The figure shows a three impurity system and their respective solubility and nucleation curves. (Note: Two of the impurities are assumed to be O and H. However, no proof is available at present that the impurities precipitating are  $\text{Na}_2\text{O}$  and  $\text{NaH}$ . This proof can only be obtained by chemical or x-ray analyses of the precipitate on the orifice.) Two of the impurities, oxygen and hydrogen, appear to have limited availability in the system and, therefore, have upper concentration limits of 15 and 24 ppm, respectively. By operating the system at various cold trap temperatures, the

plugging indicator can indicate one or various pairs of the impurities. The cases outlined above are explained as follows:

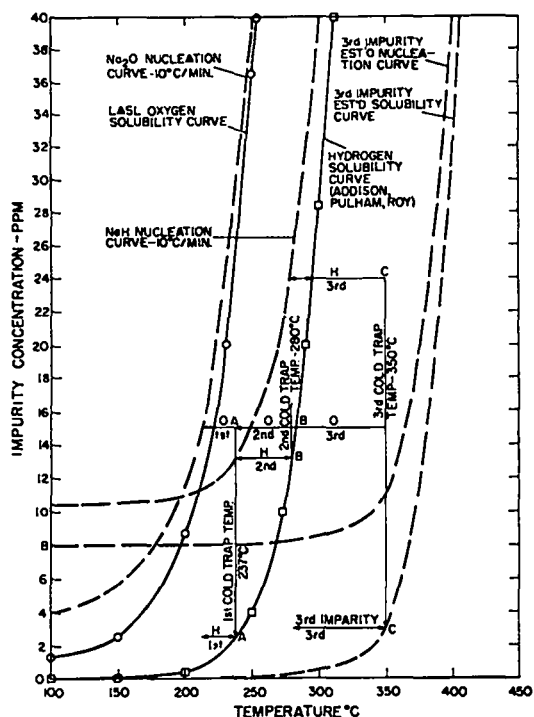


Fig. 462-4. Precipitation of impurities on an oscillating plugging meter orifice from a three impurity system.

(1) Cold Trap Temperature of 237-240°C

The concentration of oxygen is 15 ppm and hydrogen 2.5 ppm. As the temperature of the orifice drops, a temperature for nucleation of  $\text{Na}_2\text{O}$  at  $212^\circ\text{C}$  is first reached. The  $\text{Na}_2\text{O}$  nucleates, and the meter temperature then oscillates about the  $\text{Na}_2\text{O}$  saturation temperature of  $222^\circ\text{C}$ . There is sufficient hydrogen in the system to slowly nucleate  $\text{NaH}$  on the  $\text{Na}_2\text{O}$  precipitate. When the plug is converted, the temperature increases to  $237^\circ\text{C}$  and oscillates about this temperature. The third impurity is probably not involved because of its very low solubility at this cold trap temperature.

(2) Cold Trap Temperature of  $280^\circ\text{C}$

The oxygen and hydrogen concentrations are 15 and 13.2 ppm. As the orifice is cooled below

$280^\circ\text{C}$ , the hydrogen nucleation curve is reached first and  $\text{NaH}$  is precipitated. If cooling is stopped, no  $\text{Na}_2\text{O}$  can precipitate. However, if cooling is continued an increase in growth rate should be noted between  $222$  and  $212^\circ\text{C}$  as the  $\text{Na}_2\text{O}$  starts to precipitate. (This increase produces the second break phenomena.) In the first case, the oscillating meter will seek out the saturation temperature of the hydride and will oscillate about the  $280^\circ\text{C}$ . No change in equilibrium temperature will be noted since the third impurity is also saturated at  $280^\circ\text{C}$ . The plug will probably be  $\text{NaH}$  because the concentration of the third impurity is still quite small and nucleation of this impurity is improbable. In addition, by continuously dissolving off and then precipitating on the plug, the minor impurity is probably eliminated from the surface.

(3) Cold Trap Temperature of  $350^\circ\text{C}$

The third impurity solubility has increased to a significant level at  $350^\circ\text{C}$ . The solubility curve shown in Figure 462-4 is estimated to indicate the phenomena observed. The curve and the specie precipitating are unknown at present. The concentrations of the three impurities are estimated at 24, 15, and 3 ppm for H, O, and the third impurity. As the temperature is dropped below  $350^\circ\text{C}$ , the first nucleation curve intersected is that of hydrogen at  $280^\circ\text{C}$ . The oscillating meter then seeks out the hydrogen saturation temperature of  $295^\circ\text{C}$ . After about one half hour, the third impurity begins to precipitate on the plug, and the saturation temperature shifts up to the  $350^\circ\text{C}$  level.

c. Mass Transfer Coefficients

Data from the oxygen and hydrogen plugging runs were processed to generate mass transfer coefficients with use of Equation I.

$$K_i = \frac{\rho_{r_0} \left[ \left( 1 - P_{F_{i-1}} \right)^{\frac{1}{2}} - \left( 1 - P_{F_i} \right)^{\frac{1}{2}} \right]}{\int_{t_{i-1}}^{t_i} (C - C_e) dt} \quad (1)$$

$\rho$  = density of precipitate in grams of impurity per  $\text{cm}^3$

$r_0$  = radius of bare orifice

$P_F$  = fraction of orifice plugged

$C$  = concentration of impurity in sodium in ppm

$C_e$  = concentration of impurity in equilibrium with its precipitate at the orifice temperature.

K = mass transfer coefficient in grams of impurity/(cm<sup>2</sup> h ppm)

t = time in hours

To use the equation a solubility curve is necessary

in addition to a relation between flow rate and fraction at plug. The data obtained are summarized in Table 462-IV.

TABLE 462-IV  
MASS TRANSFER COEFFICIENTS FOR OXYGEN<sup>†</sup> AND HYDROGEN<sup>†</sup>

Type of Operation	Conditions				Mass Transfer Coefficient g (Impurity)/cm <sup>2</sup> -h-ppm
	Velocity Range cm/sec	% Plug	Temperature of Orifice, °C	Impurity <sup>†</sup> & ppt	
Na <sub>2</sub> O Nucleation: 8°C/min; 11°C Depression; Saturation Temperature = 213°C					
Precipitation	193-323	10-55	193	Oxygen(Na <sub>2</sub> O)	1.17 x 10 <sup>-1</sup>
Precipitation	323-404	55-69	196	Oxygen(Na <sub>2</sub> O)	6.09 x 10 <sup>-2</sup>
Dissolution	408-347	72-60	220	Oxygen(Na <sub>2</sub> O)	4.45 x 10 <sup>-2</sup>
Dissolution	408-363	72-64	213-224-213	Oxygen(Na <sub>2</sub> O)	2.27 x 10 <sup>-2</sup>
Precipitation	363-408	64-72	213-202-213	Oxygen(Na <sub>2</sub> O)	2.50 x 10 <sup>-2</sup>
NaH Nucleation: 3°C/min; 25°C Depression; Saturation Temperature = 280°C					
Precipitation	196-221	0-16.5	255-233	H(NaH)	7.82 x 10 <sup>-4</sup> † 1.44 x 10 <sup>-3</sup> ‡
Precipitation	221-272	16.5-35	233-223	H(NaH)	1.27 x 10 <sup>-3</sup> † 1.65 x 10 <sup>-3</sup> ‡
Precipitation	272-331	35-52	223-221	H(NaH)	1.28 x 10 <sup>-3</sup> † 1.61 x 10 <sup>-3</sup> ‡
Precipitation	331-398	52-65	221-240	H(NaH)	1.19 x 10 <sup>-3</sup> † 1.57 x 10 <sup>-3</sup> ‡
Precipitation	398-423	65-71	240-253	H(NaH)	7.28 x 10 <sup>-4</sup> † 1.09 x 10 <sup>-3</sup> ‡
Precipitation	448-465	75-79	268°C	H(NaH)	2.45 x 10 <sup>-4</sup> † 5.0 x 10 <sup>-4</sup> ‡
Precipitation	469-486	79-83	266	H(naH)	1.93 x 10 <sup>-4</sup> † 3.9 x 10 <sup>-4</sup> ‡
Dissolution	511-488	89-84	280-288-280	H(NaH)	1.28 x 10 <sup>-3</sup> † 2.4 x 10 <sup>-3</sup> ‡
Precipitation	500-511	86-89	258-280	H(NaH)	3.00 x 10 <sup>-4</sup> † 5.2 x 10 <sup>-4</sup> ‡
Dissolution	511-495	89-85	280-285-280	H(NaH)	1.72 x 10 <sup>-3</sup> † 3.22 x 10 <sup>-3</sup> ‡

<sup>†</sup> Assumed impurities - presence not verified by chemical analysis.

<sup>‡</sup> The Addison, Pulham, and Ray hydrogen solubility curve was used:  $\log(w/o H_2) = 6.211 - 5021/T$ .

<sup>‡</sup> The McClure hydrogen solubility curve was used:  $\log(w/o H_2) = 2.200 - 2800/T$ .

The above data contain some interesting relationships.

(1) Na<sub>2</sub>O precipitation and dissolution rate constants are approximately equal.

(2) NaH precipitation and dissolution rate constants are not equal. The dissolution constant is approximately 6 times larger than the precipitation constant. The precipitation may be reaction rate controlled while the dissolution may be at least partly liquid phase diffusion controlled.

(3) The rate constants for Na<sub>2</sub>O transport are larger than those for NaH. For precipitation the factor is 50 and for dissolution 7.5.

#### d. Plugging Indicator Study Loop

Design of a small plugging indicator study loop will be started. The purpose of this loop will be two-fold. First, a prototype automatic plugging indicator with an associated plug initiation loop for use on fairly clean systems will be designed, and; second, a provision for visual and analytical examination of the plugged orifice will be made.

#### B. Direct Current Resistivity Meter Study (G. E. Meadows)

##### 1. General

The dc resistivity meter has the capability of detecting dissolved, particulate, and gas-bubble

impurities in system sodium if the temperature of the sodium in the meter can be adequately controlled. The present work involves the testing of a LASL designed dc meter which includes a thermostated section for careful temperature control. The instrument will be tested on Analytical Loop No. 2 and will be used to detect oxygen in cold trapped and soluble getter systems. CaO particulates may be detected with the meter.

## 2. Current Results

The dc resistivity meter has been installed on Analytical Loop No. 2. No data will be obtained until the remaining portions of the loop are completed.

### C. Evaluation of UNC EMF Cells (G. E. Meadows)

#### 1. General

The UNC thoria-yttria solid electrolyte EMF cell has demonstrated the capability of indicating oxygen activity in sodium. However, such characteristics as life time, sensitivity, response time, drift, temperature coefficients, effects of vibration, and of H and C impurities have not been clearly determined. At LASL EMF cells have been installed on the cold trap loop and Analytical Loop No. 2 for use in the cold trap kinetic studies and soluble getter studies. Many of the above characteristics will be determined for these particular instruments as the indicated research progresses.

#### 2. Current Results

##### a. Analytical Loop No. 2

Two meter housings are installed; however, no data on the meters will be obtained until the loop is completed.

##### b. Cold Trap Loop

The increase in response time<sup>3</sup> of the one operating cell in the cold trap loop continued as additional cold trap runs were made. At the end of the series, the meter was operating but was not responding within a one day period to changes in concentration from 10 to 2 ppm.

## VI. SAMPLING AND ANALYSIS - Laboratory Methods

### A. Vacuum Distillation Studies (G. E. Meadows, L. A. Waldschmidt)

#### 1. General

The vacuum distillation technique has been shown to be a valuable method for analyses of oxygen in sodium.<sup>4</sup> As a result, the method is routinely used on many of the experimental loops at LASL. However, the versatility of the method can be increased as the interaction on the analytical result of other sodium impurities such as NaH and Na<sub>2</sub>CO<sub>3</sub> is better understood. Also, the method may be expanded to include analysis of metallic impurities in sodium such as Ca, Fe, Ne, and Cr. The research at LASL is directed toward refinement of the oxygen analysis methods and the determination of these metallic impurities with vacuum distillation.

#### 2. Current Results

##### a. Analytical Loop No. 1 - Distillation Analyses

In Table 462-V is a listing of 28 sodium samples taken from Analytical Loop No. 1 for vacuum distillation analysis for dissolved oxygen with the full-flow sampler.

Table 462-V  
Vacuum Distillation Analyses  
from Analytical Loop No. 1

Number of Samples	Cold Trap Temperature	Average Value ppm O	Std. Dev. ppm
4	250°C	41.2	± 1.3
16	225°C	21.2	± 2.4
8	122°C	1.4	± .3

The two high temperature determinations are 4 ppm higher than the values as determined by Rutkauskas. The low temperature value is 0.1 ppm below Rutkauskas' curve.

##### b. Off-Gas from Distillation

Observations conducted on sodium samples removed for vacuum distillation analysis for dissolved oxygen have indicated that there is a small quantity ( $\sim 10^{-5}$  -  $10^{-6}$  liters) of gas evolved from the sodium metal during the final stages of distillation. The evolution occurs while the sample is being distilled at a constant temperature ( $\sim 360^\circ\text{C}$ ) and is associated with the removal of the final portion of the metallic sodium from the nonvolatile residue. Samples analyzed by gas chromatographic techniques have shown the evolved gas to be composed primarily of hydrogen with traces of methane. Mass spectrometric scans of

the gas have shown no additional constituents below mass 40. The quantity of the gas released has been observed to be a function of the loop cold trap temperature with the lower cold trap temperature giving a smaller gas release.

A phosphorus compound has been detected in vacuum distillation residue samples removed from Analytical Loop No. 1. When the sodium samples are hydrolyzed the resulting phosphine ( $\text{PH}_3$ ) has been identified by mass spectrometer scans and also by oxidizing the phosphine to phosphate ion and subsequent spot test for phosphate. A small effort is being applied to analysis of off-gas species from sodium as one possible tool for identification and determination of impurities in sodium.

## B. Study of Gamma Ray Activation Analysis for C and O

(D. M. Holm, G. E. Meadows, W. J. Heyman, B. K. Barnes, J. L. Parker)

### 1. General

Many analytical techniques for the analysis of oxygen such as vacuum distillation and amalgamation methods are not specific for a given compound and give oxygen concentrations by assuming the nature or form of the final residue being extracted or analyzed by flame photometry. Thus, analytical techniques are required which can give concentrations of oxygen and other impurities such as carbon directly without making assumption about the chemical form of the impurity.

Photon activation of oxygen and carbon has this property of determining total impurity concentration regardless of its chemical nature. The sodium sample is irradiated by high energy photons ( $\sim 20$  Mev); the sodium is extruded and then is transported pneumatically to the counter where the positron annihilation radiation is detected in a very large segmented NaI crystal. The resulting count rate vs time curve is decomposed by computer analysis into O, C, and K decay curves. Thus, O and C can be determined from one sample if the interferences of K and Na are kept at low levels.

### 2. Current Results

#### a. Radiation Detection Equipment and Techniques

Testing of the large NaI crystal assembly has been completed and results reported previously<sup>3</sup> were confirmed. In addition, the use of the assembly in

conjunction with a Ge(Li) detector as a pair spectrometer has been investigated. A triple coincidence is required between the Ge(Li) detector and both ends of the NaI crystal assembly. Thus, only events in which a positron annihilation gamma ray goes into each NaI crystal are accepted for analysis. This enhances the double-escape peak with respect to the single-escape peak and the full-energy peak, which are almost completely suppressed. Figure 462-5 shows the type of data which may be obtained with this detector-assembly combination.

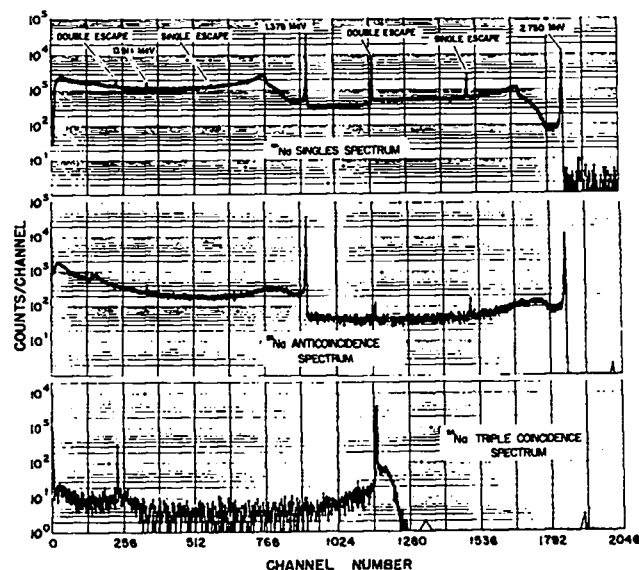


Fig. 462-5.  $^{24}\text{Na}$  spectra taken with a Ge(Li) detector in three modes of operation with the large NaI crystal assembly. The anticoincidence spectrum is used in most gamma ray analysis, and the other modes are used for analyzing complex spectra.

Experiments to determine the response of the large NaI assembly to different gamma-ray sources in various locations within the diametrical hole are nearly finished. The results of these experiments will be used to determine the optimum modes of operation for the various uses ( $^3\text{He}$  activation, photon activation, and gamma ray spectroscopy) of this assembly.

A target for sodium activation is being built for use in the electron analog of the Los Alamos Meson Physics Facility. The use of this facility will give a large increase in beam current over that available at the White Sands installation where the first proof testing of the proton activation technique was done.

## b. Sodium Handling Equipment

The sodium handling equipment (shear, extruder, and rabbit) which will be used in the evaluation of the gamma ray activation analytical technique for the determination of oxygen and carbon in sodium has been completed and has undergone operational check-out. A thief-tube sampler system for removing the characterized sodium samples to evaluate this technique has been installed on Analytical Loop No. 1. Samples will be taken in the near future for gamma ray analyses for carbon in sodium.

## c. Absorption Spectrophotometry Development for Metal Impurity Analyses (G. E. Meadows, L. A. Waldschmidt)

### 1. General

Soluble getter and corrosion studies require that various metal impurity concentration be known as a function of operating conditions. One technique for determining these concentrations is absorption spectrophotometry. Refinement of this technique is being made to detect low level concentration (~1 ppm) both in vacuum distillation residues and in bulk sodium samples. The impurities to be studied are Ca, Mg, K, Fe, Ni, and Cr.

### 2. Current Results

Effort has continued on the development of atomic absorption spectrophotometric analytical procedures for the determination of trace-level metallic impurities (other than sodium) remaining in the residue and condensate following distillation. The same procedures are also being investigated for impurities in bulk sodium samples. The reactor grade sodium in Analytical Loop No. 1 has been analyzed for Ca, Mg, and K using these procedures. Duplicate samples removed for spectrochemical analyses have agreed within analytical error with the atomic absorption techniques developed.

## d. Total Carbon Analysis Development (K. S. Bergstresser)

### 1. General

The low temperature combustion technique for total carbon analysis is being refined. By using a high sensitivity gas chromatograph for quantitative measurement of the CO<sub>2</sub> produced, it is hoped that carbon concentrations in the 1 ppm range can be determined.

## 2. Current Results

### a. Carbon

An all-metal system for low-temperature combustion of Na in the determination of C at the 1 to 10 ppm concentration level was designed and some parts tested. A major section of this analytical system is the Ni chamber for combustions at temperatures below 700°C. This unit was tested satisfactorily with temporary connections to supply and reagent lines. Permanent installation of these facilities to the Ni chamber are in progress.

Determination of the CO<sub>2</sub> will be made by gas chromatography following separation by acidification of the basic combustion products (Na<sub>2</sub>O and Na<sub>2</sub>CO<sub>3</sub>), and collection of the released CO<sub>2</sub> in a molecular sieve trap. Equipment for these operations and for calibration of the chromatograph (Varian Aerograph Model 1532-2B) was assembled and tested.

### b. Investigation of Residues from the Vacuum Distillation of Metallic Sodium

Initial testing was completed of the equipment for investigating the nature of residues following vacuum distillation of metallic Na. The inert atmosphere enclosure has maintained O<sub>2</sub> and H<sub>2</sub>O concentrations in the Ar atmosphere at less than 1 and 4 ppm, respectively. The inductively heated vacuum distillation apparatus, and various equipment for sampling and transferring samples operated satisfactorily. Further work with the distillation will be deferred until the low-temperature combustion method for determining C is operative.

## e. Development of Remotely Operated Distillation Samplers for EBR-II (W. R. Wykoff, D. N. Dunning, J. R. Phillips H. M. Ruess, E. O. Swickard)

### 1. General

At the request of the AEC, part of the effort directed to a study of in-line sampling associated with the vacuum distillation analytical method has been redirected to the design and construction of remotely operated, integral sampling and distillation units for installation on the primary coolant loop of EBR-II. A version of the sampling system is also being developed for the nonradioactive secondary sodium system of EBR-II. The sampling system design is a modified engineering loop version of the

laboratory model integral full-flow vacuum distillation sampling system currently in use on the Analytical Loop No. 1 and cold trap experimental facilities at the LASL. The entire sampling system will be fabricated of Type 304 stainless steel, and separation of sodium from the nonvolatile impurities will be accomplished by induction heating. The work coil of the induction heater is located within the metal envelope surrounding the distillation zone.

## 2. Current Results

The sample transfer mechanism, which is the heart of the remotely operated basic sampler unit has been developed to the point that a mockup is operating satisfactorily. Design of the prototype sampler is now in progress.

The vacuum-inert gas system has been designed and the prototype unit has been fabricated and tested. A test loop for pre-reactor testing of the sampler system has been completed.

Agreements have been reached with the EBR-II personnel as to the general design of an overflow pot on the Analytical Chemistry Loop to provide a constant-head source of sodium for the sampler.

Much of the control circuitry for the sampler unit has been designed and a prototype unit is under construction. Final design must be coordinated with the design of the basic sampler unit.

## VII. COVER GAS AND MAINTENANCE ATMOSPHERES

### A. Development of a High Temperature Quadrupole Mass Spectrometer for Cover Gas Analysis ( J. P. Brainard, D. C. Kirkpatrick, C. R. Winkelman)

#### 1. General

The purpose of this research is to develop a method for continuous on-line analysis of high temperature (up to 650°C) cover gas in an LMFBR. The analyzer must be capable of detecting impurities such as nitrogen, oxygen, hydrogen, carbon dioxide, methane, and fission products in the cover gas with a sensitivity varying from the part-per-million range to the percent range. A response time of about one minute is necessary if the analytical data are to serve as the error signal furnished to activate devices for continuous control of cover gas composition.

A quadrupole mass spectrometer was obtained in order to meet the above requirements. It is believed that reasonably representative sampling can be accomplished by transporting the sample gas in sodium loop containment materials and at sodium loop temperatures until it has passed through the spectrometer for analysis.

## 2. Current Results

An apparatus has been designed and nearly fabricated to measure gas beam distribution from various sources. The objective is to create a high temperature molecular beam as efficiently as possible (using the smallest quantity of gas) for the injection of the cover gas into the ion source of our gas analyzer.

The first nozzle that will be tried is a tube of 7 mil i.d. The gas density distribution is measured by an ionization gauge. A tube which is attached to the ionization gauge absorbs the gas flux at the point of measurement. At equilibrium, the gas density in the gauge is approximately six times that of the beam density at the point of interest. As a result, the sensitivity of the measurement is increased.

Collimated hole structures have been shown to be an efficient nozzle for the formation of molecular beams.<sup>5</sup> The ability to fabricate a 1/2-mil multi-tube collimated hole structure has been confirmed by a manufacturer.

The Fabri-tek digital averager which will process the quadrupole analyzer data has been repaired and has been interfaced with the Quadrupole 250. The signal preamplifier and sweep amplifier, however, were found to lack the necessary stability. Fabri-tek will purchase some better quality amplifiers. The averager has again been sent back to Fabri-tek to have a cyclic printout and memory dump capability added.

## REFERENCES

1. "Quarterly Status Report on the Advanced Plutonium Fuels Program," January 1 - March 31, 1968, Report LA-3933-MS, Los Alamos Scientific Laboratory.
2. Addison, C. C., Pulham, R. J., and Roy, R. J., J. Chem. Soc. (1965), 115-121.
3. "Quarterly Status Report on the Advanced Plutonium Fuels Program," April 1 - June 30, 1968, Report LA-3993-MS, Los Alamos Scientific Laboratory.

4. V. J. Rutkauskas, "Determination of the Solubility of Oxygen in Sodium Using the Vacuum Distillation Analytical Technique," Report LA-3879, Los Alamos Scientific Laboratory, 1968.
5. J. A. Giordmaine and T. C. Wang, "Molecular Beam Formation by Long Parallel Tubes," J. Appl. Phys. 31, 463 (1960).

PROJECT 463  
CERAMIC PLUTONIUM FUEL MATERIALS

Person in Charge: R. D. Baker

Principal Investigator: J. A. Leary

1. INTRODUCTION

The principal goals of this project are to prepare pure, well characterized plutonium fuel materials, and to determine their high temperature properties. Properties of interest are (1) thermal stability, (2) thermal expansion, (3) thermal conductivity, (4) phase relationships by differential thermal analysis, (5) structure and phase relationships by x-ray diffraction, high temperature x-ray diffraction, neutron diffraction and high-temperature neutron diffraction, (6) density, (7) hardness and its temperature dependence, (8) compatibility including electron microprobe analysis, (9) compressive creep (deformation).

In addition to phase equilibria and general properties, specific thermodynamic properties such as free energy of formation by vaporization equilibria in the 1000-2000°C temperature range with mass spectrometer identification of vapor species, free energy of formation by electromotive force measurement in the 450-1200°C temperature range, and heat capacity and heat of transition are being determined.

II. SYNTHESIS AND FABRICATION

(M. W. Shupe, A. E. Ogard, R. L. Nance, D. Kelley)

1. Carbides

Single phase (U, Pu)C pellets can be synthesized by a process in which excess carbon is intentionally introduced in the arc melting of U, Pu and C. This excess carbon is subsequently removed by reaction with hydrogen at 850°C before the powders are processed into pellets. The chemical compositions of pellets produced by this process are shown in the Synthesis and Fabrication part of Project 464 (next section).

The effect of binders on the sintered microstructures of monocarbides was tested. Three binders (Carbowax 4000, paraffin, and naphthalene) were each added at a concentration of 0.5 w/o to the single phase (U, Pu)C powder before pressing. The Carbowax 4000 was mixed dry in a Spex grinder whereas the paraffin and naphthalene were dissolved in toluene and slurry mixed. In addition, a pellet without binder was also pressed as a control. These pellets were slowly heated to 1800°C and then sintered for 4 hr in Ar. Metallographic examination of the sintered pellets revealed ~10 v/o higher carbide phases to be present in the pellet involving Carbowax 4000 binder. The remaining pellets were single phase. The pellet in which paraffin was the binder had a superior microstructure and therefore will be pursued further. Mechanically measured densities showed that the binders did not have much effect on the sintered densities; the densities were all 90.4 to 91.9% of theoretical.

Compatibility experiments at other laboratories have indicated that excess carbon present as  $MC_2$  is more reactive towards stainless steel than is  $M_2C_3$ . Efforts are now being directed towards determination of the conditions necessary to convert completely the acicular phase observed in  $U_{0.8}Pu_{0.2}C_{1.1}$  into the reprecipitated grain boundary formation. This transformation occurs at 1650°C. Pellets of the composition  $U_{0.8}Pu_{0.2}C_{1.1}$  contain the acicular phase (or platelets) after sintering at 1800°C for 4 hr followed by 1400°C for 2 hr. Annealing at 1600°C for 24 hr does not significantly change the amount of this phase. A small

reduction in amount was found on heating at 1400°C for 24 hr but did not change when the time was increased to 36 hr. Apparently this transformation is extremely slow. The MC-M<sub>2</sub>C<sub>3</sub> mixture can be formed essentially free of the acicular phase by sintering below the transformation temperature such as 1525°C for 4 hr and never getting above 1650°C. However consolidation of the pellets at this temperature is rather poor.

A variety of carbide compositions have been prepared by arc melting, solution treating, pulverizing and grinding, cold compaction and sintering techniques. These materials were used for properties measurements. The following compositions were prepared: single phase U<sub>0.8</sub>Pu<sub>0.2</sub>C, U<sub>0.8</sub>Pu<sub>0.2</sub>C<sub>1+x</sub>, U<sub>0.8</sub>Pu<sub>0.2</sub>C + 0.5 w/o W, single phase Pu<sub>2</sub>C<sub>3</sub> and PuC<sub>0.86</sub>, and five two phase PuC<sub>x</sub> carbides where x = 1.00, 1.20, 1.38, 1.65, 2.20.

## 2. Preparation of PuO<sub>2</sub> for FFTF Quality Assurance Standards

(R. L. Nance and D. W. Kelley)

Direct air oxidation of electrorefined Pu yields PuO<sub>2</sub> of good purity. It has been demonstrated that air saturated with H<sub>2</sub>O at room temperature can controllably and completely oxidize several hundred grams of Pu to PuO<sub>2</sub> in a conveniently short time. The large particles in this product apparently have a low free surface energy which leads to lowered sintered densities of compacted shapes, compared to those obtained from some other sources such as oxalate peroxide - derived PuO<sub>2</sub>.

The goal of further development work will be the large scale preparation of PuO<sub>2</sub> by air oxidation to produce sinterable, pure powder.

Analytical results for PuO<sub>2</sub> lot P-20-23, produced by the first large scale experiment, are as follows:

Li	0.07	Fe	2	Cs	< 2
Be	< 0.001	Co	< 0.5	Ba	< 0.1
B	< 0.3	Ni	2	La	< 0.5
Na	5	Cu	2	Hf	< 0.5
Mg	10	Zn	15	Ta	< 25
Al	3	Rb	< 0.5	W	50
Si	4	Sr	< 0.1	Re	< 0.5
K	< 0.5	Y	< 0.1	Pt	< 100
Ca	10	Zr	2	Pb	< 0.5
Ti	0.2	Nb	< 50	Bi	0.5
V	< 0.5	Mo	< 0.5	U	22
Cr	2	Cd	< 0.5	Pu	88.07%
Mn	< 0.1	Sn	< 0.5	Am	38

(All results expressed as ppm in respect to Pu except for percent Pu)

## III. PROPERTIES

### 1. Differential Thermal Analysis

(J. G. Reavis)

Transition Temperatures of (U, Pu)C<sub>2</sub>: Transition temperatures of (U, Pu)C<sub>2</sub> (excess C) samples containing 20-100 m/o PuC<sub>2</sub> have been reported previously.<sup>(1)</sup> Additional samples have been observed in the composition range 0-20 m/o PuC<sub>2</sub>. The thermal arrest temperatures observed are plotted on Fig. 463-1. Tetragonal MC<sub>2</sub> has been observed in all samples quenched from the "MC<sub>2</sub> + C" and "liquid + C" regions of Fig. 463-1. High temperature x-ray diffraction studies in other laboratories have shown that UC<sub>2</sub> is cubic at temperatures above 1765°C<sup>(2)</sup> and PuC<sub>2</sub> is cubic above 1700°C.<sup>(3)</sup> UC<sub>2</sub> was observed to transform from cubic to tetragonal on cooling through 1765° (or 1785°, depending on composition),<sup>(2)</sup> and it was proposed<sup>(3)</sup> that tetragonal PuC<sub>2</sub> may be a metastable phase. Thus, although quenched MC<sub>2</sub> samples are tetragonal, the tetragonal form may not be an equilibrium form at any temperature over much of the composition range between UC<sub>2</sub> and PuC<sub>2</sub>.

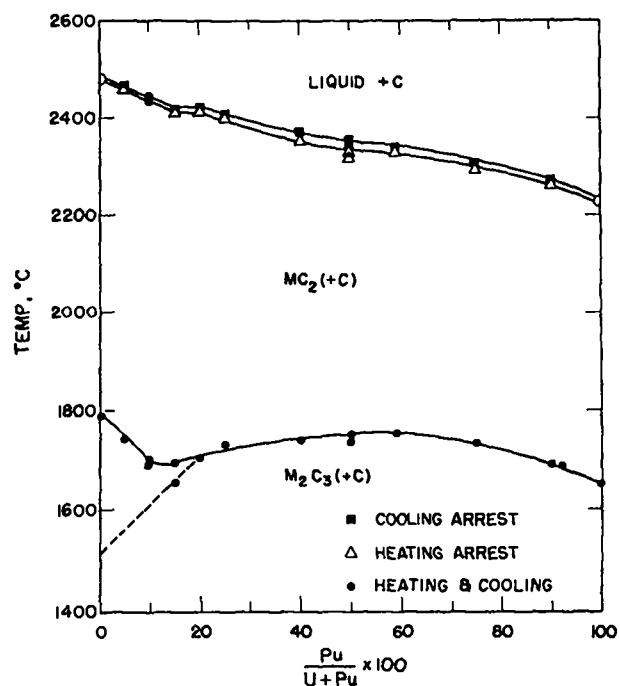


Figure 463-1. Thermal arrests observed for (U, Pu)C<sub>2</sub> samples containing excess C

### Transition Temperatures in the Pu-C System:

Samples of  $\text{PuC}_{0.86}$  and  $\text{PuC}_{0.99}$  showed slow transitions beginning at  $1600 \pm 10^\circ$  and had liquidus temperatures above  $1650^\circ$ .  $\text{PuC}_{1.6}$  exhibited the  $1650^\circ$  transition characteristic of samples containing sufficient C to form  $\text{PuC}_2$ . The melting point was  $2035 \pm 10^\circ$ . Compositions intermediate between  $\text{PuC}_{1.0}$  and  $\text{PuC}_{1.6}$  showed anomalous behavior. Weak thermal arrests were observed but were not reproducible. Additional measurements in this range of composition are needed to define the phase boundaries.

### 2. X-Ray Powder Diffraction

(C. W. Bjorklund and R. M. Douglass)

Characterization of plutonium fuel materials by x-ray diffraction powder camera techniques has been continued. The results are incorporated in other sections of this report.

A computer program<sup>(4)</sup> designed to aid in indexing x-ray powder patterns was tested with the data previously obtained for  $\alpha\text{-Pu}_2\text{S}_3$ . The program attempts to find a reduced triclinic cell which matches the observed data within a given limit of error. If such a cell is found, the program output may then be used to determine whether or not the triclinic cell may be transformed to a cell of higher symmetry. An interesting consequence of this approach is that more than one cell of higher symmetry may be found, each of which would be a valid representation of the powder pattern data. The  $\text{Pu}_2\text{S}_3$  data were treated, first, as data from the pattern of a structure of unknown symmetry to see whether the pattern could be properly indexed by the program, and, second, as data from a pattern of previously determined symmetry to determine whether cells other than the one believed to be correct might also fit the data. Ideally, either approach should lead to the same result. However, the  $\text{Pu}_2\text{S}_3$  pattern was complicated by numerous closely-spaced reflections, some of which tended to overlap, and some of which were suspected to represent impurities and/or a second phase. In addition, one second order and all first order pinacoid reflections were found to be missing from the experimental data and had to be inferred by a combination of techniques for the

program to work. No other cells of higher symmetry than the orthorhombic cell reported previously were found. The larger orthorhombic cell reported by Marcon and Pascard<sup>(5)</sup> was not found. Allbutt and Junkin<sup>(6)</sup> have also reported cell dimensions for  $\alpha\text{-Pu}_2\text{S}_3$  which agree reasonably with those found here.

### Self-Irradiation Damage

Additional measurements of the effect of self-irradiation damage on the lattice dimensions of several plutonium compounds have been made. The lattice dimensions of  $\text{PuO}_2$ ,  $\text{PuN}$ , and  $\text{Pu}_2\text{C}_3$  of normal isotopic composition continue to increase after 1877 d., and 1125 d., respectively. The relative rates of expansion decrease in the same order. The lattice dimensions obtained from the least squares curves at the times listed above indicate that the lattice expansion of  $\text{PuN}$  is not within 95% of the predicted saturation value. Corresponding values for  $\text{PuO}_2$  and  $\text{Pu}_2\text{C}_3$  are 92% and 74%, respectively.

The lattices of all samples of  $\text{PuO}_2$  enriched with a 3.75 a/o  $^{238}\text{Pu}$  have long since expanded to the predicted saturation values. The lattice dimensions are constant within experimental error. Because of a leak in one of the capillaries containing  $\text{PuO}_2$  stored in liquid nitrogen, the low temperature  $\text{PuO}_2$  time series experiments have been discontinued.

The lattice of the  $\text{Pu}_2\text{C}_3$  phase of the two-phase carbide system (enriched with 4.05 a/o  $^{238}\text{Pu}$ ) has probably expanded to its saturation value. The dimensions of the  $\text{PuC}$  phase continue to oscillate about an average value to a somewhat greater extent than would be expected from the precision of the measurements. No change has been observed in the quality of the carbide powder patterns.

### 3. High Temperature X-Ray Diffraction

(J. L. Green)

During the initial stages of testing of the x-ray diffractometer furnace, considerable difficulty was experienced in maintaining an inert atmosphere of sufficient purity to avoid sample oxidation at high temperatures. Extensive revisions were made in the cooling system in the furnace to eliminate the diffusion

of water vapor through the flexible cooling water lines in the sample chamber and also a uranium chip furnace purification system was installed in the supply line for the He cover gas. These changes appear to have eliminated the oxidation problem. Trial runs using NbC as a stand-in material have demonstrated that no observable oxidation occurs on the sample surface at temperatures up to 1800°C. As a test of the overall system, a thermal expansion coefficient determination was made on a sample of high purity NbC for the temperature interval from 800°C to 1800°C. The results of this experiment are in close agreement with the expansion data published for NbC by Houska.<sup>(7)</sup> A comparison of these data is shown in Figure 463-2. The maximum deviation of the present  $\Delta a/a_0$  data points from Houska's data is 2% and the average deviation is 1%, which are within the estimated limits of experimental error. This is considered to be an adequate demonstration of the overall accuracy of lattice parameter determinations at high temperatures and also of temperature measurement. The inert box and furnace system have been contaminated with Pu, and materials handling techniques have been found to be satisfactory with respect to contamination containment.

Work has been initiated on the preparation of samples to be used in the study of the high temperature crystallographic properties of carbon rich  $\text{PuC}_x$  compositions. Initial difficulty was experienced in the

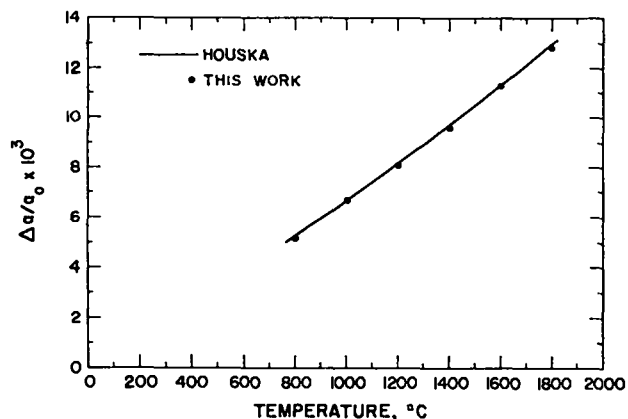
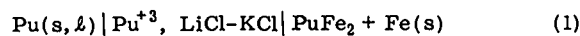


Figure 463-2. Thermal expansion data for NbC

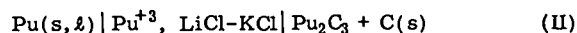
preparation of heater strip samples in this composition region. The results of a large number of trial sample preparations indicate that  $\text{Pu}_2\text{C}_3$  apparently has a relatively large thermal expansion coefficient. The samples tended to shatter during the sintering operation and did not adhere properly to the heater strip. These difficulties have been eliminated by using somewhat smaller samples and by supporting the sample with small, undercut, graphite tabs along the edges of the strip. These tabs mechanically retain the sample on the heater strip even though considerable shrinkage occurs on cooling. Proper sintering conditions have been found to be critical. The sample must be sufficiently well sintered to withstand the shock of breaking the bond formed between the sample and the graphite strip at sintering temperatures; however, if the material is oversintered, the sample surface tends to distort severely, which destroys its usefulness as a diffractometer sample. The first composition to be studied will be  $\text{PuC}_{2.2}$ . Sintering in argon at 1600°C for 4 hours appears to be optimum for samples of this material prepared from -500 mesh powders. Preliminary trials with a nominal composition of  $\text{PuC}_{4.0}$  indicate that sintering is not complete enough under these conditions; therefore, a somewhat higher sintering temperature will have to be used. Samples of the  $\text{PuC}_{2.2}$  composition are presently being prepared on complete heater strips and should be available for use in the near future.

#### 4. Thermodynamic Properties of Plutonium Compounds by Electromotive Force Techniques (G. M. Campbell and James Olson)

Galvanic cells represented schematically as



and



were monitored by galvanostatic potential determination, over a temperature range of 684 to 803°C. Special attention is being given to changes in emf with temperature. It is believed that the galvanostatic technique is sensitive enough to detect small deviations from reversibility to temperature change which is essential in knowing if the emf represents an equilibrium which does

not include complications due to slow solid state diffusion. On this basis cell (I) appears to contain complicating factors at these temperatures. Cells of type (II) give better results but the emf is significantly greater in magnitude than found by indirect measurements against a  $\text{PuRu}_2 + \text{Ru}$  electrode. An effort will be made to attain higher temperatures with this system.

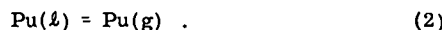
5. Thermodynamic Properties from Vaporization Studies  
(R. A. Kent)

The mass spectrometer-Knudsen cell assembly employed to study vaporization phenomena at high temperatures has been described in previous reports. Three investigations have been carried out under this program. Most of the results pertaining to the vaporization of Pu metal and PuN also have been described previously. These studies have been concluded and an investigation of the vapor pressure of Pu(g) above Pu-C solid phases as a function of composition has been initiated.

Pu: In the temperature range 1426-1658°K the vapor pressure of Pu(g) above Pu(l) is given by

$$\log P_{\text{Pu}} (\text{atm}) = (4.924 \pm 0.120) - \frac{17420 \pm 184}{T^{\circ}\text{K}} \quad (1)$$

The vapor pressure results have been combined with listed thermodynamic values for Pu(g) and estimated values for Pu(l) to calculate free energy values for the reaction



The resultant expressions are:

$$\Delta G^{\circ} = (79478 - 22.26 T) \text{ cal. mole}^{-1}, \quad 1300-1750^{\circ}\text{K}$$

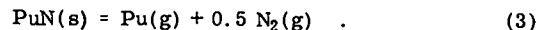
and

$$\Delta G_3^{\circ} = (80390 - 22.78 T) \text{ cal. mole}^{-1}, \quad 1750-2200^{\circ}\text{K}$$

The enthalpy and entropy of vaporization at 298°K are taken to be  $83.0 \pm 0.5 \text{ kcal. mole}^{-1}$  and  $29.1 \pm 0.5$ , respectively.

PuN: The vapor pressure of Pu(g) above solid PuN has been determined in a series of eight experiments in the range 1658-1976°K. Additional experiments have been conducted in order to determine the solubility

of Pu(l) in PuN(s) and to establish the congruency of the reaction



As yet, no high temperature heat capacity data are available for PuN. Therefore a reliable set of thermodynamic functions cannot be assembled. However, a set of thermodynamic functions for PuN have been estimated from a comparison with known functions for UN. When these functions are combined with the vapor pressure data to calculate the enthalpy of formation of PuN, the result is in excellent agreement with recent EMF<sup>(8)</sup> and calorimetric<sup>(9)</sup> studies.

Pu-C System: The vaporization behavior of most carbide systems at high temperatures is seldom straightforward. The carbide systems are characterized by compounds having a wide range of single phase composition. When such nonstoichiometric compounds are heated, the vapor pressure, and indeed the identity of the vapor species themselves, are dependent upon the composition of the solid phase or phases. This composition is likely to change during heating unless one is at a point of congruent vaporization. In addition, small amounts of impurities, such as oxygen, can often change drastically the vaporization behavior.

The U-C system, for example, has been investigated by many workers in the past ten years. Often the results of one set of investigators would be in sharp disagreement with those obtained by other workers. Only recently has an understanding of the complex vaporization behavior of this system been attained.<sup>(10)</sup> Thus, it would seem that as a logical first step in the investigation of the Pu-U-C ternary system, the Pu-C binary system should be established.

To date fifteen experiments have been conducted involving samples with nine different compositions ranging from Pu to  $\text{PuC}_{2.1}$ . The vaporization behavior of the Pu-C system may be qualitatively described as follows.

As one adds carbon to Pu(l) the pressure of Pu(g) at a given temperature drops as the Pu activity is lowered. When the low carbon boundary of the mono-

carbide is attained the pressure of Pu(g) falls rather sharply. As one continues to heat the sample and continues to add carbon, the monocarbide undergoes reaction to form Pu(g) and the sesquicarbide. The Pu(g) pressure remains invariant so long as both the monocarbide and sesquicarbide are present as solid phases. When the low carbon boundary of the single phase sesquicarbides is reached the Pu(g) pressure falls drastically. The sesquicarbide on heating gives off Pu(g) with free carbon appearing in the solid phase. Again, the Pu(g) pressure remains invariant so long as both solid sesquicarbide and free carbon are present. Above 1660°C the sesquicarbide transforms to the dicarbide with a resultant change in Pu(g) pressure. In addition, at high temperatures, small amounts of PuC<sub>2</sub> gas are formed above the solid dicarbide.

When the vapor pressure data attained above the monocarbide-sesquicarbide two phase region are combined with the thermodynamic functions for the monocarbide listed by Rand<sup>(11)</sup> the calculated free energy of formation for the monocarbide is in good agreement with the value calculated from the vapor pressure data of other workers.<sup>(12, 13)</sup> However, the results are in poor agreement with the recent EMF study.<sup>(14)</sup> Also, the vapor pressure data obtained above the two phase sesquicarbide-carbon region yield free energy of formation values which are in poor agreement with the EMF study. Finally the vapor pressure data obtained above the dicarbide are in sharp disagreement with results attained in a previous vaporization study.<sup>(15)</sup>

It is obvious that further elucidation of the Pu-C phase diagram, with special emphasis on determining the width of the sesquicarbide single phase region will be required before the discrepancies in the vapor pressure and EMF studies can be resolved.

The investigation of this system will be continued.

## 6. High Temperature Calorimetry (A. E. Ogard, G. Melton)

The high temperature heat content of U<sub>0.8</sub>Pu<sub>0.2</sub>O<sub>2.00</sub> and U<sub>0.8</sub>Pu<sub>0.2</sub>O<sub>1.98</sub> are being determined as part of a cooperative program with G. E. -Sunnyvale.

In addition, these properties are being determined for UO<sub>2</sub>, α-Al<sub>2</sub>O<sub>3</sub> and W. To date the heat contents have been determined to ~2100°C.

The heat content of the W used in the capsules is being determined from 1000°C on up to temperatures approaching 3000°C using a W mesh furnace in connection with the copper block calorimeter. In Table 463-I are shown the values of H<sub>T</sub> - H<sub>298</sub> for W recently determined in this laboratory as compared to values in the literature, (literature values were calculated from equations given in each paper). The values compare quite favorably and in the worst case at 2340°C the maximum difference is less than 5%. However, this difference is magnified if the derivative of the heat content equation is taken to obtain the equation for the heat capacity. The difference in heat capacities at 2340°C is then ~15%.

The values of H<sub>T</sub> - H<sub>298</sub> determined in this laboratory and listed in Table 463-I have been corrected for the estimated radiative heat losses that occurred during free fall into the calorimeter block. The magnitude of this correction becomes significant at temperatures over 1700°C in that it is larger than, and increasing at a faster rate than the estimated inaccuracy of the experiments. Due to the size and uncertainty of this correction along with the ~1% overall possible inaccuracy of high temperature drop calorimetry it will be necessary to define a metal such as W as a standard. In defining W as a standard it will be necessary to show that the high temperature heat contents are independent of

Table 463-I  
Heat Content of Tungsten  
H<sub>T</sub> - H<sub>298</sub>°C (cal/gram)

Temperature, °C	Hoch & Johnston <sup>(16)</sup>	Present Work	Hein & Flagella <sup>(17)</sup>	Kiril'in et al. <sup>(18)</sup>
1084	36.1	36.7	36.4	36.9
1217	41.0	41.5	41.3	42.0
1304	44.2	45.4	44.6	45.4
1437	49.2	50.2*	49.8	50.7
1508	51.9	52.1	52.6	53.5
1711	58.8	61.4*	60.8	61.9
1753	61.5	62.8	62.4	63.7
1775	62.3	63.4	63.4	64.6
1932	68.6	68.9*	70.1	71.3
1963	69.8	72.2	71.4	72.6
2100	75.4	77.8	77.4	78.7
2114	76.0	78.3*	78.1	79.3
2195	79.3	82.0	81.8	82.9
2340	86.4	88.7	88.6	89.5

\*A second capsule of similar weight but with 1/2 the surface area.

sample weight, sample size, physical form of sample, method of heat exchange between sample capsule and calorimeter, total heat input into calorimeter and rate of heat input into calorimeter. A comparison will also be needed between correcting for radiative heat loss and the method using the difference between full and empty capsules. After these factors are known something can be said about the accuracy of the heat content values of W at temperatures above 2000°C.

#### 7. Adiabatic Calorimeter

(D.G. Clifton)

A small adiabatic calorimeter, similar in design to the one built and used by Dench,<sup>(19)</sup> is being developed.

The calorimeter will be operative up to about 1400°C and will have the capability of measuring heats of reaction and of transformation of condensed phase materials for processes that proceed at reasonable rates in this temperature regime. Direct determinations of heat capacities of condensed phase material also can be made with this instrument.

The main housing of the calorimeter and its associated cooling jacket and vacuum system are fabricated and assembled and are being leak tested. The interior components of the calorimeter are either on hand or are presently being fabricated, the instrumentation development is almost completed and the total assembly of the unit will be accomplished soon.

Provision has been made for the installation of the calorimeter in a glove box. However, it will be installed initially on a temporary work bench until its operation is shown to be satisfactory.

#### 8. Intermediate Temperature Drop Calorimeter

(D.G. Clifton)

An intermediate temperature (300° to 1300°K) drop calorimeter is under development. Experiments have been conducted upon a method of sample heating utilizing a 1-1/2" I. D. Marshall resistance wound furnace with a quartz tube liner and six Pt-Pt, 10 Rh thermocouples located in such a manner as to provide a complete temperature survey over the zone containing the sample. This system provided conditions in which the longitudinal variation in the sample temperature for

a 3/4" O. D. x 2" long sample at 1000°C was about 2 to 3°C with this variation dropping to 1°C or less at a sample temperature of about 360°C. Subsequent to these experiments this design was incorporated into a furnace system and a "dropping" mechanism which is presently being fabricated. The fabrication is about 80% complete and the system is to be installed upon the receiving calorimeter, or energy measuring system.

The six Pt-Pt, 10 Rh thermocouples which will be used in the final calorimeter assembly have been calibrated against standard freezing point samples acquired from the National Bureau of Standards. The corresponding correction curves needed to get the temperature on the International Temperature Scale from the observed emf values have been obtained.

#### IV. ANALYTICAL CHEMISTRY

##### 1. Electron Microprobe Examination of Various Ceramic Plutonium Materials

(E. A. Hakkila, H. L. Barker)

Ten samples of sintered carbides (MC, M<sub>2</sub>C<sub>3</sub>, etc.) from various preparatory experiments were examined to determine homogeneity and to identify inclusions. X-ray intensities of the U and Pu in adjacent crystals in nine of the samples varied by as much as 18 and 100 percent, respectively, indicating heterogeneity. Significant variations in U and Pu x-ray intensities were not observed in one sample. In three samples, long blue-white stringers were found that contained less C than the matrix. Several samples contained large white inclusions, that had less Pu, U, and C than the matrix, and small inclusions that had more Pu and less U and C than the matrix. Impurities found in inclusions were Si, Cr, Fe, Ni, and, in a few cases, Cu.

As a matter of comparison a sample of UC was examined to identify impurities and determine homogeneity. X-ray intensities of U from adjacent crystals did not differ significantly, indicating that the sample was homogeneous. Impurities found in inclusions were Fe and Cr.

##### 2. Determination of Oxygen in Refractory Oxides

(D. E. Vance, M. E. Smith)

An inert-gas-fusion-chromatographic method was developed for the determination of oxygen in refractory

oxides. The sample was heated in a graphite crucible by induction which liberated the oxygen as a mixture of CO and CO<sub>2</sub>. These gases were trapped on silica gel, desorbed and mixed with an internal standard such as Ne, then measured with a gas chromatograph. Repeated analysis of one lot of ThO<sub>2</sub>, known to contain 12.28 percent O<sub>2</sub> gave an average value of 12.24 percent. Heterogeneity of the sample resulted in rather poor precision (2.4 relative percent at the 1 $\sigma$  level). Analysis of a homogeneous sample of U<sub>3</sub>O<sub>8</sub> showed a relative standard deviation of 0.58% at the 1 $\sigma$  level. The method is now being tested by repeated analysis of a single lot of (U, Pu)O<sub>2</sub>.

### 3. Miscellaneous Services

(W. Hutchinson, W. Wilson, N. Koski, G. R. Waterbury, O. R. Simi, W. M. Myers, C. J. Martell, C. B. Collier, R. T. Phelps)

An inert-gas-fusion method was applied without difficulty to the determination of O<sub>2</sub> in twenty-six samples of (U, Pu)C, two of UC, and one PuC. The standard deviation of the method was 10 relative percent for O<sub>2</sub> concentrations greater than 50 ppm and 5 ppm for lower concentrations.

Nine samples of (U, Pu)C were analyzed without difficulties for U, Pu, C, and N, and one UC sample for U, C, and N by controlled-potential coulometric, combustion, and Kjeldahl methods. The precision (1 $\sigma$ ) was 0.2 relative percent for the coulometric titration of U and Pu, 0.5 relative percent for the combustion-gravimetric determination of C in the concentration range between 4.65 and 5.02 percent, and about 2 relative percent in measuring N in the ppm concentration range.

Four samples of PuN were analyzed for N by a Kjeldahl-titration method. The precision (1 $\sigma$ ) was 0.3 relative percent in the 5.39 to 5.50 percent N concentration range. A spectrophotometric method, which has a relative standard deviation of 2 percent, was applied to measurement of U in one (U, Pu, Na) chloride salt. No difficulties were experienced. Sodium metal, uranium metal, PuO<sub>2</sub>, PuC and (U, Pu)C were analyzed for spectrographic impurities.

### V. PUBLICATIONS

1. "A Computer Program for Calculation of Particle

Size Distribution from Sedimentation Data," James D. Olson and G. M. Campbell, Los Alamos Scientific Laboratory Report No. LA-4001 (1968).

### VI. REFERENCES

1. Annual Status Report on the Advanced Plutonium Fuels Program, July 1, 1966, to June 30, 1967, Report LA-3745-MS, p. 27.
2. Bowman, A. L., et al. Acta Cryst. 21, 670 (1966).
3. Harper, E. A., et al. Nature 219, 151 (1968).
4. Roof, R. B., Jr., "INDX: A Computer Program to Aid in the Indexing of X-Ray Powder Patterns of Crystal Structures of Unknown Symmetry," Los Alamos Scientific Laboratory Report No. LA-3920 (1968).
5. Marcon, J. P., and Pascard, R., "Sulfures et Seleniures Supérieurs de Plutonium et Des Lanthanides," J. Inorg. Nucl. Chem. 28, 2551 (1966).
6. Allbutt, M., and Junkison, A. R., "Plutonium Chalcogenides," AERE-R 5541, U. K. A. E. A. (1967).
7. Houska, C. R., Union Carbide Research Institute, Report UCRI-TR-18 (1963).
8. Campbell, G. M., manuscript accepted for publication in J. Phys. Chem., Feb. 1969.
9. Lapage, R., and Bunce, J. L., Trans. Faraday Soc. 63, 1889 (1967).
10. Storms, E. K., The Refractory Carbides, Academic Press, New York, N. Y., 1967.
11. Rand, M. H., A Thermochemical Assessment of the Plutonium-Carbon System, presented to the IAEA, Vienna, Sept. 1968.
12. Olson, W. M., and Mulford, R. N. R., Thermodynamics of Nuclear Materials, IAEA, p. 467, Vienna (1968).
13. Harris, P. S., Phillips, B. A., Rand, M. H., and Tetenbaum, M., AERE-R-5353 (1967).
14. Campbell, G. M., Mullins, L. J., and Leary, J. A., Thermodynamics of Nuclear Materials, IAEA, Vienna (1968).
15. Mulford, R. N. R., Ford, J. O., and Hoffman, J. G., Thermodynamics of Nuclear Materials, IAEA, p. 525, Vienna (1962).
16. Hoch, M., and Johnston, H. L., J. Phys. Chem., 65, (1961) 855.

17. Hein, R. A., and Flagella, P. N., GEMP-578 (1968).
18. Kirilin, V. A., Sheindlin, A. E., and Chekhovskoi, V. Ya., Dokl. Akad. Nauk SSSR 142 (6) (1962) 1323.
19. Dench, W. A., Trans. Farad. Soc. 59, 1279 (1963).

PROJECT 464

STUDIES OF Na-BONDED (U,Pu)C AND (U,Pu)N LMFBR FUELS

Person in Charge: D. B. Hall  
Principal Investigators: R. H. Perkins  
G. H. Best

I. INTRODUCTION

(U,Pu)C and (U,Pu)N are regarded as attractive alternates to mixed oxides as fuels for commercial LMFBR application. The high heavy-atom densities and thermal conductivities of the mixed carbide and nitride make it possible for these fuels to outperform mixed oxides. Full exploitation of carbides and nitrides dictates the use of a gap between fuel and clad to accommodate fuel swelling (with minimal fuel-cladding mechanical interactions) and a high thermal conductivity path across the gap to limit fuel temperature. These conditions can be met by filling an annulus between fuel and clad with sodium.

Before a satisfactory sodium-bonded fuel element can be developed, however, information is required that will identify the number and severity of problems associated with sodium bonding and will suggest solutions to these problems. Problem areas that are being studied in this experimental program are:

1. The mechanisms and kinetics of carbon transfer to claddings through the sodium bond.
2. The significant fuel and sodium variables that affect compatibility.
3. The consequences of exposing fuel to coolant sodium.
4. The behavior of sodium-bonded fuel elements under irradiation.
5. The performance limitations of the sodium bond under high-heat-flux conditions.

Efforts are now concentrated on the mixed car-

bide fuel. Type 316 stainless steel is the base cladding material being studied, though vanadium alloys developed by ANL and Westinghouse also will be tested.

As prerequisites for this compatibility program, a number of developmental efforts have been undertaken. These include establishment of (1) techniques for the production of single-phase monocarbide pellets of known composition and dimensions, (2) techniques and equipment for fuel pin loading, bonding, and inspection, and (3) techniques and equipment for determining the distribution of fission products in irradiated fuel pins.

II. SYNTHESIS AND FABRICATION OF (U,Pu)C PELLETS  
(M. W. Shupe, A. E. Ogard, S. McClanahan,  
G. Moore, R. W. Walker)

A. General

Standardized procedures for producing single-phase monocarbide pellets of known composition and dimensions have been developed. These pellets will be utilized in EBR-II irradiation experiments and compatibility testing. Basic process steps are:

1. Multiple arc melting of a physical mixture of  $^{235}\text{U}$ , Pu, and C on a 60-g scale using a graphite electrode.
2. Solution treatment of the arc melted ingot for 24 h at 1600°C.
3. Crushing and grinding of the ingot in a WC vibratory mill, followed by screening of the resulting powder to  $\leq 62 \mu$ .
4. Blending of several powder batches.
5. Elimination of excess carbon by reaction with  $\text{H}_2$  at 850°C.

6. Cold compaction at 20 tsi into pellets without the use of binders or sintering aids.
7. Sintering the pellets in Ar at 1800°C.
8. Characterization of the pellets by linear dimensioning, weighing, metallography, x-ray diffraction analysis, chemical analysis including U, Pu, C, N, O, and spectrochemical analysis for trace impurities, electron microprobe analysis, radiography for determination of possible internal cracks, and isotopic analysis of the U and Pu isotopes.

#### B. Current Results

In addition to the 1012 (U,Pu)C pellets previously reported, 464 more pellets were prepared this period. The single phase monocarbide pellet inventory remaining is 925. This is 80 pellets over the requirement schedule so efforts will be devoted to refinement of process variables. No effort was allocated for the preparation of nitride pellets for compatibility testing during this period.

The results of characterization of pellets produced by the above process during this period are shown in Table 464-I. These results were obtained on statistically selected samples from the different lots. A typical pellet microstructure of (U,Pu)C is shown in Fig. 464-1.

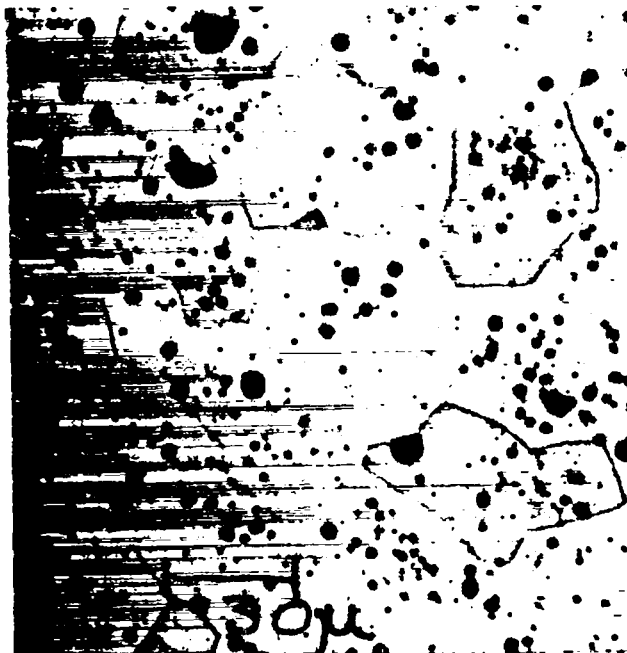


Fig. 464-1. Typical single-phase (U,Pu)C, electrolytic etch, 380X.

For irradiation studies in EBR-II, 330 pellets of single-phase (U,Pu)C were loaded into vacuum-tight transfer cans under a pure Ar atmosphere for transfer to the fuel pin loading facility. Statistical compilations for samples taken from this block of pellets are as follows: All pellets were x-ray radiographed and were found to be free of detectable cracks and chips. The average chemical composition is  $(U_{0.797}Pu_{0.203})(C_{0.97}O_{0.006}N_{0.005}H_{0.001})$ . The average density obtained by immersion techniques is  $89.1 \pm 1.6\%$  of theoretical. Averaged analyses for

Table 464-1  
Characterization of  $U_xPu_yC_z$  Pellets

Material No.	X	Y	Z	O	N	Diam (in.)	% of Theor. Density	Pellet Microstructure
23	0.795	0.205	0.98	0.005	0.004	0.262	(90.4)	MC
24	0.795	0.205	0.96	0.005	0.004	0.265	90.4	MC
25	0.795	0.205	0.97	.....	0.004	0.263	89.4	MC
26	0.795	0.205	0.96	0.005	0.004	0.263	89.8	MC
27	0.795	0.205	0.98	.....	.....	0.263	90.1	MC, I

Note: I indicates < 0.5 v/o impurity phase.

Densities in ( ) are mechanically measured.

impurities are shown in Table 464-II. The average x-ray lattice dimension was found to be  $4.956 \pm 0.001 \text{ \AA}$ . Single-phase monocarbide microstructures

Table 464-II  
Average Spectrochemical Analysis  
of  $U_{0.8}Pu_{0.2}C$  Pellets

Element	ppm	Element	ppm
Li	< 1	Ni	20
Be	< 1	Cu	40
B	< 1	Zn	< 10
Na	< 2	Sr	< 5
Mg	< 5	Zr	< 100
Al	< 10	Nb	< 50
Si	100	Mo	< 10
P	< 50	Cd	< 10
Ca	< 5	Sn	< 2
Ti	< 50	Ba	< 10
V	< 5	Ta	< 1000
Cr	< 10	W	20
Mn	< 2	Pb	< 2
Fe	60	Bi	< 2
Co	< 5		

Note: The "<" sign is a normal limit of detectability.

were found; no uncombined metal or higher carbide phases were present. A few inclusions were found in some specimens, generally less than  $3 \mu$  wide and the amounts were much less than 0.5 w/o as determined by point counting methods. Examination of etched samples by electron microprobe showed the samples to be homogeneous on a macro scale.

The diametral characteristics for the 330 pellets packaged for transfer for EBR-II irradiations are shown in Fig. 464-2.

In addition, 149 pellets of single-phase  $^{238}U$  insulator pellets were prepared during this period. Using the provided transfer containers, 105 of these single-phase UC pellets have been loaded and are waiting transfer. A typical single-phase UC microstructure is shown in Fig. 464-3.

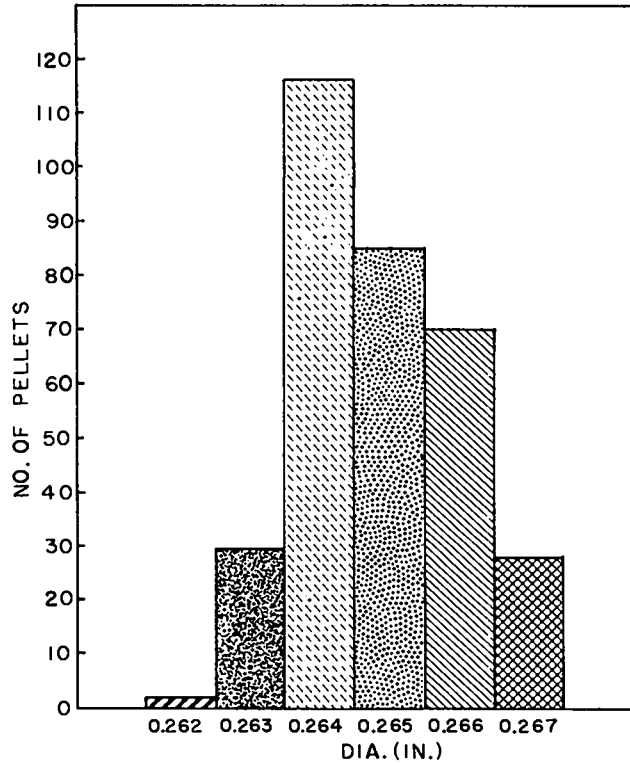


Fig. 464-2. Diametral characteristics of single-phase (U,Pu)C pellets for irradiations.

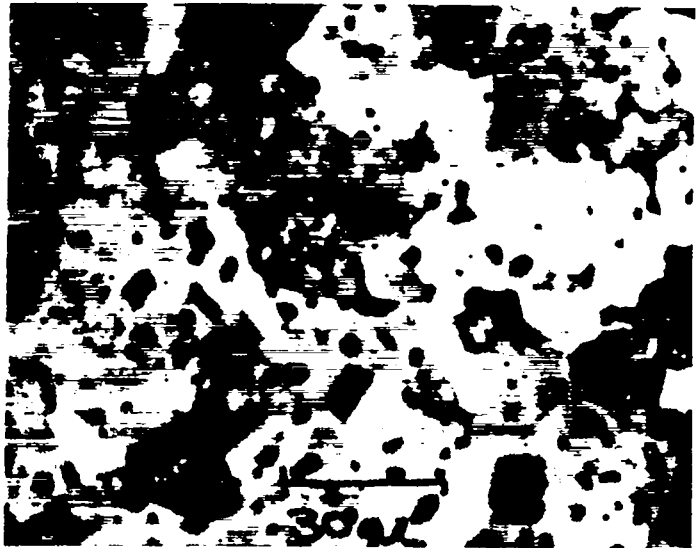


Fig. 464-3. Typical single-phase UC, stain etch, 380X.

### III. LOADING FACILITY FOR TEST CAPSULES (D. N. Dunning)

#### A. General

A prerequisite to a compatibility program involving (U,Pu)C and sodium is a satisfactory

capsule loading and bonding facility. There is little point to obtaining well-characterized materials for testing if these materials are contaminated before they are placed in test. Sodium and (U,Pu)C are sufficiently reactive that all operations must be performed either in vacuum or in a high-quality inert atmosphere. A loading facility for handling these materials is now operational, though it is not yet complete. An inert-atmosphere glovebox and an inert-gas cleanup system to facilitate handling fuel pellets prior to their insertion into capsules have been installed, but they have not yet been made operational.

#### B. Current Results

An investigation of gas purity in inert boxes during loading operations has been initiated and initial data have been obtained. At present the monitoring equipment on the sodium loading facility consists of a Model 303 CEC moisture monitor and a Model 207E Westinghouse oxygen meter on the box discharge line and a Thermox Model 1 oxygen meter in the box interior. Attempts to cross-check the oxygen meters have not been successful because the Westinghouse unit is sensitive to gas flow rate at low flow rates.

Inert gas samples from the sodium loading box were taken at various times during operations for analysis on a mass spectrometer (CEC Model 21-620). The following information was obtained:

1. Prior to the introduction of sodium, the CEC moisture monitor indicated 4.5 ppm  $H_2O$  and the oxygen meter indicated  $\sim 1$  ppm  $O_2$  were present in the glovebox atmosphere. Mass spectrometer analyses indicated a trace to 4 ppm  $H_2O$ , 10 ppm  $O_2$ , and no  $H_2$  were present.
2. After introduction of sodium into the glovebox, the moisture monitor indicated 4.5 ppm  $H_2O$ , and the oxygen meter reading was below 0.1 ppm. This meter gives low readings when hydrogen is present, so it is assumed that the low oxygen reading was due to hydrogen in the box atmosphere. Mass spectrometer analyses of gas samples indicated a trace to 4 ppm  $H_2O$ , 5 to 10 ppm  $O_2$ , and 2 to 4 ppm  $H_2$  were present.
3. After an additional 4 days of standby

(no manipulations within the box) with sodium in the glovebox, the instrument readings were unchanged, and the mass spectrometer indicated that 4 ppm  $H_2O$ , 6 to 7 ppm  $O_2$ , and 3 to 6 ppm  $H_2$  were present.

#### IV. CARBIDE FUEL COMPATIBILITY STUDIES (F. B. Litton, L. A. Geoffrion, J. H. Bender)

##### A. General

The objectives of this program are to study the interactions among single-phase mixed (U,Pu)C, a sodium bond, and potential cladding materials, i.e., to investigate the technology related to sodium-bonded fuel elements. There are two approaches to the experimental work. One approach is to determine the reactions occurring between  $(U_{0.8}Pu_{0.2})C$  and potential cladding materials, using Type 316 stainless steel and a high-strength vanadium-base alloy as the first and second choices of cladding material, respectively. A second concurrent set of experiments is designed to study the mechanism of carbon transport through sodium, the effect of impurities such as oxygen, and the carburizing potential of sodium in mutual contact with carbides and the preferred cladding materials.

Capsules containing sodium-bonded, single-phase (U,Pu)C are tested in sodium loops at 750°C for periods up to 10,000 h. High-purity, thoroughly-characterized sodium is used for the studies. Fuels of known composition are used in all tests. Most of the testing is performed on single-phase (U,Pu)C fuel in which the Pu/U ratio is maintained at 0.2, but some experiments are being carried out on material containing a second phase (either metallic or carbon-rich). Other experiments are being carried out on stoichiometric and hyperstoichiometric UC to determine the effect of plutonium addition on the behavior of the carbide fuel.

##### B. Current Results

###### 1. Stabilities of Metal Carbides

A literature search on the stabilities of metal carbides of interest to this program has been completed. The data on fuel carbides are shown in Table 464-III. Information from several sources were compared and evaluated, and it is thought that these values are the most accurate. The mixed

sesquicarbide appears to be almost as stable as UC. The standard free energies of formation of possible reaction product carbides from elements that are present in potential clad materials are recorded in Table 464-IV. On the basis of the standard free energies of formation for the pure compounds, chromium and molybdenum carbides appear to be the most stable carbides in Type 316 stainless steel. A

high-strength vanadium alloy for LMFBR application has not been selected; however, probable constituents of this alloy include iron, chromium, titanium, zirconium, and tungsten. Titanium, zirconium, and chromium carbides should form in preference to vanadium carbide.

Available free-energy data for the principal impurities in bond sodium are shown in Table 464-V.

Table 464-III  
Free Energy of Formation vs Temperature of Fuel Carbides

- $\Delta G_T^\circ$ , kcal/mole Carbon

Temp (°C)	(U <sub>0.8</sub> Pu <sub>0.2</sub> ) <sub>2</sub> C <sub>3</sub> <sup>(1)</sup>	UC <sup>(2)</sup>	PuC <sup>(3)</sup>	U <sub>2</sub> C <sub>3</sub> <sup>(2)</sup>	Pu <sub>2</sub> C <sub>3</sub> <sup>(3)</sup>	UC <sub>2</sub> <sup>(2)</sup>
450	18.4	18.3	15.5	17.0	13.9	10.9
550	18.0	18.5	15.3	17.0	13.4	11.3
650	17.6	18.7	15.1	17.1	12.9	11.7
750	17.2	18.8	14.9	17.1	12.5	12.1

Table 464-IV  
Free Energy of Formation vs Temperature for Potential Clad Carbides

- $\Delta G_T^\circ$ , kcal/mole Carbon<sup>(4)</sup>

Temp (°C)	Fe <sub>3</sub> C	Ni <sub>3</sub> C	Cr <sub>23</sub> C <sub>6</sub>	Mo <sub>2</sub> C	Mn <sub>3</sub> C	VC	TiC	ZrC	WC
450	-2.1	-6.9	17.5	6.7	3.5	11.3	42.5	36.5	8.4
550	-1.5	-6.7	17.6	--	3.5	11.2	41.8	--	--
650	-0.9	-6.5	17.8	--	3.6	11.0	41.5	--	--
750	-0.3	-6.4	17.9	--	3.6	10.9	41.3	--	--

Table 464-V  
Free Energy of Formation vs Temperature for Potential Carbides in Bond Sodium

- $\Delta G_T^\circ$ , kcal/mole Carbon

Temp (°C)	Na <sub>2</sub> C <sub>2</sub> <sup>(5)</sup>	CaC <sub>2</sub> <sup>(4)</sup>	Al <sub>4</sub> C <sub>3</sub> <sup>(4)</sup>	SiC <sup>(4)</sup>	K <sub>2</sub> C <sub>s</sub>	MgC <sub>2</sub> <sup>(4)</sup>
450	6.6	8.9	10.9	11.6	--	-10.5
550	--	9.4	10.9	11.4	--	--
650	--	9.8	10.8	11.2	--	--
750	*	10.2	10.5	11.0	--	--

\*Decomposition temperature 1073°K.

2. Compatibility of Mixed Carbides with Type 316 Stainless Steel

Three Type 316 stainless steel capsules (0.3-in. o.d. x 0.010-in. wall x 3 in. long) were metallographically examined after being tested in sodium at 750°C for 4000 h. The capsules contained essentially single-phase  $(U_{0.804}Pu_{0.196})(C_{0.95}O_{0.016})$  pellets bonded with about 1 g sodium.

The metallographic structures of the capsules and pellets were not altered during the compatibility test. Although one localized area on a capsule surface darkened when etched, there was no evidence of carburization of the capsule wall. There was also no evidence to indicate reaction with the sodium bond during the compatibility test.

3. Compatibility of Mixed Carbide with V-15Ti-7.5Cr Alloy

Five capsules of V-15Ti-7.5Cr were loaded with essentially single-phase mixed carbide pellets selected from two compositions:  $(U_{0.807}Pu_{0.203})(C_{0.967}O_{0.005})$  and  $(U_{0.814}Pu_{0.186})(C_{0.950}O_{0.008})$ . The capsules were 0.3-in. o.d. x 0.010-in. wall x 3 in. in length and contained 1.0 g of bond sodium. Two capsules were tested at 650°C in hot-trapped sodium for 1000 h and three at 750°C for 1000 h.

After the 650°C test there was no evidence of reaction on either the pellets or the interior surfaces of the capsules. The microstructures are shown in Figs. 464-4 and 464-5. However, during

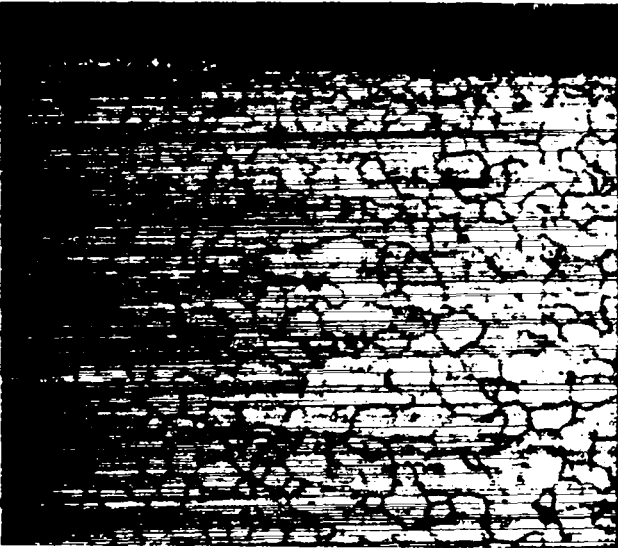


Fig. 464-4. Microstructure of V-15Ti-7.5Cr alloy capsule tested at 650°C for 1000 h. Etched, 400X.



Fig. 464-5. Microstructure of mixed carbide pellet tested at 650°C for 1000 h. Etched, 300X.

the 750°C test, plutonium penetrated one of the three capsules. The reaction layer on the surface of the bottom pellet is shown in Fig. 464-6.

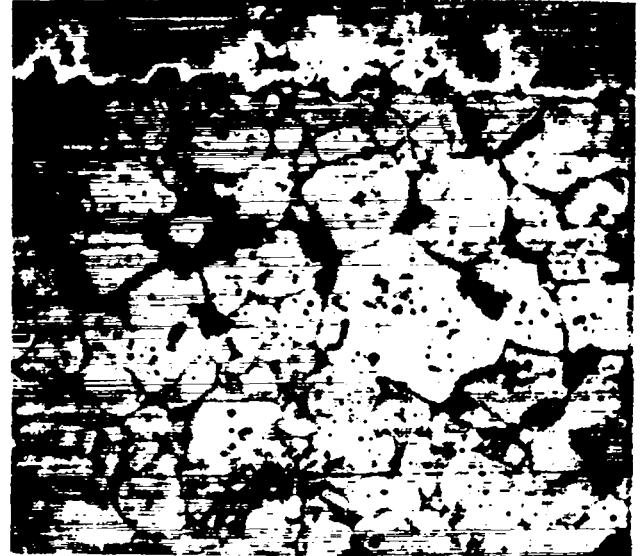


Fig. 464-6. Reaction layer at surface of carbide pellet. Etched, 300X.

Attack on the capsule was observed opposite this reaction layer and along the wall at the junction of the bottom and middle pellets. The attack on the capsule wall is shown in Fig. 464-7. Examination of the remaining two capsules tested at 750°C failed to show any reaction between the pellets and the clads.

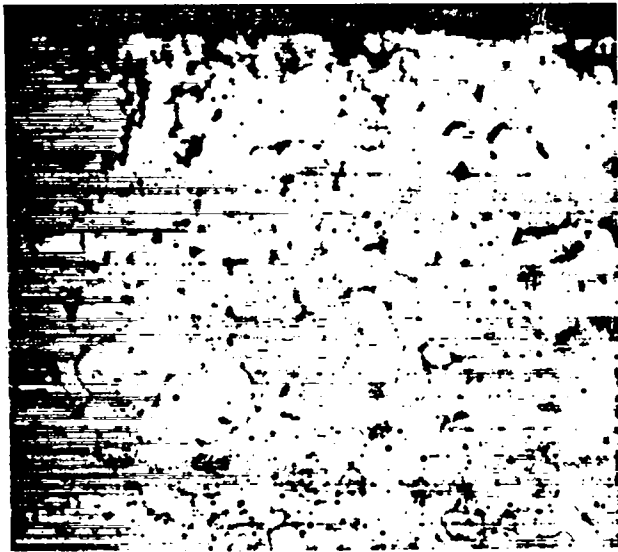


Fig. 464-7. Microstructure of capsule wall showing attack. Etched, 300X.

A diffusion zone was observed on the outside of the capsules which were tested at 650°C. This diffusion zone is shown in Fig. 464-8. A similar,



Fig. 464-8. Diffusion zone on outside of V-15Ti-7.5Cr alloy capsule. Tested in 650°C sodium for 1000 h. Etched, 400X.

but less pronounced, diffusion layer was observed on the exterior of the capsules tested at 750°C.

#### 4. Effect of Oxygen in Bond Sodium on Compatibility

In experiments with defected capsules containing (U,Pu)C, it was shown that carbon was trans-

ferred by loop sodium from essentially single-phase pellets to the Type 316 stainless steel container. Oxygen in the sodium was suspect, so additional experiments have been carried out to show conclusively that oxygen addition to the bond sodium results in carbon transfer.

Essentially single-phase mixed monocarbide pellets were loaded in Type 316 stainless steel capsules, and ~ 5 g of bond sodium containing ~ 1.25% oxygen was added to each capsule. These capsules, along with controls (no oxygen addition to the bond sodium), were tested for 1000 h at 550, 650, and 750°C. Metallographic examination after test showed that carbon was moved from single-phase mixed monocarbide pellets to the Type 316 stainless steel in capsules containing excess oxygen in the sodium bond. No carbon transfer was observed in the capsules containing low-oxygen sodium. The extent of carburization at 550°C is shown in Fig. 464-9. A Widmanstatten-type precipitate was



Fig. 464-9. Carburization of Type 316 stainless steel containing oxygen-contaminated sodium and (U,Pu)C pellets. Heated at 550°C for 1000 h. Etched, 300X.

observed near the surfaces of the fuel pellets that reacted with oxygen. This is shown in Fig. 464-10. These surfaces were cracked and tended to disintegrate. X-ray analyses showed that the products from the disintegration of the pellets (residue remaining in the capsules after sodium distillation) consisted of a mixture of (U,Pu)O<sub>2</sub> and (U,Pu)C. The surface material from the fuel pellet consisted

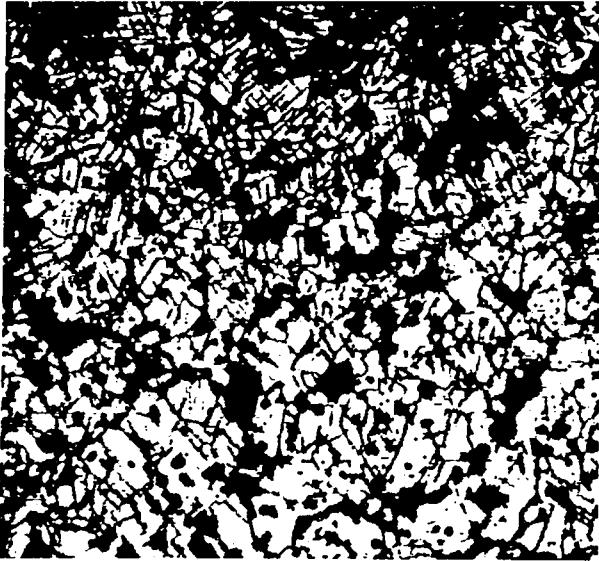


Fig. 464-10. Surface of fuel pellet that reacted with oxygen in the sodium bond. Heated at 750°C for 1000 h. Etched, 300X.

largely of dioxide and some monocarbide. In contrast to this, examination of the surface material from a pellet from a control capsule showed only the presence of (U,Pu)C. Chemical analysis of a pellet from a control capsule tested at 650°C for 1000 h showed that it contained 4.60% C, 0.12% O, and 230 ppm N. A pellet heated in oxygen-contaminated sodium contained 4.53% C, 0.68% O, and 270 ppm N.

The carbon transfer may result from precipitation of either carbon or a higher carbide in the fuel during the reaction of oxygen from the sodium with the fuel. The most probable thermodynamically stable phases are carbon and sesquicarbide. The data do not indicate the presence of sesquicarbide.

##### 5. Effect of Sesquicarbide Content on the Compatibility of Type 316 Stainless Steel with Sodium-Bonded Carbide Pellets

The objective of this study is to determine if sodium-bonded hyperstoichiometric fuel pellets are compatible with Type 316 stainless steel when the structure consists of sesquicarbide distributed in a monocarbide matrix. The experimental program consisted of two approaches: (1) heat-treat specimens of uranium carbide (5.13% C, 0.39% O) for 24 and 100 h at 1600°C to convert the UC<sub>2</sub> to the U<sub>2</sub>C<sub>3</sub> phase, followed by testing in sodium, and (2) determine the equilibrium phases in uranium carbide

(5.13% C, 0.39% O) after repeated compatibility tests in Type 316 stainless steel capsules.

Compatibility tests were completed on two capsules containing heat-treated specimens of uranium carbide and three capsules containing as-received specimens. Each of the capsules contained ~ 5 g of -10 to +14 mesh powder and ~ 5 g of sodium metal. They were tested for 1000 h at 750°C. The capsules were inverted at temperature to separate the bulk of the sodium from the uranium carbide. Residual sodium was removed from the specimens by dissolution in 95% ethyl alcohol, followed by washing in dilute acidic ethyl alcohol to remove traces of sodium oxide, and vacuum drying.

Extensive carburization was observed on the capsules containing specimens that were not heat-treated, in contrast to limited carburization on the capsule containing the specimen heat-treated for 24 h, and localized carburization on the capsule containing the specimen heat-treated for 100 h. The capsules containing as-received uranium carbide were bulk carburized to a depth of 0.003 in. and carburized in the grain boundaries to at least 0.010 in. The capsule containing uranium carbide heat-treated for 24 h was bulk carburized to a depth of 0.001 in. and carburized in the grain boundaries to a depth of about 0.005 in. The capsule containing uranium carbide heat-treated for 100 h was carburized only on localized regions during the compatibility test. The extent of carburization was confirmed by microhardness measurements as shown in Table 464-VI.

The differences in the ability of hyperstoichiometric uranium carbide subjected to different heat treatments to carburize the stainless steel capsules are attributed to differences in the dicarbide content. However, the stability of the dicarbide phase is related to the oxygen content of the uranium carbide. Consequently, a small arc-melted UC<sub>1.04</sub> ingot of low oxygen content for further compatibility tests was prepared. After this material was heat-treated for 116 h at 1350°C, a preliminary x-ray pattern indicated the presence of the equilibrium phases, UC and U<sub>2</sub>C<sub>3</sub>. To conclude this phase of the experimental program, fuel pellets containing about 10 v/o (U,Pu)<sub>2</sub>C<sub>3</sub> are being prepared by United Nuclear Corporation and Group CMB-11 at LASL.

Table 464-VI  
 Microhardness of Type 316 Stainless Steel Capsules  
 After Compatibility Tests with Uranium Carbide  
 (DPH, 25 g load, 50 sec)

Distance from Surface (in. x 10 <sup>-3</sup> )	Uranium Carbide As-Received	Uranium Carbide Heat-Treated (24 h at 1600°C)	Uranium Carbide Heat-Treated (100 h at 1600°C)	
			Uncarburized Area	Carburized Area
1	322	274	128	193
2	--	254	135	168
3	--	201	131	143
4	--	220	142	135
5	270	193	122	138
6	--	193	160	128
7	--	186	151	118
8	--	193	162	111
9	--	193	143	128
10	243	188	151	114

6. Behavior of Vanadium-Titanium Alloys in Hot-Trapped Sodium

Vanadium has been proposed as a backup cladding material to stainless steel for the liquid-metal fast breeder reactor. Vanadium alloys have the potential of contributing low neutron absorption,<sup>6</sup> little susceptibility to fast-neutron damage, good strength at relatively high temperatures,<sup>7</sup> and suitable compatibility with sodium<sup>8</sup> and potential fuel materials. However, there is a need for acquiring a comprehensive background on the corrosion of vanadium alloys in sodium of known impurity content.

Specimens of the alloys listed in Table 464-VII were tested for 1000 h in hot-trapped, forced-convection sodium loops at 450, 550, 650, and 750°C. Additional 4000-h tests were run at 650 and 750°C, as shown in Table 464-VIII. The corrosion tests were conducted on six annealed specimens from each material (total surface area of about 19.5 cm<sup>2</sup>) and the average weight change was calculated. One specimen was used for metallographic, electron microprobe, and microhardness examinations, and the other five specimens for chemical analysis.

The weight losses of the vanadium alloys in 450°C sodium after 1000 h, shown in Table 464-VII, were comparable to those observed for Type 304 and 316 stainless steels. However, at higher temperatures, the stainless steel specimens continued to

show little weight change, while the vanadium alloys predominantly gained weight. This weight gain appeared to be a function of both temperature and oxygen content of the sodium. Assuming a density of 6.0 g/cm<sup>3</sup> for vanadium alloys, a weight loss of 0.6 mg/cm<sup>2</sup> is equivalent to a metal loss of 1 micron. The weight changes recorded in Table 464-VII for the vanadium alloys were small, but the weight gains in some cases and losses in others indicated that two mechanisms may be involved in the behavior of these alloys in sodium: (1) dissolution (mass transfer), and (2) adsorption and subsequent diffusion of impurities into the vanadium alloys.

The titanium-containing binary alloys tested at 650 and 750°C gained more weight than vanadium by a factor of two in both the 1000- and 4000-h tests. The V-15Ti-7.5Cr alloy performed poorly in the 650 and 750°C tests. In tests at 650°C the V-15Cr-5Ti alloy gained considerably less weight than the V-15Ti-7.5Cr alloy.

A brownish deposit, which was identified by x-ray diffraction analysis as titanium nitride, was observed on the vanadium specimens after the 1000-h, 750°C-tests. The surfaces in all other tests were metallic, from bright metallic to a matte finish.

An extremely hard zone at the surface of titanium-bearing alloys was observed after the 550°C, 1000-h corrosion test. The specimens of these alloys that were tested at 650 and 750°C also exhibited

Table 464-VII  
Corrosion of Alloys in Hot-Trapped Sodium, 1000-h Test

Material	Weight Change (mg/cm <sup>2</sup> ) at Indicated Specimen Temp (°C)			
	450°	550°	650°	750°
V	None	-0.37	-0.02	+0.25
V-10Ti	-0.01	+0.11	+0.03	+0.47
V-20Ti	-0.02	--	+0.04	+0.44
V-40Ti	None	+0.09	+0.11	+0.39
V-15Ti-7.5Cr	-0.01	+0.04	+0.24	+0.83
V-15Cr-5Ti	-0.01	--	--	--
Type 304 SS	-0.01	None	-0.04	-0.23
Type 316 SS	-0.01	None	-0.04	--

Table 464-VIII  
Corrosion of Alloys in Hot-Trapped Sodium, 4000-h Test

Material	Weight Change (mg/cm <sup>2</sup> ) at Indicated Specimen Temp (°C)	
	650°	750°
V	+0.08	+0.58
V-10Ti	+0.18	+1.25
V-20Ti	+0.16	+1.14
V-40Ti	+0.60	+1.78
V-15Ti-7.5Cr	+0.59	+1.72
V-15Cr-5Ti	+0.12	--
Type 304L SS	None	-1.02
Type 316L SS	-0.01	-1.48

thin hardened zones near the sample surfaces, but hardening was less pronounced in these cases. The unalloyed vanadium specimens exhibited neither hardness increases nor hardness gradients after test. Apparently the diffusing species in the vanadium samples had little effect on hardness. The microhardness of Type 304 stainless steel was not affected by the corrosion tests.

Chemical analyses for oxygen, carbon, and nitrogen were obtained on specimens heated for 1000 h at 500 and 650°C, and for 4000 h at 750°C. These analyses, which are shown in Tables 464-IX, 464-X, and 464-XI, are compared to the content of those elements in as-received specimens. With the exception of unalloyed vanadium, which decreased in oxygen content at the 650 and 750°C test temperatures, oxygen and carbon were the primary impurities

absorbed by the alloys during the tests, although some of the specimens increased in nitrogen content.

A randomly selected test specimen from each series of corrosion tests was mounted in stainless steel clamps and polished for metallographic examination. The samples were etched by swabbing with a 1:1:2 mixture by volume of hydrofluoric acid, nitric acid, and water.

The characteristic microstructure of vanadium after corrosion testing is shown in Fig. 464-11. The primary microstructural feature is the absence of a diffusion zone at the surface. A diffusion zone in unalloyed vanadium was not observed on any of the examined test specimens.

A typical view of the microstructure of V-40Ti alloy is shown in Fig. 464-12. The binary titanium alloys and the V-15Ti-7.5Cr alloy showed a hardened

Table 464-IX  
Analyses of Test Specimens after 1000 h at 550°C  
in Sodium Containing 5-9 ppm Oxygen

Material	Composition (ppm)					
	Oxygen	Change in Oxygen Content	Carbon	Change in Carbon Content	Nitrogen	Change in Nitrogen Content
V	790	+400	520	+100	440	+190
V-10Ti	3300	+2840	520	+290	580	+444
V-40Ti	2800	+2380	470	+299	400	+224
V-15Ti-7.5Cr	2500	+1805	580	+347	340	-120
V-15Cr-5Ti	1700	+930	820	+567	460	+353

Table 464-X  
Analyses of Test Specimens after 1000 h at 650°C  
in Sodium Containing 2-5 ppm Oxygen

Material	Composition (ppm)					
	Oxygen	Change in Oxygen Content	Carbon	Change in Carbon Content	Nitrogen	Change in Nitrogen Content
V	110	-280	700	+280	320	+70
V-10Ti	1500	+1040	460	+230	210	+74
V-20Ti	2100	+1380	590	+393	160	+13
V-40Ti	1300	+880	215	+44	65	-111
V-15Ti-7.5Cr	820	+125	390	+157	225	-235

Table 464-XI  
Analyses of Test Specimens after 4000 h at 750°C  
in Sodium Containing 1-3 ppm Oxygen

Material	Composition (ppm)					
	Oxygen	Change in Oxygen Content	Carbon	Change in Carbon Content	Nitrogen	Change in Nitrogen Content
V	85	-305	1120	+700	*	
V-10Ti	3000	+2540	1000	+770	< 50	--
V-20Ti	3000	+2280	1120	+923	320	+173
V-40Ti	2300	+1880	500	+329	365	+189
V-15Ti-7.5Cr	2200	+1505	585	+352	365	-95

\*Insufficient for analysis.

diffusion area at the surface and a zone of precipitation immediately underneath it. In addition, these alloys showed general precipitation of a second phase throughout the cores of the test specimens. The V-15Cr-5Ti alloy did not show these general characteristics. A view of this alloy after testing at 550°C is shown in Fig. 464-13.

Intergranular corrosion was observed at the surface of V-20Ti alloy after heating in sodium for 4000 h at 750°C; this is shown in Fig. 464-14. Corrosion occurred along the grain boundaries which

contained a complex two-phase precipitate. General precipitation of a second phase was observed along the grain boundaries as well as within the matrix in this specimen.

In contrast to the two phase precipitate in the V-20Ti alloy, a crystalline phase was observed in the V-15Ti-7.5Cr alloy (Fig. 464-15). No intergranular corrosion of the V-15Ti-7.5Cr alloy was observed after 4000 h at 750°C.



Fig. 464-11. Microstructure of unalloyed vanadium. Heated in sodium at 550°C for 1000 h. Etched, 200X.

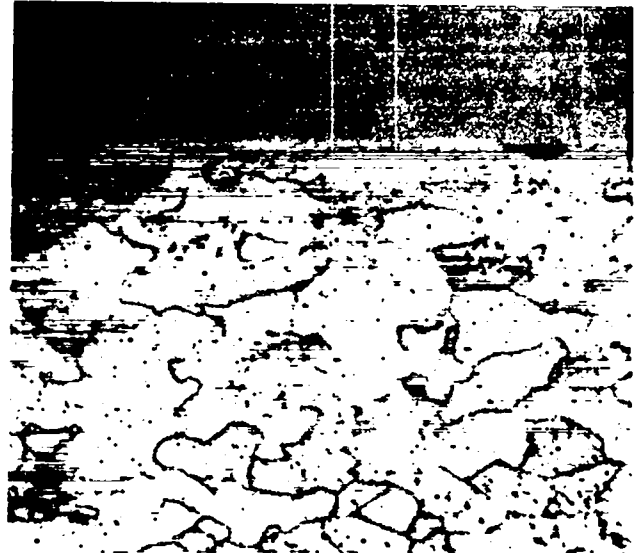


Fig. 464-13. Microstructure of V-15Cr-5Ti alloy. Heated in sodium at 550°C for 1000 h. Etched, 600X.



Fig. 464-12. The surface of V-50Ti alloy. Heated in sodium at 550°C for 1000 h. Etched, 600X.



Fig. 464-14. Intergranular corrosion at the surface of V-20Ti alloy. Heated in sodium at 750°C for 4000 h. Etched, 1200X.

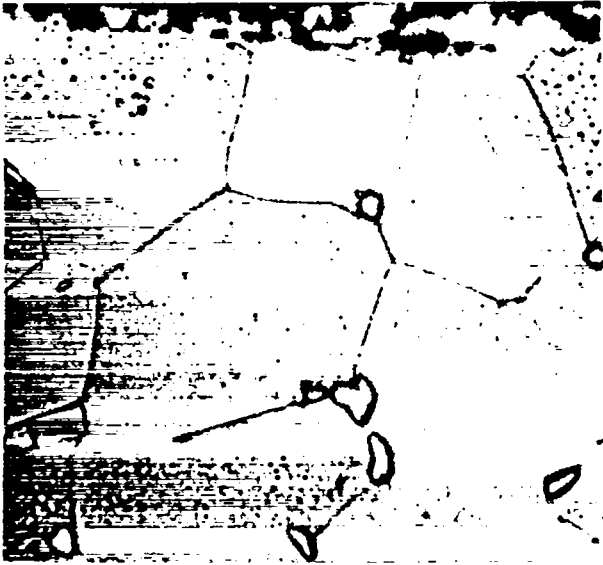


Fig. 464-15. Crystalline precipitates in the grain boundaries of V-15Ti-7.5Cr alloy. Heated in sodium at 750°C for 4000 h. Etched, 1340X.

V. EBR-II IRRADIATION TESTING  
(J. O. Barner)

A. General

The purpose of these irradiations is to evaluate candidate fuel/sodium/clad systems for the LMFBR program. In the reference design, pellets of single-phase (U,Pu)C are separated by a sodium bond from a cladding of Type 316 stainless steel or other high-temperature alloy. Seven fuel-element tests are planned in the initial group of a continuing series of EBR-II irradiation experiments.

The capsules are to be irradiated under the following conditions:

1. Lineal power: 29.15 to 30.20 kW/ft (max).
2. Fuel composition:  $(U_{0.8}Pu_{0.2})C$ , (single-phase, sintered, fully enriched).
3. Fuel density: 90% of theoretical.
4. Smear density: 80%.
5. Clad size: 0.300-in.-o.d. x 0.010 in.-wall.
6. Fuel size: 0.265-in.-diam x 0.25-in.-high pellets.
7. Clad type: 316 SS.
8. Maximum clad temperature: 1250°F.
9. Maximum fuel centerline temperature: 2130°F.
10. Burnup: 0.22 to 0.66 g fissioned per  $cm^3$ .

B. Current Results

LASL-42B is currently operating in the EBR-II

reactor at a maximum power of  $\sim 29.5$  kW/ft. The capsule has accumulated 818 MWD burnup out of a projected 3125 MWD ( $\sim 17,600$  MWD/T).

The remaining six irradiation capsules will be loaded during the next quarter.

VI. GAMMA SCANNING AND RELATED STUDIES  
(D. M. Holm, W. M. Sanders, B. M. Moore,  
B. K. Barnes)

A. General

Gamma scanning is a nondestructive technique for obtaining information on the distribution of fission products and activation products in fuel elements. A new advanced semiconductor detector system has been constructed for this purpose, and additional apparatus has been built for determining gamma-ray spectra of short-lived fission products from fast fission of plutonium.  $^3He$  activation has also been studied as a method of determining the concentration and distribution of impurities in stainless steel.

B. Current Results

1. Semiconductor Detector System

The intrinsic full-energy peak efficiency for the 25-cm<sup>3</sup> Ge(Li) detector was measured, and corrections were applied for gamma-ray leakage through the sides of the lead collimators and for absorption in the rabbit and end station. Figure 464-16 shows the percentage of the gamma rays that are located in the full-energy peak striking the detector at a particular energy. The decrease in efficiency with decreasing energy below 0.1 MeV is caused by absorption in the aluminum case of the cryostat and the  $n^+$  layer of germanium.

The first model of new gold conical collimators was fabricated. These collimators are designed to increase the counting rate of the detector without a loss in spatial resolution on the sample.

2. Development of Techniques

Experiments were performed to determine the ratio of  $^{101}Rh$  to  $^{102}Rh$  in a low-activity sample. The low activity coupled with complex decay schemes of the isotopes presented new problems in counting. Various combinations of detectors and geometries were tested to determine the optimum conditions for counting. The two low-energy lines (127 and 197 keV)

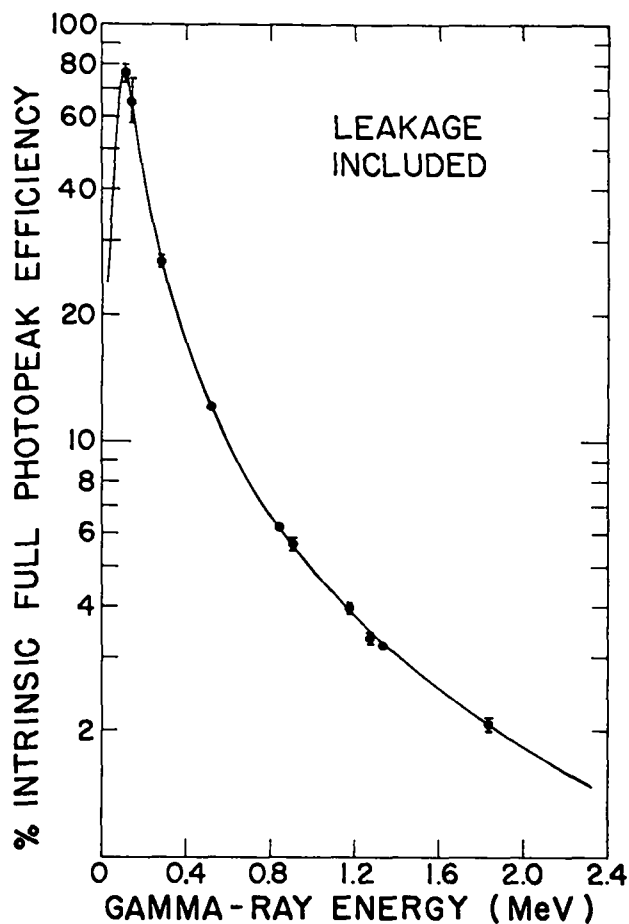


Fig. 464-16. Intrinsic full-energy peak efficiency for 25-cm<sup>3</sup> Ge(Li) detector with corrections for gamma-ray leakage and absorption.

from <sup>101</sup>Rh could not be seen in the spectrum taken with a 6-cm<sup>3</sup> Ge(Li) detector, but they were easily detected with a 25-cm<sup>3</sup> Ge(Li) detector. The difference in the results from the two detectors is caused by the better resolution, total efficiency, and peak-to-total ratio of the larger detector. The low activity of the sample required that the sample be placed near the detector, but the gamma rays in cascade prevented normal anticoincidence operation. Therefore, a hollow tantalum cylinder was placed around the sample to form a collimator that shielded the large (13-1/2-in.-diam by 6-in.-long) NaI anticoincidence detectors from the source (Fig. 464-17). This configuration reduced the Compton continuum under the 127- and 197-keV peaks to one-eighth and one-fourth, respectively, of its value for the single spectrum taken with the germanium detector alone.

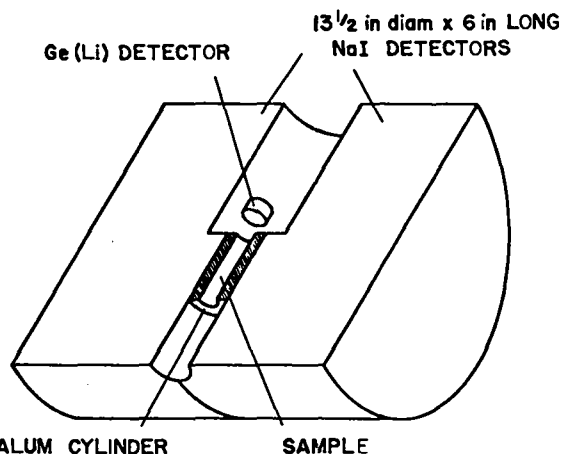


Fig. 464-17. Counting geometry for low-activity sample.

A disk from an irradiated UO<sub>2</sub>-PuO<sub>2</sub> (2 wt %) fuel rod was borrowed from Pacific Northwest Laboratory (PNL). The results from scanning this sample are summarized in Figs. 464-18 and 464-19. The sample was about 0.5 in. in diameter and 0.125 in. thick. It was scanned with a 0.031-in.-diam pinhole, and each spectrum was accumulated for 160 min. The photomicrographs shown below the data plots are at approximately the same scale as the plots. PNL had taken microsamples from the holes in the sample; these holes were removed by polishing in the sample that was scanned. Consultations with personnel at PNL reveal good correlation of our results with those obtained from microsampling. Our results have more data points and have less uncertainty than those obtained from microsampling. It appears that the <sup>106</sup>Rh concentrates at the interface of melting (shown by a saddle in the center of Fig. 464-18) and at the recrystallization interface (peaks on both sides of the saddle. The dimensions of the peaks are similar to those expected from two well-defined ring concentrations that are less than 0.020 in. in radial thickness. Therefore, pinhole collimators smaller than 0.031-in. diam should give a better indication of the actual distribution.

### 3. <sup>3</sup>He Activation

Because the Van de Graaff accelerator is used to accelerate many different ions, care must be

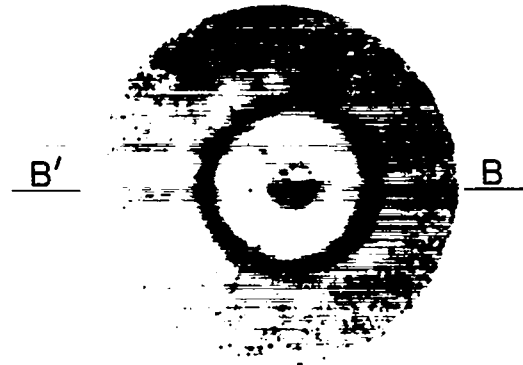
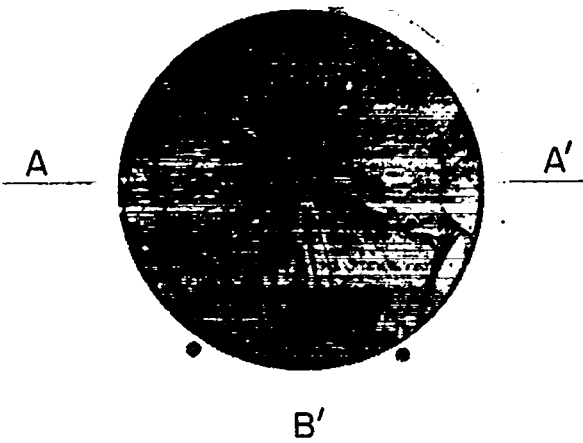
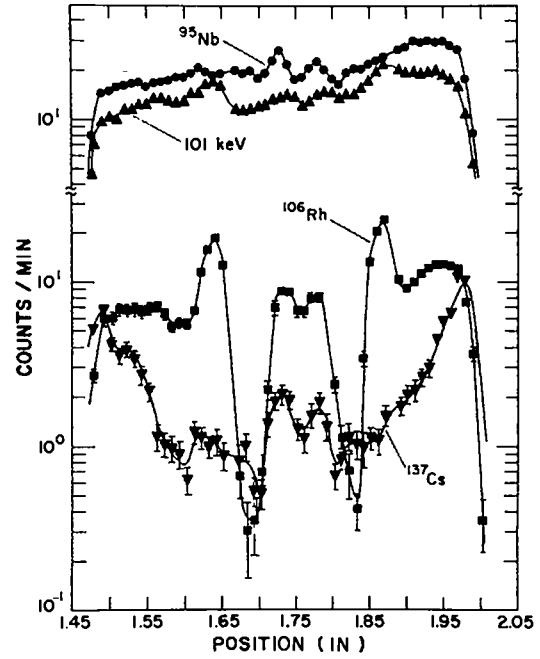
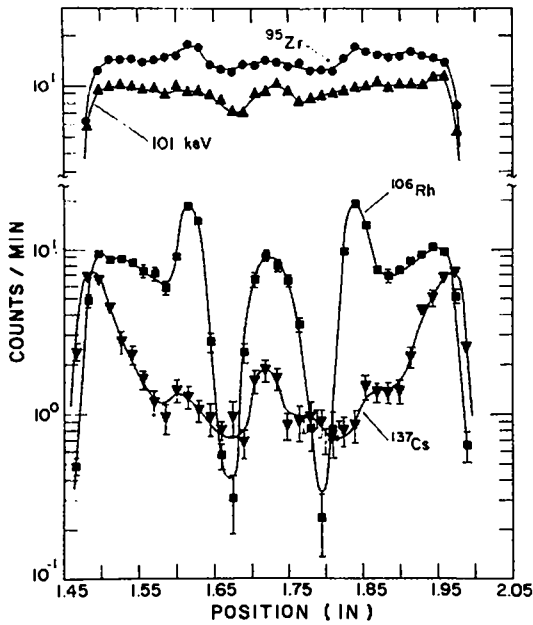


Fig. 464-18. The distributions of <sup>95</sup>Zr, <sup>106</sup>Rh, <sup>137</sup>Cs, and an unidentified peak at 101 keV as obtained from a diametrical pinhole scan (0.031 in. diam) across the A-A' axis of a disk fuel section. The photomacrograph at the bottom shows that recrystallization took place in the central part of oxide fuel during the irradiation.

Fig. 464-19. The distributions of the same isotopes and sample shown in Fig. 464-18, but across the line B'-B. The beta-gamma autoradiograph taken soon after termination of irradiation correlates very well with the <sup>106</sup>Rh distribution.

taken to ensure a pure beam of <sup>3</sup>He ions when doing an activation analysis. The ion source normally puts out <sup>3</sup>He<sup>+</sup> and <sup>3</sup>He<sup>++</sup> beams. The former beam is much more intense than the latter but is frequently contaminated with singly charged tritons or single charged hydrogen molecules (pd<sup>+</sup> and ppp<sup>+</sup>). Similarly, the <sup>3</sup>He<sup>++</sup> beam can be contaminated with doubly charged hydrogen molecules. A postacceleration electron stripper foil of thin carbon has been

added to the accelerator to eliminate these beam contaminations. After acceleration the singly charged ion beam is passed through the foil, which strips off electrons from all isotopes. The resulting <sup>3</sup>He<sup>++</sup> ions are separated from the other ions by a 90° bending magnet. Since the beam is more intense, it can be collimated to a smaller angular deviation for the same final intensity. The new experimental arrangement incorporates two vernier slit

systems to collimate the beam and has a vacuum pumping station near the target chamber to allow a better final vacuum in the chamber. This better vacuum should reduce deposition of carbon and oxygen on the target while running. The new chamber also allows more precise positioning of the beam and the target with respect to the beam.

Six germanium crystals were activated to study the surface contamination of oxygen on the crystals. Four were bombarded by 10.0-MeV  $^3\text{He}$  particles and two by 6.5-MeV  $^3\text{He}$  particles. The samples were allowed to decay for approximately 2 h after bombardment so short half-life activity, particularly from  $^{11}\text{C}$ , would decay. During this period, both Ge(Li) high resolution spectra and NaI total absorption spectra were taken at 4-min intervals to identify the radioactive isotopes in the sample. After the initial decay period, the samples were alternately lapped on a diamond lapping plate to remove thin ( $\sim 1\text{-}3\ \mu$ ) layers of the crystal and counted as above to determine the remaining activity. This was done to study the distribution of the radioactive material with depth. The crystals were lapped a total of 10-25  $\mu$ , which removed most of the activity. They were then counted overnight to give better data on the remaining activity. Preliminary results indicate possible cross contamination between the layers of the crystal via the lapping plate.

## VII. SODIUM-BOND HEAT TRANSFER STUDIES (J. O. Barner, K. Meier)

### A. General

The purpose of this project is to evaluate methods for determining the effects of fuel-pin defects on heat transfer properties of the sodium bond. Such defects could arise in a number of ways. For example, a void in the sodium bond could: (1) be present before insertion in the reactor, (2) come from dewetting of the pellet due to change in composition as fission products are formed, (3) form from a hot spot on the pellet and consequent local vaporization of the sodium, and/or (4) be produced from desorbed or fission-product gases. Of these, probably the most serious defect would be the presence of fission gas bubbles in the bond region.

There appear to be three methods of obtaining

the high heat fluxes necessary for "defect analysis": (1) in-pile experiments, (2) out-of-pile experiments utilizing a central, high-heat-flux heater, (3) out-of-pile experiments utilizing an induction heat source with the heat flow direction reversed. These three methods are all receiving consideration for use in sodium-bond heat transfer studies.

### B. Current Results

Much of the apparatus for out-of-pile testing of sodium bonds utilizing a central, high-heat-flux heater was constructed during this reporting period. The graphite rod heater was fabricated. The sodium test loop was fabricated and instrumented with a flowmeter and thermocouples to measure heat flux to the sodium. The heater was installed in the test loop and prepared for testing. Associated control instrumentation was also completed.

A 45 kVA transformer which provides power to the graphite heater was tested at rated voltage. After slight modifications, performance was satisfactory.

The heater was tested at 4kW, which is approximately 1/3 of the rated power. The heat flux produced in the 10-min test was 500,000 Btu/h-ft<sup>2</sup> at the heater surface.

The UC cylinder which fits over the heater to simulate (U,Pu)C fuel was designed. Fabrication is 70% complete.

Design work is 50% complete on apparatus to inject bubbles into the sodium bond. The heater lower support section is also being designed.

## VIII. ANALYTICAL CHEMISTRY

### A. General

Specific analytical techniques have been developed and evaluated to cope with the problems encountered in the investigation of fuel-clad compatibility. The results of many of these special analyses are given in several sections of the report in Project 464. A brief summary of some of the techniques, and the problems to which they were applied, is given below.

### B. Current Results

#### 1. Electron Microprobe Examination (E. A. Hakkila, H. L. Barker)

Variations in C, Cr, Fe, Ni, and Mo concentrations were determined along the inner walls of

eight Type 316 stainless steel capsules that had been sodium-bonded to (U,Pu)C. Diffusion of carbon into the stainless steel occurred at darkened areas of the walls of each sample. In one capsule the Cr, Fe, and Ni concentrations were lower at the darkened areas than at other areas, but significant variations in Cr, Fe, Ni, or Mo x-ray intensity as a function of proximity to the sample surface were not observed in the other samples.

Carbon concentration gradients from the inner surface to a depth of 250 microns into the interior of the wall were found in one type of "as-received" stainless steel capsules, but not in another type.

The following impurity phases were identified in six (U,Pu)C samples that had been tested in sodium-bonded stainless steel capsules: (1) precipitates, containing more plutonium and less uranium than the matrix, that were contaminated with Fe, W, and Si, either singly or together, (2) precipitates containing only tungsten, and (3) precipitates containing more uranium and less plutonium than the matrix. The U, Pu, and C distributions in the matrix were uniform.

## 2. Miscellaneous Services (N. Koski, W. Wilson, L. Thorn, G. Waterbury)

An inert-gas-fusion method was applied to the determination of O<sub>2</sub> in the following corrosion test specimens that had been held in sodium at various elevated temperatures: ten vanadium-base alloys, four niobium-base alloys, one uranium metal, one thorium metal, four stainless steels, one Nb-Zr alloy, and one Nb-W alloy. Oxygen was determined by this method also in seventeen (U,Pu)C pellets prior to corrosion testing, one (U,Pu)C pellet that had been heated in sodium at 650°C for 1000 h, and two UC samples. The method performed satisfactorily in these applications.

Two sodium samples that had contacted (U,Pu)O<sub>2</sub> powder were analyzed spectrophotometrically for uranium. In the multimicrogram concentration range, uranium is determined with a precision (1  $\sigma$ ) of 3 relative percent.

Controlled-potential coulometric and combustion-gravimetric methods were applied to measurement of U, Pu, and C in sixteen pre-test (U,Pu)C samples and to C in two pellets that had been tested for 1000 h in 650°C sodium. The coulometric

methods for measuring uranium and plutonium had a relative standard deviation of 0.2 to 0.3%, and the combustion-gravimetric method for determining carbon had a precision (1  $\sigma$ ) of 0.5 relative percent. The methods performed satisfactorily.

Spectrophotometric methods were applied to measurement of nitrogen in seventeen pre-test (U,Pu)C samples and two (U,Pu)C pellets held in sodium at 650°C for 1000 h, and to determination of tantalum in two pre-test samples of (U,Pu)C. The relative standard deviations were 3% in determining nitrogen at the ppm concentrations, and 5% for the low ppm concentrations of tantalum found.

## 3. Spectrographic Impurities (O. R. Simi, W. M. Myers, C. J. Martell, C. B. Collier, J. A. Mariner, R. T. Phelps)

Impurities normally determined by emission spectrography were determined in a number of samples of (U,Pu)C, PuO<sub>2</sub>, V-Ti alloys, sodium, and stainless steels. The significance of the impurities found is interpreted elsewhere in the various experimental programs.

## IX. REFERENCES

1. G. M. Campbell, private communication.
2. Edmund K. Storms, The Refractory Carbides, Academic Press, New York and London, 1967.
3. G. M. Campbell, L. J. Mullins, and J. A. Leary, "Thermodynamic Properties of Plutonium Compounds by EMF Techniques" in Thermodynamics of Nuclear Materials, 1967, IAEA, Vienna, 1968.
4. F. D. Richardson, "The Thermodynamics of Metallurgical Carbides and of Carbon in Iron," J. Iron and Steel Inst., Sept. 1953.
5. C. E. Wicks and F. E. Block, "Thermodynamic Properties of 65 Elements - Their Oxides, Halides, Carbides, and Nitrides," U. S. Bureau of Mines, Bulletin 605, 1963.
6. David Okrent, "Neutron Physics Considerations in Large Fast Reactors," Power Reactor Technology 7, 107, 1964.
7. K. F. Smith and R. J. Van Thyne, "Selected Properties of Vanadium Alloys for Reactor Application," Report ANL-5661, Argonne National Laboratory, May, 1957.
8. Harry A. Levin and Sherman Greenberg, "An Exploratory Study of the Behavior of Niobium- and Vanadium-Base Alloys in Oxygen-Contaminated Sodium," Report ANL-6982, Argonne National Laboratory, January, 1968.

9. V. J. Rutkauskas, "Determination of the Solubility of Oxygen in Sodium by Vacuum Distillation," Report LA-3879, Los Alamos Scientific Laboratory, September, 1968.

PROJECT 465  
REACTOR PHYSICS  
Person in Charge: D. B. Hall  
Principal Investigator: G. H. Best

---

## I. INTRODUCTION

Basic to the evaluation of various fast breeder concepts and proposals are the analytical techniques and physical data used in the analyses. Valid comparisons between different concepts and proposals depend on minimization of differences in results due to the methods of analysis. To this end, the Los Alamos Scientific Laboratory is cooperating with other AEC laboratories and contractors in the development of evaluated cross section data and associated processing codes. In addition, the Laboratory is working on the development and maintenance of digital computer programs pertinent to the nuclear analysis of fast breeder concepts. Finally, the Laboratory is evaluating the performance characteristics of various fast breeder reactor concepts.

## II. CROSS-SECTION PROCUREMENT, EVALUATION, AND TESTING (M. E. Battat, D. J. Dudziak, R. J. LaBauve)

### A. General

Accurate predictions of reactor design parameters, such as critical mass, sodium worth, and spectral response, require the development and maintenance of up-to-date basic microscopic nuclear data files. To meet this need, a national cooperative program is in progress to prepare an evaluated nuclear data file (ENDF/B). The large amount of experimental data which is becoming available, together with the theoretical data being generated by newly developed physics codes, makes the maintenance of ENDF/B a continuing task. In addition, a large effort is also needed in evaluating and testing the microscopic data prior to use in reactor calculations.

### B. Data Testing

The Data Testing Subcommittee of the CSEWG has examined in detail the calculational results submitted by various laboratories for ZPR-3 Assembly

48. It was concluded that it would be necessary to specify the procedures for data testing much more closely in order to clear up some of the ambiguities. It was also agreed that an additional  $^{235}\text{U}$ -fueled fast reactor benchmark was necessary, and ZPR-3 Assembly 11 was selected for this purpose. Calculations for both these benchmark problems were completed, and the results were transmitted to the Chairman of the Data Testing Subcommittee. Multi-group constants were generated by the ETOE and MC<sup>2</sup> codes from the ENDF/B data tapes received in July 1968 from BNL. Calculations to determine  $k_{\text{eff}}$  and real and adjoint fluxes were performed with both the MACH1 (diffusion)<sup>1</sup> and DTF-IV (transport)<sup>2</sup> codes. Central reactivity worths and perturbation cross sections were also computed. Tables I and II give selected results for ZPR-3 Assembly 48. These results were obtained using the fine-group and ultrafine-group options in MC<sup>2</sup>, and diffusion theory and transport theory.

At this time, the Data Testing Subcommittee has received results for the two fast reactor benchmark problems from LASL, ANL, and BNL. Results from other laboratories are expected in the near future; the calculations will be compared when all of the results are received.

### C. Shielding

The UK to ENDF/B data file translation codes (LUTE and LATEX) are being revised to account for photon production at neutron energies above those for which level de-excitation schemes are well known. This photon production is entered in the UK format files as being associated with a particular level, but the excitation cross section for that level is not the appropriate cross section to produce the photon. The reason for this is that the photon production cross section is for excitation of the level and for cascading through the level.

TABLE I

ZPR 3 ASSY 48 DATA COMPARISONS. CENTRAL ACTIVATION RATIOS RELATIVE TO U-235 FISSION.  
 MACH1=DIFFUSION THEORY. DTF-IV=TRANSPORT THEORY (S-4 OPTION).  
 FOR ALL PROBLEMS, BLANKET XSEC FOR U-235, U-238, AND FE CALCULATED USING ULTRAFINE GROUP OPTION (ZERO BUCKLING) IN MC\*\*2.  
 FOR ALL FINE GROUP PROBLEM, CORE XSEC USED IN BLANKET (EXCEPT FOR U AND FE).  
 FOR ULTRAFINE GROUP PROBLEM, MG AND AL FINE GROUP XSEC USED IN CORE. CORE XSEC USED IN BLANKET (EXCEPT FOR U AND FE).

	ALL FINE GROUP XSEC MACH1	DTF-IV	ULTRAFINE GROUP XSEC MACH1	DTF-IV
K-EFFECTIVE	0.9688	0.9834	0.9697	0.9838
FISSION RATIOS				
NP-237	2.26E-01	2.25E-01	2.12E-01	2.12E-01
U-238	3.21E-02	3.21E-02	3.05E-02	3.05E-02
PU-239	9.39E-01	9.39E-01	9.20E-01	9.20E-01
PU-240	2.40E-01	2.40E-01	2.26E-01	2.26E-01
CAPTURE RATIOS				
U-238	1.41E-01	1.40E-01	1.42E-01	1.40E-01
PU-239	1.87E-01	1.86E-01	1.96E-01	1.96E-01
PU-240	2.09E-01	2.09E-01	2.18E-01	2.17E-01
U-235	2.72E-01	2.71E-01	2.81E-01	2.80E-01

TABLE II

ZPR 3 ASSY 48 DATA COMPARISONS. CENTRAL REACTIVITY WORTHS.  
 PERTURBATION CROSS SECTIONS IN MILLIBARNS.  
 MACH1=DIFFUSION THEORY. DTF-IV=TRANSPORT THEORY (S-4 OPTION).  
 FOR ALL PROBLEMS, BLANKET XSEC FOR U-235, U-238, AND FE CALCULATED USING ULTRAFINE GROUP OPTION (ZERO BUCKLING) IN MC\*\*2.  
 FOR ALL FINE GROUP PROBLEM, CORE XSEC USED IN BLANKET (EXCEPT FOR U AND FE).  
 FOR ULTRAFINE GROUP PROBLEM, MG AND AL FINE GROUP XSEC USED IN CORE. CORE XSEC USED IN BLANKET (EXCEPT FOR U AND FE).

MATL	MAT	ALL FINE GROUP XSEC		-----ULTRAFINE GROUP XSEC-----		
		MACH1 DELTA K/MOLE	DTF-IV SIG-PERT	MACH1 DELTA K/MOLE	MACH1 SIG-PERT	DTF-IV SIG-PERT
C	1010	-1.14E-06	-4.70E+00	-2.29E-07	-6.91E-01	-2.19E+00
NA	1059	-1.52E-06	-5.93E+00	-7.18E-07	-2.07E+00	-3.62E+00
MG	1014	-6.13E-06		-5.53E-06		-1.70E+01
AL27	1015	-4.73E-06		-4.33E-06		-1.35E+01
CR	1018	-1.05E-05	-3.17E+01	-1.08E-05	-3.04E+01	-3.19E+01
MN55	1019	-2.06E-05	-6.09E+01	-2.19E-05	-6.20E+01	-6.35E+01
FE	1020	-8.05E-06	-2.47E+01	-8.74E-06	-2.30E+01	-2.46E+01
NI	1021	-1.18E-05	-3.60E+01	-1.07E-05	-3.01E+01	-3.22E+01
MO	1025	-8.42E-05	-2.41E+02	-9.44E-05	-2.66E+02	-2.66E+02
U235	1044	9.76E-04	2.68E+03	9.96E-04	2.64E+03	2.69E+03
U238	1047	-7.07E-05	-2.04E+02	-7.61E-05	-2.14E+02	-2.16E+02
NP237	1048	-2.69E-04	-8.02E+02	-3.33E-04	-9.81E+02	-9.67E+02
PU239	1051	1.30E-03	3.59E+03	1.31E-03	3.51E+03	3.56E+03
PU240	1053	2.26E-04	6.08E+02	2.04E-04	5.28E+02	5.38E+02
PU241	1054	1.90E-03	5.25E+03	1.96E-03	5.27E+03	5.35E+03
PU242	1055	1.91E-04	5.15E+02	1.71E-04	4.48E+02	4.56E+02

The translations of Drake's sodium and calcium evaluations are being extended to account for this additional photon production. The data are being entered in ENDF/B format with reaction type number MT = 110. At an August 6, 1968, meeting of the Codes and Formats Subcommittee of the Shielding Subcommittee of the CSEWG at Los Alamos, we recommended the inclusion of a photon production cross section, using MT = 110, in the ENDF/B file. No official action was taken, so in the interim we are placing a unit cross section in file 3 (MF = 3) and the photon production cross sections in file 15 as photon yields. This system, with the exception of using MT = 110, fits within the present ENDF/B system without compromising any of the data.

Detailed input specifications have been devised for the photon production code, LAPH, using as a model the DTF-IV system of flags for repeat, interpolate, and terminate. A major portion of the LAPH input for a spatially dependent gamma-source problem is identical to the DTF-IV input for the corresponding physical regions. Other inputs include: DTF-IV broad-group flux vectors (i.e., flux dump); resonance cross sections, weighting functions, and fine-group energy structure from MC<sup>2</sup>; and other control input. Also, a procedure is being devised to extract fine-group structures from MC<sup>2</sup> for resonance cross sections, resonance weighting functions, smooth cross sections, smooth weighting functions, and energy mesh.

Studies of the fast neutron biological dose attenuation by metal shields succeeded by thin hydrogenous shields have been completed. Since the work reported<sup>3</sup> at the ANS 1968 Annual Meeting, a study has been made of the effect of finite polyethylene shields. That is, the backscatter contribution in an effectively infinite thickness of polyethylene, as used in previous calculations, was removed. As would intuitively be expected, the backscatter contribution is significant (up to 16%), but its fractional contribution to the biological dose is essentially the same for all lead thicknesses. Thus, the effect on the removal cross section of the lead is minimal; a maximum change of 0.3% was found in the removal cross sections of lead followed by 9 cm of polyethylene.

### III. REACTOR ANALYSIS METHODS AND CONCEPT EVALUATIONS

#### A. General

A continuing task in fast reactor analysis and evaluation is the improvement of computer programs and the development of new computational methods. In addition to new methods, advances are constantly being made in computer technology which make possible the extension of existing calculational techniques.

#### B. Variational Principles Applied to Transport Problems (R. E. Alcouffe)

When performing one-dimensional transport calculations on two-dimensional systems, the leakage must be estimated in the spatial direction transverse to the calculation. In DTF-IV, this is done by using a buckling type of correction to the total cross section. Since this estimate is unsatisfactory when the medium in the transverse direction is large, it is desirable to have a more precise estimate. For this more precise estimate, it would be desirable to preserve the simplicity of the buckling type of correction.

In order to formulate such a method, the neutron transport process is written as a variational problem. For example, for two-dimensional cylindrical geometry, the problem is to find the stationary conditions of the functional

$$J = \sum_{g=1}^G \int_0^1 d\xi \int_0^\pi d\omega \int_0^R r dr \int_{Z_0}^{Z_f} dZ \left\{ \phi_g^\dagger(r, Z, \xi, \omega) \cdot \left[ \frac{\mu}{r} \frac{\partial(r\phi_g)}{\partial r} + \xi \frac{\partial\phi_g}{\partial Z} - \frac{1}{r} \frac{\partial}{\partial\omega} (\eta\phi_g) + \sigma_{Tg}(r, Z) \phi_g - \sum_{g'=1}^G \sigma_{g',g}^0(r, Z) \phi_{0g'}(r, Z) \right] \right\} + \text{B.C.}, \quad (1)$$

where the terms have their usual meanings<sup>4</sup> and B.C. stands for boundary condition terms.

In order to obtain one-dimensional equations, the functional is reduced by using trial functions for the dependent variable  $\phi_g(r, Z, \xi, \omega)$  and its adjoint. An axial (Z-direction) equation can be derived from the trial functions

$$\phi_g(r, Z, \xi, \omega) = \psi_g(r, \xi, \omega) a_g(Z, \xi)$$

$$\phi_g^\dagger(r, Z, \xi, \omega) = \psi_g^\dagger(r, \xi, \omega) a_g(Z, \xi). \quad (2)$$

The functions  $\psi_g$  and  $\psi_g^\dagger$  are assumed to come from a previous transport calculation in the radial direction, in which the axial leakage has been estimated by some appropriate method. The reduced equations have the form

$$\begin{aligned} \xi \frac{\partial a}{\partial Z} + \sigma'_{Tg}(\xi, Z) a_g - \sum_{g'=1}^G \sigma_{g'g}^{0'}(Z) a_{0g'}(Z) &= 0 \\ -\xi \frac{\partial a}{\partial Z} + \sigma'_{Tg}(Z, \xi) a_g^\dagger - \sum_{g'+1}^G \sigma_{gg'}^{0'}(Z) a_{0g'}^\dagger &= 0, \end{aligned} \quad (3)$$

where

$$\begin{aligned} \sigma'_{Tg}(Z, \xi) &= \left\{ \int_0^\pi d\omega \int_0^R r dr \psi_g^\dagger(r, \xi, \omega) \left[ \frac{\mu}{r} \frac{\partial r \psi_g}{\partial r} - \frac{1}{r} \frac{\partial}{\partial \omega} (\eta \psi_g) + \sigma_{Tg} \psi_g \right] \right\} / \left\{ \int_0^\pi d\omega \int_0^R r dr \psi_g^\dagger(r, \xi, \omega) \psi_g(r, \xi, \omega) \right\} \\ \sigma_{g'g}^{0'}(Z, \xi) &= \left\{ \int_0^\pi d\omega \int_0^R r dr \psi_g^\dagger(r, \xi, \omega) \sigma_{g'g}^{0'}(r, Z) \psi_{g'0}(r) \right\} / \left\{ \int_0^\pi d\omega \int_0^R r dr \psi_g^\dagger(r, \xi, \omega) \psi_g(r, \xi, \omega) \right\} \end{aligned} \quad (4)$$

An analogous equation may also be developed for the radial direction using the trial functions

$$\begin{aligned} \phi_g(r, Z, \xi, \omega) &= \chi_g(Z, \xi) b_g(r, \xi, \omega) \\ \phi_g^\dagger(r, Z, \xi, \omega) &= \chi_g^\dagger(Z, \xi) b_g^\dagger(r, \xi, \omega). \end{aligned} \quad (5)$$

The radial equations are written as

$$\begin{aligned} \frac{\mu}{r} \frac{\partial (rb)}{\partial r} - \frac{1}{r} \frac{\partial (\eta b)}{\partial \omega} + \sigma''_{Tg} b_g - \sum_{g'=1}^G \sigma_{g'g}^{0''} b_{0g'} &= 0 \\ -\mu \frac{\partial b}{\partial r} + \frac{1}{r} \frac{\partial (\eta b)}{\partial r} + \sigma''_{Tg} b_g^\dagger - \sum_{g'=1}^G \sigma_{gg'}^{0''} b_{0g'}^\dagger &= 0 \end{aligned} \quad (6)$$

where

$$\begin{aligned} \sigma''_{Tg}(r, \xi) &= \left\{ \int_{Z_0}^{Z_f} dZ \chi_g^\dagger(Z, \xi) \left[ \xi \frac{\partial \chi_g}{\partial Z} + \sigma_{Tg}(r, Z) \chi_g(Z, \xi) \right] \right\} / \left\{ \int_{Z_0}^{Z_f} dZ \chi_g^\dagger(Z, \xi) \chi_g(Z, \xi) \right\} \\ \sigma_{g'g}^{0''}(r, \xi) &= \left\{ \int_{Z_0}^{Z_f} dZ \chi_g^\dagger(Z, \xi) \sigma_{g'g}^{0''}(r, Z) \chi_{g'0}(Z) \right\} / \left\{ \int_{Z_0}^{Z_f} dZ \chi_g^\dagger(Z, \xi) \chi_g(Z, \xi) \right\} \end{aligned} \quad (7)$$

It is apparent that Eqs. 3 and 6 can be used in a cyclic manner to generate one-dimensional transport solutions starting from some initial estimate of either the radial or axial leakage. The process will be considered successful if the eigenvalues resulting from the transverse calculations are essentially the same. Presumably, this eigenvalue

will be a better approximation to the two-dimensional eigenvalue than that resulting from a single one-dimensional "buckled" calculation. Also, the composite two-dimensional flux which can be constructed from the one-dimensional traverses should serve as an excellent flux guess for a detailed two-dimensional  $S_n$  calculation.

Since the trial functions used in the above development come from DTF-IV  $S_n$  calculations, the information may be in either a  $P_n$  moments form or the discrete angle  $S_n$  form. If the leakage is

large, it is necessary to retain a large number of terms in the moments expansion in order to represent the flux adequately at the boundary, and thus give a good estimate of the leakage. The additional terms significantly complicate the evaluation of the parameter (Eqs. 4 and 7), especially in a cylindrical geometry. Therefore, to conserve simplicity and accuracy, the trial functions are taken to be in the discrete angle form. This can be done most conveniently by recasting the functional of Eq. 4 into its discrete space-angle form in each of the transverse directions. For example,

when the trial function is in the radial direction, the functional may take the form

$$J = \sum_{g=1}^G \sum_{m=1}^{MM} \sum_{i=1}^{IM} \int_0^1 d\xi \int_{Z_0}^{Z_f} dz \left\{ \phi_{i,m,g}^\dagger \left[ w_m \mu_m (A_{i+1} \phi_{i+1,m,g} - A_i \phi_{i,m,g}) + \left( \alpha_{m+1} \phi_{i,m+1,g} - \alpha_m \phi_{i,m,g} \right) + w_m \left( \xi \frac{\partial \phi_{i,m,g}}{\partial Z} + \sigma_{Tg} \phi_{i,m,g} - \sum_{g'=1}^G \sigma_{g',g}^0 \phi_{0,i,g'} \right) \right] \right\} \quad (8)$$

where the notation is taken from Eq. 10 of Ref. 2. The index  $i$  refers to the  $r$  dimension and  $m$  is the angular index consistent with cylindrical geometry.

A scheme based upon this functional has been programmed for the CDC 6600 and is currently being tested on a variety of realistic problems.

C. Collapsing of Cross-Section Sets (J. S. Philbin, B. M. Carmichael)

Tests have been performed to verify the accuracy obtainable when using regular-flux-weighted cross sections in reactor calculations. These cross sections were generated by the REGFLX code.

The preservation of  $k_{eff}$  when using spectrum collapsed cross sections for two reactors, UHTREX and a large fast reactor, is summarized in Figs. 1 and 2.

Although UHTREX is a thermal reactor, five fast groups are required in the broad-group structure for good agreement with the  $k_{eff}$  value calculated

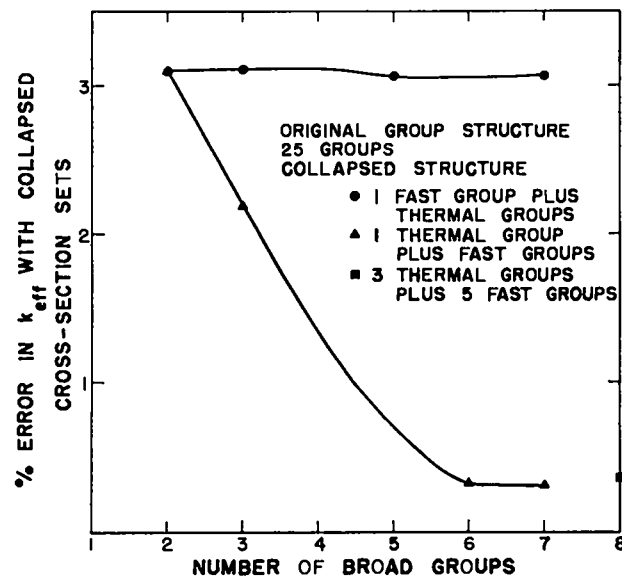


Fig. 1. Preservation of  $k_{eff}$  for UHTREX reactor.

with 25 groups (13 thermal, 12 fast groups). With only one fast group, the error was greater than 3%.

The preservation of  $k_{eff}$  under group collapse on the large fast reactor was slightly better than on UHTREX. The error remains below 2% even with only two broad groups.

The total fluxes in each broad energy group were checked against the total fluxes of the fine groups within each broad group,

$$\sum_{g \in G} \phi_g = \phi_G,$$

for which the agreement was always within 0.2%.

A pure spatial collapse was performed on four UHTREX cells. The homogenized cross sections agreed exactly with those generated in EFFXS. These homogenized cross sections were then used in CHILE to calculate  $k_{\infty}$  of the respective cells. These values agreed well with  $k_{\infty}$ 's calculated in the heterogeneous DTF-IV cell calculations. The differences were 0.025%, -0.001%, 0.004%, and 0.006% for the four cells.

REGFLX is now available for use on the DTF-IV codes. A dummy subroutine, EXFINP, can be equipped to call REGFLX and perform any collapsing routine specified by the user.

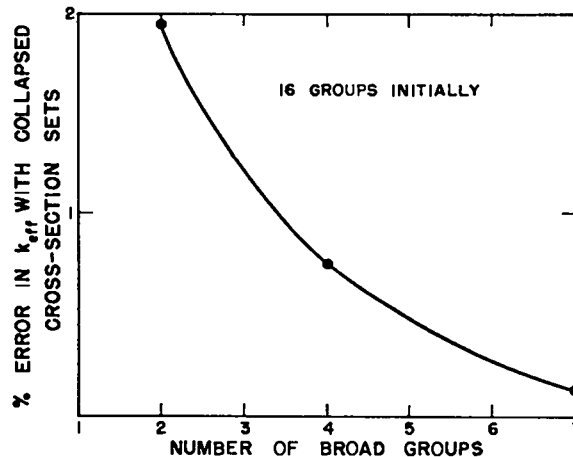


Fig. 2. Preservation of  $k_{eff}$  for a large fast reactor.

D. Preparation and Maintenance of Code Packages  
(M. E. Battat, J. C. Vigil)

1. Calculation of Central Worths. As discussed previously,<sup>5</sup> a discrepancy of 7-8% has been observed in the central reactivity worths computed by: (1) direct k-eigenvalue change using the DTF-IV neutron transport code ( $S_8$  option), and (2) perturbation theory, using the DTF-IV fluxes and currents. The system investigated was the JEZEBEL assembly with a centrally located  $^{239}\text{Pu}$  sample.

If  $(\text{Mdk/dM})_0$  is defined as the central void coefficient, where  $M$  = critical sphere mass, and the subscript refers to the mass change  $dM$  being made at  $r = 0$ , the observed discrepancy can be explained as follows:

- With respect to order  $n$  of  $S_n$  approximation, for the eigenvalue-difference method, the calculated  $(\text{Mdk/dM})_0$  for  $S_8$  is 1.5% larger than  $(\text{Mdk/dM})_0$  for  $S_\infty$ .
- With respect to order  $n$  of  $S_n$  approximation, for perturbation theory, the calculated  $(\text{Mdk/dM})_0$  for  $S_8$  is 3.5 to 5% (depending on mesh spacing) less than  $(\text{Mdk/dM})_0$  for  $S_\infty$ .
- With respect to DTF-IV flux and adjoint eigenfunctions, the " $r = 0$  transient" (where the first radial interval fluxes or adjoints in the sample region are smaller than the corresponding quantities in the second interval) phenomenon results in a 1.5% underestimate in the perturbation theory value of  $(\text{Mdk/dM})_0$  for  $S_8$ .

[G. E. Hansen provided this explanation of our calculations.]

2. ANCON. An additional feedback option has been incorporated into the ANCON code.<sup>6</sup> This additional option gives the reactivity feedback when the temperature coefficient is of the form

$$\frac{d\rho}{dT} = \frac{a}{T^b} \quad (9)$$

where  $\rho$  is the reactivity,  $T$  is the temperature ( $^{\circ}\text{K}$ ), and  $a$  and  $b$  are arbitrary constants. Equation 9 is the form commonly used for Doppler coefficients.

The reactivity feedback,  $F(T)$ , due to a change in temperature from  $T_0$  to  $T$  is given by the integral of Eq. 9. Results are

$$F(T) = a \ln(T/T_0) \quad \text{for } b = 1$$
$$F(T) = \frac{a}{1-b} (T^{1-b} - T_0^{1-b}) \quad \text{for } b \neq 1 \quad (10)$$

A feedback term of the type shown in Eq. 10 is available for each lump in the heat-balance equations. Different values of the constants  $a$  and  $b$  may be specified for each lump.

3. DAC. The DAC code has been modified to reduce data handling. This new version, called DAC-2, reads reactor specifications, unperturbed cross sections, and both regular and adjoint fluxes and currents directly from the 2DF output tapes. For the old version of DAC, tapes containing fluxes and currents had to be prepared from cards punched by 2DF. Also, reactor specifications and cross sections were input on cards in the old version.

E. Reactor Analysis

1. Transient Analysis (G. C. Hopkins). A transient analysis is being conducted for an oxide-fueled 1000-MW fast breeder reactor.<sup>7</sup> Parameters necessary for the analysis have been generated by PARAM, and transients resulting from various reactivity insertions are being studied using one and two energy groups in ANCONMG.

2. Steady-State Analysis (T. J. Hirons, R. D. O'Dell). Analytical methods are being developed for evaluating the performance potentials of carbide-fueled and metal-fueled fast breeder reactors. A 1000-MWe mixed-oxide fast breeder reactor<sup>7</sup> is being utilized as a model during the technique development. It is intended that parametric nuclear design analyses be made on such a reactor for use as a reference in evaluating the comparative performance potential of the other fuels. These studies will take cognizance of and be coordinated with the fuels and materials studies being conducted by this Laboratory.

The code to be used in this analysis is 2DB,<sup>8</sup> a two-dimensional diffusion theory burnup code. Recent modifications<sup>9</sup> have been incorporated into the LASL version of the code. The input format of the code was changed to permit the use of input parameter and data card formats that are virtually identical to those used in the 2DF code. An addition has been made to the code which allows the calculation and printing of the contribution to the

breeding ratio from each zone in the reactor. This information can be useful in determining trends in the breeding ratio.

It was found that a sinusoidal flux input guess produced a 10 to 50% reduction in computer running time from that required for no initial flux guess. Therefore, a subroutine (SINUS) was written and added to the 2DB code to generate the appropriate sinusoidal flux guess for any combination of reflective and vacuum boundary conditions. The value of  $k_{\text{eff}}$  was insensitive to the flux input guess, but local flux values were somewhat sensitive to the initial guess with a convergence criterion of  $10^{-5}$ . However, a convergence criterion of  $10^{-6}$  gave a fully converged flux profile.

Several parametric studies of the 2DB code were made using this fast breeder reactor. The over-relaxation factor,  $\beta$ , which is used in the point-wise relaxation scheme for accelerating convergence, was varied from 1.0 to 2.0. A value of 1.4 to 1.5 gave the quickest convergence of the code. However, it appears that the optimum value of  $\beta$  depends on the particular reactor being analyzed. A study of the convergence criterion  $\epsilon$  was made to determine the accuracy of the eigenvalue with respect to the magnitude of  $\epsilon$ . The results indicate that the maximum possible error in  $k_{\text{eff}}$  is about  $\pm 6\epsilon$  as opposed to the value  $\pm 3\epsilon$  given in the 2DB report.

The variation of  $k_{\text{eff}}$  with mesh point spacing was also studied in detail. Since the reactor is nearly symmetric in the vertical direction, the system can be accurately treated by considering only half rather than the whole reactor as was done previously. Halving the vertical dimension permitted much finer mesh studies within the storage limitations of the code. With this change, mesh spacings could be reduced to the order of a mean free path, and in a subsequent 2DB run, the  $k_{\text{eff}}$  value for the system stabilized at about 1.004 (clean core, all rods out). A mesh parameter involving both the relative magnitude of the flux as well as the local degree of curvature of the flux can be used to systematize the mesh selection.

Accordingly, a mesh parameter,  $MPX_i$ , at point  $i$  in direction  $X$  is defined as

$$MPX_i \equiv \frac{1}{\phi_{\text{max}}} \left| \frac{d^2 \phi_i}{dX^2} \right| (\Delta X_i)^2 \\ \equiv \frac{|\phi_i - 2\phi_{i+1} + \phi_{i+2}|}{\phi_{\text{max}}}, \quad (11)$$

where

- $\phi_{\text{max}}$  is the maximum total flux in the reactor
- $\phi_i$  is the total flux at point  $i$
- $\phi_{i+1}$  is the total flux at point  $i+1$  (in direction  $X$ ).

If a mesh spacing is established so that  $MPX$  is essentially uniform throughout the system (e.g.,  $MPX = 1\%$ ), then there are neither too many nor too few mesh points in a particular region. The use of the  $MPX$  criterion to establish a mesh typically results in fewer required mesh points than when the mesh is selected arbitrarily. For example, for a mesh that results in an  $MPX$  of about 0.6% throughout the above LMFBR (half-core model), a total of some 800 mesh points produces the same value of  $k_{\text{eff}}$  as did an arbitrary mesh selection involving some 1400 mesh points. The running times were about 4 min for the former case and about 10 min for the latter.

Testing of the ENDF/B cross-section data as generated from  $MC^2$  (see Section II) has continued on the reactor. A criticality run with 2DB and eight-group cross sections generated from the core spectrum alone resulted in a  $k_{\text{eff}}$  of 1.0060. Three different cross-section sets based on core, axial-blanket, and radial-blanket spectra were then used together in 2DB, and a  $k_{\text{eff}}$  of 1.0065 was obtained. Although the difference in eigenvalues between these two runs is small, more significant changes should be observed when the different cross-section sets are used in burnup calculations, since atom densities and flux distributions are constantly changing. The output spectra of these 2DB runs are generally softer than the infinite medium spectra used to generate the group cross sections. Attempts are being made to obtain a better matching of input and output spectra before detailed burnup analysis is begun. The  $MC^2$  code has the option of

taking an input spectrum along with input atom densities, which may be helpful in the generation of a more accurate set of group constants.

A criticality calculation was performed using a 16-energy-group cross-section set which was obtained by dividing each of the previously used 8 groups in half. The 16-group calculation with the 2DB code yielded a  $k_{eff}$  of 1.0003. Additional studies will be made to ascertain the sensitivity of the system to energy-group structure.

The spatially self-shielded cross sections of the boron control rods were calculated and used to determine the worth of the entire set of 85 rods in the reactor. Results of the 2DB runs with and without rods indicate an overall reactivity worth of about 6%. This figure agrees generally with that given in the design report.<sup>7</sup> It is interesting to note that when the self-shielded boron cross sections are not used, the calculated rod worth is more than twice as large as the 6% figure quoted above.

Preliminary burnup calculations have been made with 2DB to establish estimates on the reactivity loss due to burnup. Results indicate a 4 to 5% reactivity loss in going from an initial clean core to the beginning of an equilibrium cycle, and a 2% loss over an equilibrium cycle using the proposed refueling plan.<sup>7</sup> However, these numbers should be considered approximate, since no attempt was made to bring the reactor to critical after each refueling interval and the exact isotopic plutonium content to be supplied has not been determined.

Two different criticality calculations were performed on the LMFBR with the 2DF two-dimensional transport code. The first was performed using the full-core model with 1320 mesh points and the second using the half-core (axially symmetric) model with 1632 mesh points. The 2DF and corresponding 2DB results are shown in Table III.

TABLE III

COMPARISON OF  $k_{eff}$  FROM 2DF AND 2DB

Core Model	$k_{eff}$	
	2DF	2DB
Full core (1320 mesh)	1.0076	1.0060
Half core (1632 mesh)	1.0084	1.0042

#### IV. COOPERATIVE ARRANGEMENTS

W. H. Hannum has returned from his assignment at the United Kingdom Atomic Energy Research Establishment at Winfrith, England. Reports of his work and his visits to other research centers have been distributed.

#### V. REFERENCES

1. D. A. Meneley et al., "MACH1, a One-Dimensional Diffusion Theory Package," ANL-7223, Argonne National Laboratory (1966).
2. K. D. Lathrop, "DTF-IV, a FORTRAN-IV Program for Solving the Multigroup Transport Equation with Anisotropic Scattering," LA-3373, Los Alamos Scientific Laboratory (1966).
3. Donald J. Dudziak, "Attenuation of Fast-Neutron Biological Dose in Nonhydrogenous Shields Followed by Their Hydrogenous Shields," Trans. Am. Nucl. Soc. 11 (1), 197 (1968).
4. B. G. Carlson and K. D. Lathrop, "Transport Theory; The Method of Discrete Ordinates," LA-3251-MS, Los Alamos Scientific Laboratory (1965).
5. "Quarterly Status Report on the Advanced Plutonium Fuels Program, April 1 to June 30, 1968, and Second Annual Report, FY 1968," LA-3993-MS, Los Alamos Scientific Laboratory (1968).
6. J. C. Vigil, Nucl. Sci. Eng. 29, 392 (1967).
7. "Liquid Metal Fast Breeder Reactor Design Study (1000 MWe UO<sub>2</sub>-PuO<sub>2</sub> Fueled Plant)," GEAP-4418, General Electric (1963).
8. W. W. Little, Jr. and R. W. Hardie, "2DB, a Two-Dimensional Diffusion-Burnup Code for Fast Reactor Analysis," BNWL-640, Battelle Northwest Laboratory (1968).
9. W. W. Little, Jr. and R. W. Hardie, "2DB User's Manual," BNWL-831, Battelle Northwest Laboratory (1968).

PROJECT 466

FAST REACTOR METALLIC FUEL STUDIES

Persons in Charge: R. D. Baker  
D. B. Hall  
Principal Investigators: W. J. Maraman  
R. H. Perkins

---

I. INTRODUCTION

The objective of this program is the development of metal fuels for fast reactor application. Much of the primary effort is placed on preparation and fabrication development of the U-Pu-Zr alloys. Supporting effort is directed toward areas of physics and system evaluation, determining of physical and chemical properties of the fuel, and fuel-cladding interactions.

Irradiation testing is an essential part of the evaluation of a potential fuel alloy for fast reactor application. A knowledge of its intrinsic swelling rate as a function of alloy composition, metallurgical history, irradiation temperature, and total burnup must be obtained. The fission gas release rates and the limits of lattice-retained gas as a function of the above parameters are also required. In addition, the compatibility of fuels and claddings during irradiation at temperatures of interest to the LMFBR program must be determined.

II. FUEL PREPARATION AND FABRICATION  
(D. R. Harbur, B. N. Robbins, E. L. Grady,  
K. A. Johnson)

A. General

The initial goals of this task are to prepare high-purity, homogeneous U-15Pu-10Zr to U-15Pu-15Zr alloys, to fabricate these alloys into fuel pins of the EBR-11 size, and to fully characterize these pins. The major effort has been directed toward the preparation of a high-purity, homogeneous alloy. Several fabrication methods have been considered, and installation of equipment for the more promising of these methods is continuing. Extrusion and

characterization of as-cast U-15Pu-12.7Zr rods have been initiated.

B. Current Results

Two methods for preparing and casting U-Pu-Zr alloys have been evaluated. It has been concluded that the cold crucible technique, whereby the molten alloy is in contact with a water-cooled crucible, while feasible, still requires a great deal of development work to make it applicable to this alloy program. The zirconium segregation due to a zone-refining effect associated with the liquid-to-solid interface within the alloy button can only be eliminated by levitation of the entire charge. Another disadvantage of the cold crucible technique for a production-oriented program is the size limitation, which is related to the induction generator power available.

The advantages of the more conventional technique of induction melting and alloying in a bottom-pour crucible followed by direct casting are well known. The only reservation for this method was the extreme reactivity of the molten U-Pu-Zr alloys with most conventional crucible materials. Colloidal  $Y_2O_3$  coatings on graphite crucibles held up well but the oxygen and carbon content of the alloys prepared in these crucibles were about 500 and 400 ppm, respectively. A NbC coating on graphite crucibles has proven to be virtually inert to the molten U-Pu-Zr alloys. The niobium and carbon concentrations in four different castings prepared in NbC-coated graphite crucibles were about 20 and 200 ppm, respectively. The chemical analyses of one casting is given in Table I.

Table I  
Chemical Analyses of Feed and As-Cast U-Pu-Zr Lot No. 8023  
(Impurities in ppm)

	Arc-Cast U-Zr	Refined Pu	As-Cast U-Pu-Zr	
			Top	Bottom
Pu		100.00%	15.03%	15.10%
Zr	(~ 15%)	< 0.1	12.7%	12.2%
H		10		
Li	< 0.5	< 0.005		< 1
Be	< 0.5	0.01		< 1
B	< 0.5	< 0.3		< 1
C		20	190	190
O	100	20	180	260
Na	< 2	1		2
Mg	< 1	1		7
Al	5	1		12
Si	20	4		70
K		< 0.5		
Ca	< 5	2		< 5
Ti		< 0.2		
V	< 100	< 0.5		
Cr	< 2	< 0.5		< 10
Mn	15	< 0.1		25
Fe	75	4.2		78
Co	< 5	< 0.5		
Ni	< 5	0.5		12
Cu	5	0.6		25
Ga		2.2		
Sr		< 0.1		< 5
Y		< 0.1		
Mo	< 25	< 0.5		
Cd	< 2	< 0.5		< 10
Sn	< 2	< 0.5		< 2
Ba		< 0.1		< 10
Pb	< 2	< 0.5		< 2
Bi		< 0.5		< 2
Nb				20

Minimizing the oxygen content in these U-Pu-Zr alloys is an acute problem. The oxygen content of crystal-bar zirconium is 170 ppm. Arc-melted U-15Zr prepared from crystal-bar zirconium and high-purity uranium has an oxygen content between 70 and 130 ppm. U-Pu-Zr alloys prepared by co-melting the U-15Zr binary with high-purity plutonium in NbC-coated graphite crucibles followed by chill casting into an aluminum mold at ambient temperature have an oxygen content between 180 and 260 ppm. If the surface of the U-15Zr binary becomes oxidized and this tarnished surface is not removed prior to melting, the oxygen content of the casting produced is increased to 500 ppm. An additional 300 ppm O is dissolved into the alloy if it is poured into a Y<sub>2</sub>O<sub>3</sub>-coated mold.

The present method being used to prepare homogeneous U-15Pu-12.7Zr alloys is to inductively heat the arc-melted U-15Zr binary with plutonium to 1400°C in a NbC-coated graphite crucible, mechanically stir

the melt for 15 min, followed by bottom pouring into either aluminum molds at ambient temperature or Y<sub>2</sub>O<sub>3</sub>-coated graphite molds which are heated to 600°C or above. Chemical and metallographic examination of these castings have showed them to be homogeneous.

As the oxygen and carbon contents of the U-Pu-Zr alloys have been lowered, the machining properties of these cast rods has greatly improved. Figure 1 shows a U-15Pu-12.7Zr rod being machined with a carbide tool. The ends of the rod can be faced off with no edge chipping, and as can be seen from the photograph the cuttings are in the form of curled turnings.

Two different lots of 0.375-in.-diam rods, prepared by casting in Y<sub>2</sub>O<sub>3</sub>-coated graphite molds heated to 600°C, have been used for the determination of as-cast tensile properties. Metallographic examination of these rods showed a small amount of centerline porosity.

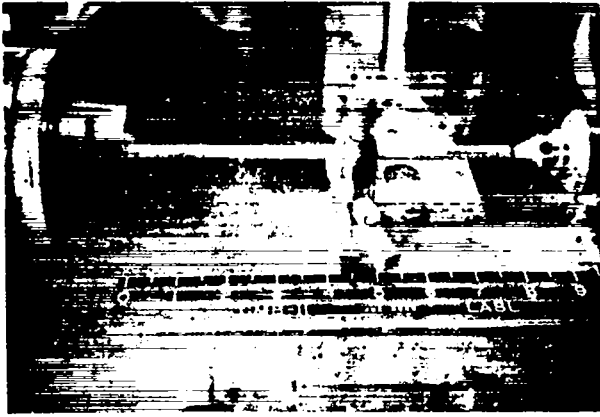


Fig. 1. U-15Pu-12.7Zr rod being machined with a carbide tool. Note the curled turnings.

Two tensile bars machined from these rods have been mechanically tested at 25°C. The stress-strain curves are shown in Fig. 2. As can be seen,

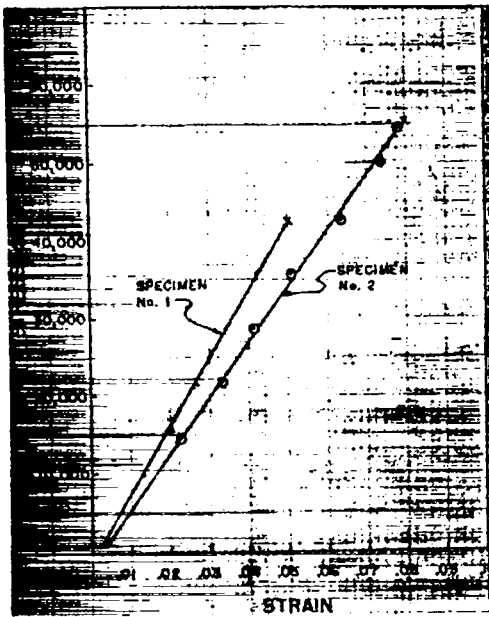


Fig. 2. Stress-strain curves for U-15Pu-12.2Zr and U-15Pu-12.6Zr tensile bars at 25°C at a strain rate of 0.015 in./min.

the strain was linear with stress up to the point of fracture, making a yield stress measurement impossible. No elongation was measurable in the 2-in. gage section of these 0.300-in.-diam test bars. The ultimate tensile strength, hardness, density and chemical analysis for these tensile bars are given in Table II. It is known that the densities of these test bars were lowered by center line porosity and it is believed that the tensile values were also lowered by this porosity.

An aluminum mold with a 0.75-in.-diam, 14-in.-long cavity is used for making chill-cast rods; one rod is cut into seven extrusion billets. Three extrusions of the U-15Pu-12.7Zr alloy have been made between 490 and 540°C using an M-2 tool steel die having a 60° included angle. The force necessary for these extrusions was 25 to 32 tons. The extrusion ratio was 4 to 1 starting with a 0.73-in.-diam billet. The WS<sub>2</sub> lubricant used held up well during these extrusions. A smooth surface on the extruded rods was obtained for all of the extrusion rates tested (0.3 to 0.9 in./min). The densities and hardnesses of the chill-cast billets were unchanged by the extrusion process, remaining at 15.1 g/cc and 41 Rc, respectively. A photomicrograph of a chill-cast U-15Pu-12.5Zr alloy rod with oxygen and carbon contents of 220 and 190 ppm, respectively, is shown in Fig. 3. The microstructure of this extruded material is shown in Fig. 4. The low oxygen content of this alloy is evident from the small amount of oxygen-stabilized, α-Zr present (small white particles).

Table II  
Properties of As-Cast U-Pu-Zr Alloys

No.	U (w/o)	Pu (w/o)	Zr (w/o)	C (ppm)	O (ppm)	Hardness (Rc)	Density (g/cc)	Ultimate tensile strength (25°C)
1	72.7	15.0	12.2	250	430	35-37	14.8	42,300
2	72.3	15.0	12.6	430	780	33-35	14.9	55,100



Fig. 3. Microstructure of as-cast U-15Pu-12.5Zr alloy rod chill cast into an aluminum mold at 25°C. 750X.



Fig. 4. Microstructure (longitudinal view) of extruded alloy shown in Fig. 3. Extrusion temperature was 500°C. 750X.

### III. IRRADIATION EFFECTS STUDIES

(J. A. Horak, R. L. Cubitt, L. B. Lundberg)

#### A. General

All long-term irradiations of metal fuels to date have had the effects of thermal cycling (due to reactor shutdowns and changes in power level) imposed upon the effects due to irradiation. Some of the detrimental effects to the fuel caused by this thermal cycling are:

1. The internal stresses produced by the volume changes associated with the alpha-gamma phase transformation in uranium-base alloys could be the source of microcracking.
2. Upon cooling, as alpha grains nucleate and grow from the existing gamma grains, the fission products (those that are insoluble and/or above their solubility limits) are swept ahead of the new alpha grains and end up in the alpha grain boundaries. The reverse process occurs on heating. The agglomeration of these elements produces a brittle and/or weak phase (usually intermetallic) resulting in a decrease in the mechanical strength and

ductility of the fuel. This phase could exhibit a lower corrosion resistance to hot sodium than the parent fuel.

3. Possibly even more important is the relocation of fission gases during thermal cycling; the agglomeration of fission gases during repeated phase transformations could very well be responsible for the extensive swelling and cracking observed in many of the fuel alloy irradiated to date.

It is evident that thermal cycling of unirradiated material does not provide the information necessary to separate the effects due to irradiation from those due to combined irradiation and thermal cycling.

One of the prime objectives of this program is to determine the effects of irradiation in the absence of thermal cycling. Irradiations will be conducted in the Omega West Reactor where there are instrumented facilities capable of maintaining the irradiation temperature within 5°C of the setpoint at fuel/clad interface temperatures up to at least 700°C, with or without reactor power. Parallel experiments will involve thermal cycling to accurately

assess the effects of thermal cycling during irradiation on the properties to be studied.

#### B. Current Results

The major effort during the past quarter has been devoted to the rehabilitation of the electrical and gas control systems for the environmental irradiation cells at Omega West Reactor. Current plans are to insert the first fueled experiment in the reactor in about one month.

Preirradiation physical measurements on the U-5Fs alloys for this experiment have been obtained. In addition, a practice loading of the primary fuel assembly and sodium bonding of the fuel to the cladding have been conducted. A diffusion couple of U-Fe has been made and will be included in this irradiation.

### IV. METAL FUEL COMPATIBILITY TESTING (L. B. Lundberg)

#### A. General

The aim of this task is to study the compatibility of potential fast reactor metallic fuels (e.g., U-Pu-Zr alloys) with potential cladding materials (e.g., Type 316 stainless steel). This will be accomplished by studying the mechanisms and kinetics of reactions between the fuels and claddings both in-pile and out-of-pile in temperature regions of interest to LMFBR designers. The emphasis will be on out-of-pile studies with neutron irradiation being added as an experimental variable. To attempt to understand some of the reactions which will occur between the complex candidate fuel and cladding alloys, some experiments will be performed to study the reactions between the pure components of these alloys (e.g., U vs Fe).

#### B. Current Results

A U-Fe diffusion couple annealed 194 h at 600°C has been examined metallographically. A diffusion zone  $3.3 \times 10^{-3}$ -in. wide was observed on the as-polished sample. This is almost 50 times the thickness of the reaction zone reported by Kittel<sup>1</sup> for a U-Fe couple annealed 192 h at 600°C. On the other hand, Kittel reports a reaction layer thickness for U-347 SS of the same order of magnitude as was seen in this experiment for U-Fe. It would not be too surprising to find, after further experimentation, that there is a closer correlation between

the diffusion rates of uranium-iron and uranium-austenitic stainless steels than is indicated by the earlier work of Kittel.

This sample has been submitted for electron microprobe analysis, but the results are not yet available. The microprobe analysis is being performed to (1) obtain concentration-penetration data, (2) identify the phases in the reaction zone, and (3) verify the metallographic observations. It is hoped that this sample will be available for inclusion in the first OWR metal fuels irradiation experiment. Since this sample has experienced some out-of-pile annealing, is diffusion bonded and will be well characterized, it could prove very useful in providing significant early indication of the effects of neutron irradiation on the compatibility of metal fuels and cladding.

Five additional U-Fe couples and five (U-5Fs)-316SS couples have been assembled and are awaiting encapsulation in heavy-walled stainless steel tubes. The U-Fe couples will be sealed in a helium atmosphere only, but the (U-5Fs)-316SS couples will be immersed in sodium with helium in the void space.

A diffusion bonding press has been designed and is being constructed. This device is being built to pre-bond metallic diffusion (compatibility) couples before submitting them to long-term anneals, either in-pile or out-of-pile. Pre-bonding appears to be more convenient over the long run than clamping unbonded specimens in low thermal expansion holders for bonding and subsequent diffusion during the long-term anneal.

### V. ANALYTICAL CHEMISTRY

#### 1. Electron Microprobe Examination of U-Pu-Zr Alloys (E. A. Hakkila, H. L. Barker)

Five samples of early preparations of U-Pu-12.5Zr alloys were examined to identify phases. Light matrix areas were found to contain more zirconium and less uranium than dark areas, but significant differences in plutonium content between these two phases were not observed. Irregularly-shaped white precipitates in which zirconium was the major constituent, and a light needle-like phase that contained more uranium and less plutonium than the matrix were identified.

2. X-ray Spectrophotometric Determination of Pu and Zr in U-Pu-Zr Alloys  
(R. G. Hurley, E. A. Hakila)

An x-ray fluorescence spectrometric method was developed for determining plutonium and zirconium in 200-mg samples of U-12Pu-15Zr alloys to supplement the controlled-potential coulometric and spectrophotometric methods now applied to these measurements. In this method thorium was used as an internal standard, and the intensities of the  $K_{\alpha}$  x-ray for zirconium and the  $L_{\alpha_1}$  x-ray for plutonium were measured relative to the intensity of the  $L_{\alpha_1}$  x-ray for thorium. Repeated determinations of zirconium and plutonium at three known concentrations in prepared solutions that also contained uranium showed that the precisions ( $1 \sigma$ ) were about 1%, respectively, in measuring between 10 and 20% of each element. The method included an arithmetic correction to eliminate interference caused by overlap of the  $K_{\alpha}$  x-ray for zirconium by the plutonium and uranium x-rays. A Fortran program for use on a CDC 6600 computer was written for this problem. Of the other elements that might cause interference by x-ray overlap or absorption, concentrations of at least 3% were tolerated, except for Pt, Bi, and Sr for which the concentrations could not exceed 1%, 0.2%, and 0.15%, respectively. The method has been applied successfully to analysis of two U-Pu-Zr alloys to date.

3. Miscellaneous Services  
(W. Hutchinson, W. Wilson, L. Thorn, G. Nelson, G. R. Waterbury)

An inert-gas fusion method was applied to the measurement of  $O_2$  in 23 samples of U-Pu-Zr alloy and two U-Zr alloys. The standard deviation of the method is 10 relative percent in the  $O_2$  concentration range between 90 ppm and 0.12% found in these samples. No difficulties were experienced.

A microcombustion method performed satisfactorily in measuring carbon in 14 U-Pu-Zr alloys. For the carbon concentration range between 190 ppm and 0.26% found in these alloys, the precision ( $1 \sigma$ ) is 10 relative percent.

A controlled-potential coulometric titration method for measuring plutonium, and spectrophotometric methods for measuring Zr, Ga, W, and Nb were applied to analyses of 39 U-Pu-Zr alloys. The relative standard deviations were 0.1% in measuring the

plutonium, 1% in measuring zirconium, and 2% in measuring Ga, W, and Nb.

VI. REFERENCES

1. J. H. Kittel, "Layer Formation by Interdiffusion between Some Reactor Construction Metals," Report ANL-4937, Argonne National Laboratory, June, 1949.

PROJECT 471

OTHER ADVANCED SYSTEMS - RESEARCH AND DEVELOPMENT

Person in Charge: D. B. Hall  
Principal Investigator: E. O. Swickard

1. HIGH TEMPERATURE NEUTRON DETECTOR TEST  
(E. O. Swickard, J. L. Bacastow)

A. General

Two high temperature neutron detectors were purchased from each of three manufacturers for evaluation. The detectors have  $^{235}\text{U}$  coated electrodes with integral, mineral-insulated cables. Purchase specifications required that both the detector and cable operate at  $600^\circ\text{C}$ . The test objective was the determination of the effect of temperature on the following: (1) pulse height distribution; (2) neutron counting sensitivity, (3) detector and cable resistance, (4) detector and cable capacitance; and (5) detector and cable noise.

Detectors with their integral signal cables were installed in four 17-ft high furnaces that contain a helium atmosphere at a few psig. Electrical heaters on the outside of the furnace tube were wired so that those in the detector region and those in the cable region are independently controllable.

The initial test of all detectors was made at ambient (room) temperature. Following testing at each temperature, detectors were allowed to cool to room temperature and the test sequence executed. Comparison of data from successive room temperature tests indicates the observed performance degradation caused by high temperature. Because of changes in pulse counting equipment, it is not appropriate to compare initial and final room temperature performance for the Westinghouse and Reuter Stokes detectors. For those detectors final room temperature performance can be compared to a reference intermediate room temperature test for which there was no change in counting equipment.

The evaluation of the detectors has now been completed, and a preliminary report has been prepared.<sup>1</sup> A summary of the results is presented here in Figs. 471-1 through 471-10. Figures 471-1 through 471-6 are plots of counting rate versus voltage for initial (or reference) and final room temperatures.

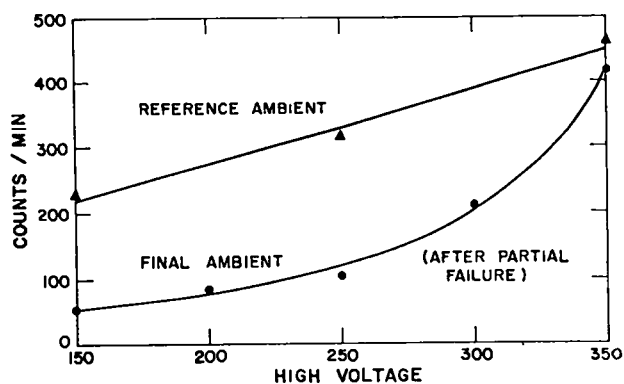


Fig. 471-1 Counting Rate vs. Voltage - Reuter Stokes No. 1 (room temp.)

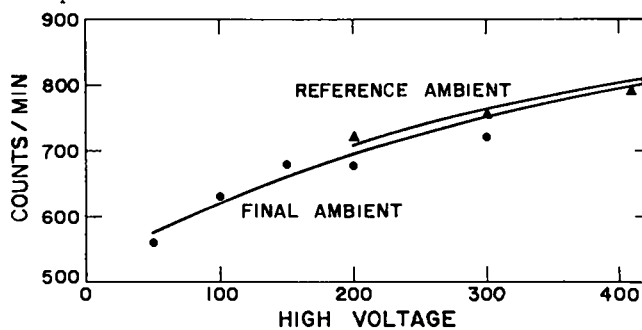


Fig. 471-3 Counting Rate vs. Voltage - Westinghouse No. 1 (room temp.)

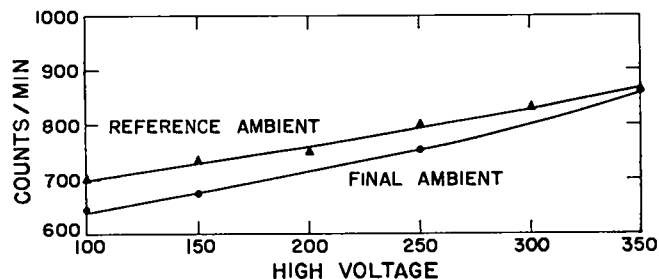


Fig. 471-2 Counting Rate vs. Voltage - Reuter Stokes No. 2 (room temp.)

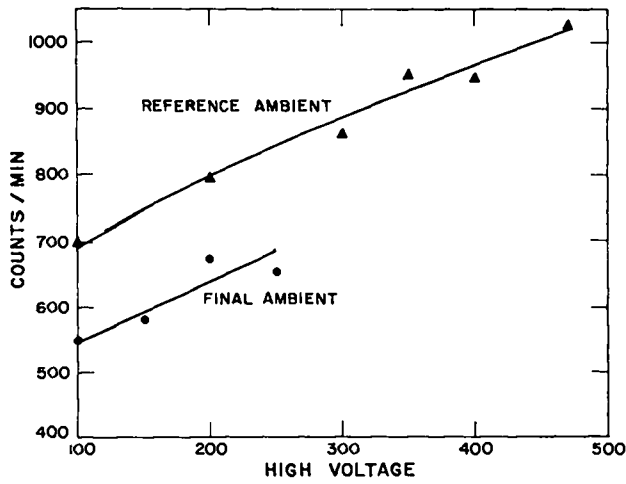


Fig. 471-4 Counting Rate vs. Voltage - Westinghouse No. 2 (room temp.)

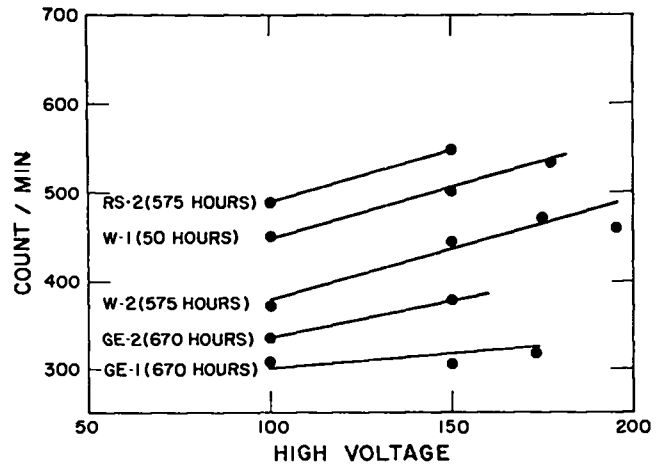


Fig. 471-7 Neutron Counts vs. Voltage After Being Held at 600°C Detector and Cable Temperature for Time Indicated.

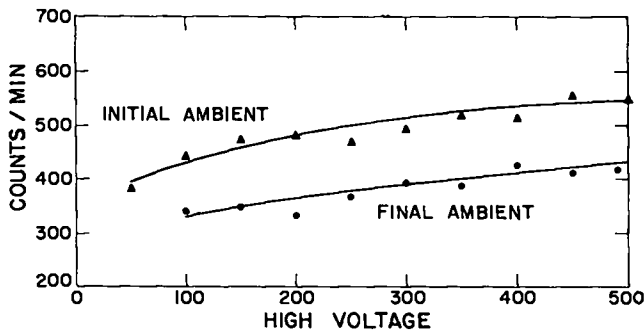


Fig. 471-5 Counting Rate vs. Voltage - General Electric No. 1 (room temp.)

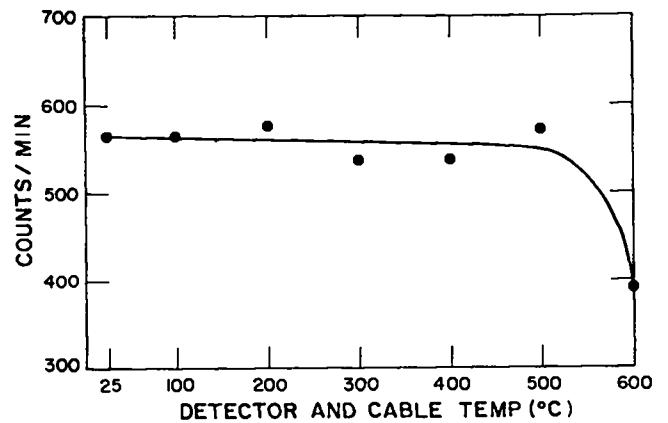


Fig. 471-8 Neutron Counts at 100 Volts vs. Temperature. Reuter Stokes No. 2.

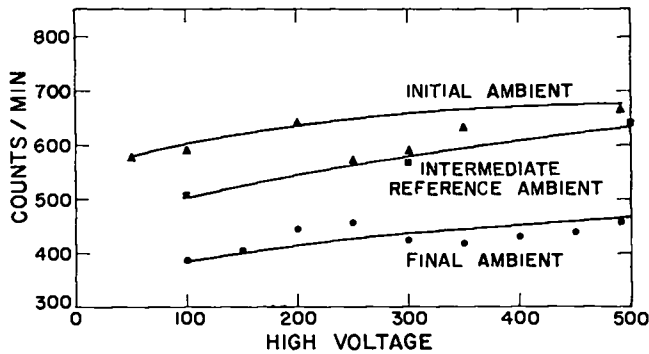


Fig. 471-6 Counting Rate vs. Voltage - General Electric No. 2 (room temp.)

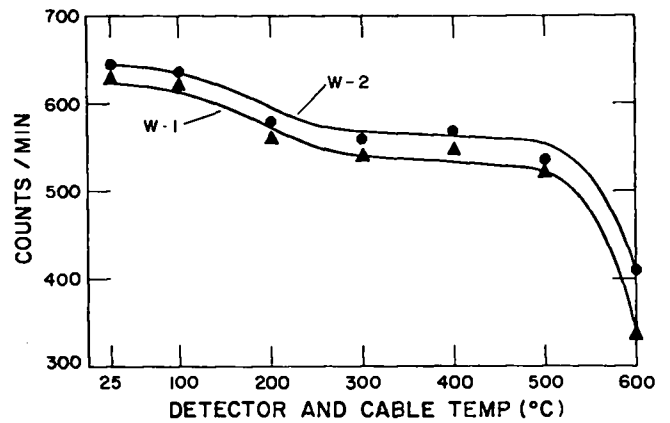


Fig. 471-9 Neutron Counts at 200 Volts vs. Temperature. Westinghouse Nos. 1 and 2.

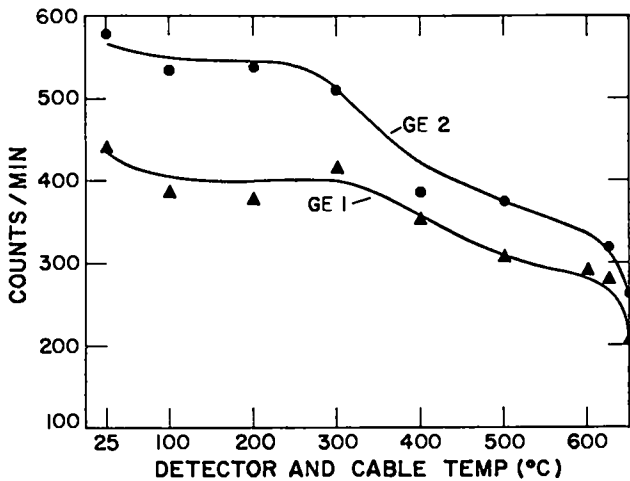


Fig. 471-10 Neutron Counts at 100 Volts vs. Temperature. General Electric Nos. 1 and 2.

Figure 471-7 is a plot of counting rate versus voltage for all detectors (except Reuter Stokes No. 1 which failed at 600°C) after being held at 600°C for the times indicated. All detectors have about the same change in counting rate versus voltage characteristic.

Figures 471-8, 471-9, and 471-10 are plots of counting rate versus temperature for a constant voltage.

## II. EQUATION OF STATE OF REACTOR FUELS (B. C. Goplen)

### A. General

The maximum credible accident (MCA) is a concept useful in calculating a maximum possible, but highly improbable, reactor accident. The various finite difference codes available, such as RAC and AXI, have proven adequate in handling the prompt critical, fast reactor excursion analysis. However, results of these calculations are highly dependent upon the assumed equation of state for the reactor fuel. Use is commonly made of the law of corresponding states in calculating a theoretical equation of state; however, the applicability of this law at such high temperatures and pressures has not been proven, and no direct experimental evidence is available. To remedy this situation, LASL has engaged in an experimental program to measure directly the equation of state of various fast reactor fuels (beginning with uranium dioxide) using high explosive

shock techniques.

In shock experiments, measurements are made of shock and particle velocities for a large number of "shots," which form a loci of points referred to as the Hugoniot line. Application of the laws of conservation of mass, momentum, and energy allows conversion to the thermodynamic variables energy, pressure, and specific volume through the Hugoniot equation. Thermodynamic identities and finite difference steps can then be used to extrapolate results along adiabatics extending below the Hugoniot line. In general, temperature rises encountered in these experiments are of the order of a few hundred degrees at most, but with extremely high pressures. To obtain results more applicable to the fast reactor excursion domain, use is made of low density fuel samples in the tests. Basically what happens is that the energy associated with crushing the voids goes into molecular excitation, or thermal energy. The result is higher temperatures and lower pressures which are more in line with those of reactor interest.

Uranium dioxide testing has been divided into two stages. Phase I involves establishing the basic Hugoniot for each of four density levels. This has been accomplished for densities of 3.16, 4.27, 6.30, and 10.31 g/cc. Classification of the effort prevents presentation of the data in this report; however, there is substantial evidence of two large volume changes, at least one of which is caused by a solid-solid transition. Phase II testing involves the use of standard materials to establish differential measurements which can be translated to Grunheisen ratios. These ratios will allow extrapolation of the low density data gathered in Phase I. Phase II has been completed for the densities of 6.30 and 10.31 g/cc. A complete analysis will be attempted following completion of the 4.27 g/cc series of shots.

### III. REFERENCES

1. "Test of Six High Temperature Neutron Detectors to 650°C," J. L. Bacastow and E. O. Swickard, LA-DC-9611, Los Alamos Scientific Laboratory (1968).

SPECIAL DISTRIBUTION

Atomic Energy Commission, Washington

Division of Research

D. K. Stevens

Division of Naval Reactors

R. H. Steele

Division of Reactor Development and Technology

L. J. Colby  
G. W. Cunningham  
D. E. Erb  
Nicholas Grossman  
W. H. Hannum (2)  
K. E. Horton  
J. R. Humphreys  
R. E. Pahler  
J. M. Simmons (2)  
E. E. Sinclair  
Bernard Singer  
A Van Echo  
C. E. Weber  
G. W. Wensch  
M. J. Whitman

Division of Space Nuclear Systems

G. K. Dicker  
F. C. Schwenk

Idaho Operations Office

DeWitt Moss

Ames Laboratory, ISU

O. N. Carlson  
W. L. Larsen  
M. Smutz

Argonne National Laboratory

F. G. Foote  
Sherman Greenberg  
J. H. Kittel  
W. B. Loewenstein  
R. E. Macherey  
M. V. Nevitt

Idaho Falls, Idaho

D. W. Cissell  
R. C. Robertson

Atomics International

R. W. Dickinson, Director  
Liquid Metals Information Center  
J. L. Ballif

Babcock & Wilcox Co.

C. Baroch  
J. H. MacMillan

Battelle Memorial Institute

D. L. Keller  
S. J. Paprocki

Brookhaven National Laboratory

D. H. Gurinsky  
C. Klamut

Combustion Engineering, Inc.

S. Christopher

Donald W. Douglas Laboratories

R. W. Andelin

General Electric Co., Cincinnati, Ohio

V. P. Calkins

General Electric Co., Sunnyvale, California

R. E. Skavdahl

Gulf General Atomic, Inc.

E. C. Creutz

Idaho Nuclear Corporation

W. C. Francis

IIT Research Institute

R. Van Tyne

Lawrence Radiation Laboratory

Leo Brewer  
J. S. Kane  
A. J. Rothman

LMFBR Program Office

Alfred Amorosi  
D. K. Butler (Physics)  
L. R. Kelman (Fuels & Materials)  
J. M. McKee (Sodium Technology)

Mound Laboratory

R. G. Grove

NASA, Lewis Research Center

J. J. Lombardo

Naval Research Laboratory

L. E. Steele

Oak Ridge National Laboratory

G. M. Adamson  
J. E. Cunningham  
J. H. Frye, Jr.  
C. J. McHargue  
P. Patriarca  
O. Sisman  
M. S. Wechsler  
J. R. Weir

Pacific Northwest Laboratory

F. W. Albaugh  
E. A. Evans

FFTF Project

E. R. Astley  
B. M. Johnson  
D. W. Shannon (2)

U. S. Department of Interior

Bureau of Mines, Albany, Oregon  
H. Kato

United Nuclear Corporation

A. Strasser

Westinghouse, Advanced Reactors Division

W. E. Ray

Westinghouse, Advanced Research Division

E. C. Bishop

Westinghouse, Bettis Atomic Power Laboratory

E. J. Kreigh